Supporting Information

Heterometallic Cooperativity in Divalent Metal ProPhenol Catalysts: Combining Zinc with Magnesium or Calcium for Cyclic Ester Ring-Opening Polymerisation

Weronika Gruszka,[a] Haopeng Sha,[a] Antoine Buchard,[b] Jennifer A. Garden*[a]

[a] *EaStCHEM School of Chemistry, University of Edinburgh, Edinburgh, EH9 3FJ, UK*

[b] *Department of Chemistry, University of Bath, Claverton Down, Bath, BA2 7AY, UK*

E-mail: j.garden@ed.ac.uk

Table of Contents

General experimental details

All manipulations requiring inert conditions were performed under an argon atmosphere using standard Schlenk techniques or in a glove box. All reagents and solvents were obtained from Sigma-Aldrich, Fischer Scientific, Honeywell or Acros Organics and were used without further purification unless described otherwise. Dry THF, toluene and hexane were collected from a solvent purification system (Innovative Technologies), dried over activated 4 Å molecular sieves and stored under argon. THF-d_8 and toluene-d_8 NMR solvents for NMR were degassed by three freeze-pump-thaw cycles and stored over activated 4 Å molecular sieves under argon. *Rac*-lactide (*rac*-LA), L-lactide (L-LA) and D-lactide (D-LA) were purified by double recrystallisation from toluene and sublimation. Benzyl alcohol (BnOH), ε-caprolactone (ε-CL), δ-valerolactone (δ-VL) and hexamethyldisilazane (HMDSH) were dried over CaH_2 and distilled under reduced pressure prior to use. ^{1}H, ^{13}C and 2D NMR (COSY, HSQC and DOSY) spectra were recorded on a Bruker AVA500, PRO500, AVA400 and AVA600 spectrometers at 298 K at 400 MHz, 500 MHz and 600 MHz and referenced to the residual solvent peaks (^{1}H: δ 3.58 for THF-d_8 and δ 2.08 for toluene-d_8, ^{13}C: δ 67.21 for THF-d_8 and δ 137.48 for toluene-d_8). The reported DOSY masses (to the nearest whole number) and aggregation states were determined by comparison to a calibration plot made with a range of standards (HMDSH, $Zn(HMDS)_2$, β-diketiminate ligand (BDIH) and (BDI)Zn(HMDS)) with molar masses varying from 161.4 to 643.4 g mol^{-1} in THF-d_8 and toluene-d_8.[1] SEC analyses of the filtered polymer samples were carried out in GPC grade THF at a flow rate of 1 mL min^{-1} at 35 °C on a 1260 Infinity II GPC/SEC single detection system with mixed bed C PLgel columns (300 x 7.5 mm). APPI-MS analysis was performed using a Bruker Daltonics 12T SolariX Fourier Transform Ion Cyclotron Resonance Mass Spectrometer using atmospheric pressure photoionisation (APPI). MALDI-ToF MS analyses were performed using a Bruker Daltonics UltrafleXtreme™ MALDI-ToF/ToF MS instrument. The sample to be analysed, dithranol or 2,5-dihydroxybenzoic acid matrix and KI (cationising agent) were dissolved in THF at 10 mg mL^{-1} and the solutions were mixed in a 2:2:1 volume ratio, respectively. A droplet (2 µL) of the resultant mixture was spotted on to the sample plate and submitted for MALDI-ToF MS analysis.

General computational details

All density-functional theory (DFT) calculations were performed using the Gaussian16 suite of codes (revision A.03).[2] Geometries were fully optimised without any symmetry or geometry constraints. The nature of all the stationary points as minima was verified by calculations of the vibrational frequency spectrum at 298 K and characterised by no imaginary mode. Only the intermediates of lowest free enthalpy found are reported here. Free enthalpies were calculated within the harmonic approximation for vibrational frequencies. DFT optimisation was carried out using the ωB97XD long-range corrected (LC) hybrid functional developed by Chai and Head-Gordon that includes an empirical

dispersion correction.[3,4] The 6-311++g(d,p) basis set was used for N, O, Zn, Mg, Ca atoms and the 6-31g(d) basis set was used for C and H atoms. Solvent effects in THF were considered using conductor-like polarisable continuum model (CPCM).[5,6] In order to facilitate DFT optimisations, calculations were carried out on a model version of the Trost ProPhenol ligand used experimentally, using no methyl group in the *para* position of the phenol ring. Based on our previous work, we assumed that the *R*,*R* configuration of the ligand at the nitrogen atoms was retained upon metal(s) coordination.[7] Full coordinates for all the stationary points, together with computed energies and vibrational frequency data, are available *via* the corresponding Gaussian16 output files and calculation spreadsheet, stored in the open-access digital repository, DOI:10.6084/m9.figshare.15785475.

Synthesis and characterisation of $Ca(HMDS)_2(THF)_2$

$Ca(HMDS)_2(THF)_2$ was synthesised following a literature procedure.[8] CaI_2 (2.95 g, 10.03 mmol) was added to a solution of KHMDS (4.00 g, 20.05 mmol) in dry THF (10 mL) in the glove box. The resulting mixture was stirred vigorously for 48 h under reflux under an argon atmosphere. The solution was then filtered through a plug of celite/glass wool, followed by removal of THF *in vacuo* and second filtration through celite/glass wool in pentane (10 mL). Pentane was subsequently removed *in vacuo* resulting in a pale orange powder (1.04 g, 21%). ^{1}H NMR (500 MHz, THF-d_8) δ 3.62 (m, 8 H), 1.77 (m, 8 H), 0.00 (s, 36 H) ppm. ^{13}C NMR (126 MHz, THF-d_8) δ 68.03, 26.19, 5.61 ppm.

Synthesis and characterisation of complex 1

(*S,S*)-(+)-2,6-bis[2-(hydroxydiphenylmethyl)-1-pyrrolidinyl-methyl]-4-methylphenol (500 mg, 0.79 mmol) was weighed into a Schlenk flask and dissolved in dry THF (10 mL) in the glove box. $Mg(HMDS)_2$ (270.3 mg, 0.79 mmol) was added to the ligand solution. The resulting mixture was stirred for 15 min at ambient temperature under an argon atmosphere in the glove box. $ZnEt_2$ (97.0 mg, 0.79 mmol) dissolved in dry THF (2.5 mL) was subsequently added and the reaction mixture was stirred for 16 h at ambient temperature under an argon atmosphere in the glove box. THF was subsequently removed *in vacuo*, resulting in a pale yellow powder (0.62 g, 78%). ^{1}H NMR (601 MHz, THF-d_8) δ 8.04 (d, 2 H), 7.87 (d, 2 H), 7.77 (d, 2 H), 7.62 (d, 2 H), 7.16 (q, 4 H), 7.07 (t, 4 H), 6.96 (dt, 2 H), 6.90 (dt, 2 H), 6.64 (d, 1 H), 6.59 (d, 1 H), 4.11 (d, 1 H), 3.82 (m, 2 H), 3.70 (m, 1 H), 3.62 (m, 4 H), 2.67 (dt, 1 H), 2.53 (d, 1 H), 2.33-2.43 (m, 4 H), 2.17-2.25 (m, 2 H), 2.05 (s, 3 H), 1.77 (m, 4 H), 1.19-1.54 (m, 6 H), 0.89 (t, 3 H), 0.04 (s, 19 H), -0.11-0.00 (m, 2 H). ^{13}C NMR (126 MHz, THF, for assignment, see Fig. S4) δ 158.73 (C13), 156.21 (C14), 155.88 (C14), 155.84 (C14), 155.81 (C14), 131.95 (C2), 131.89 (C2), 127.83 (C9), 127.60 (C9), 127.44 (C9), 127.34 (C9), 127.30 (C8), 126.73 (C8), 126.67 (C8), 126.63 (C8), 125.34 (C10), 125.12 (C10), 124.84 (C10), 124.80 (C10), 79.28 (C15), 76.80 (C15), 75.06 (C4), 71.07 (C4), 60.11 (C3), 58.61

(C3), 55.11 (C7), 29.77 (C5 + C6), 29.54 (C5 + C6), 20.12 (C7), 20.02 (C1), 13.65 (C12), 2.49 (HMDSH), -0.45 (C11).

Elemental analysis: Calculated for **[LMgZnEt(THF)(HMDSH)]**: C, 66.86; H, 7.65; N, 4.25%. Found: C, 66.15; H, 7.31; N, 4.11%.

m/z (APPI-MS): 753.28 $[LMgZnEt + H]^+$ (calc: 753.28).

Synthesis and characterisation of complex 2

(*S,S*)-(+)-2,6-bis[2-(hydroxydiphenylmethyl)-1-pyrrolidinyl-methyl]-4-methylphenol (500 mg, 0.79 mmol) was weighed into a Schlenk flask and dissolved in dry THF (10 mL) in the glove box. $Ca(HMDS)_2(THF)_2$ (395.9 mg, 0.79 mmol) was added to the ligand solution. The resulting mixture was stirred for 15 min at ambient temperature under an argon atmosphere in the glove box. $ZnEt_2$ (97.0 mg, 0.79 mmol) dissolved in dry THF (2.5 mL) was subsequently added and the reaction mixture was stirred for 16 h at ambient temperature under an argon atmosphere in the glove box. THF was subsequently removed *in vacuo*, resulting in a pale yellow powder (0.60 g, 75%). ^{1}H NMR (500 MHz, THF) δ 8.06 (d, 2 H), 7.76 (dd, 4 H), 7.56 (d, 2 H), 7.02-7.13 (m, 8 H), 6.78-6.90 (m, 4 H), 6.61 (dd, 2 H), 4.12 (d, 1 H), 4.01 (d, 1 H), 3.75-3.82 (m, 2 H), 3.60-3.63 (m, 4 H), 2.68 (d, 2 H), 2.60-2.63 (m, 1 H), 2.34-2.38 (m, 1 H), 2.18-2.21 (m, 2 H), 2.04 (s, 3 H), 1.84-1.91 (m, 1 H), 1.76-1.79 (m, 4 H), 1.54-1.60 (m, 2 H), 1.43-1.49 (m, 4 H), 1.17-1.21 (m, 2 H), 1.01 (t, 3 H), 0.04 (s, 19 H), -0.17--0.08 (m, 2 H). ^{13}C NMR (126 MHz, THF, for assignment, see Fig. S8) δ 161.06 (C13), 157.72 (C14), 157.06 (C14), 156.32 (C14), 156.21 (C14), 133.16 (C2), 131.52 (C2), 130.21 (C9), 127.65 (C9), 127.57 (C9), 127.20 (C8), 127.09 (C8), 127.01 (C8), 126.86 (C8), 126.47 (C9), 125.17 (C10), 124.77 (C9 + C10), 124.66 (C10), 124.37 (C10), 79.85 (C15), 79.52 (C15), 77.25 (C4), 70.42 (C4), 59.38 (C3), 58.93 (C3), 55.05 (C7), 29.90 (C5 + C6), 28.80 (C5 + C6), 20.25 (C7), 20.17 (C1), 13.96 (C12), 2.49 (HMDSH), -0.43 (C11).

Elemental analysis: Calculated for **[LCaZnEt(THF)(HMDSH)]**: C, 65.81; H, 7.53; N, 4.19%. Found: C, 66.10; H, 7.03; N, 4.15%

m/z (APPI-MS): 795.23 $[LCaZnOH + K]^+$ (calc: 795.32).

Synthesis and characterisation of complex 6

(*S,S*)-(+)-2,6-bis[2-(hydroxydiphenylmethyl)-1-pyrrolidinyl-methyl]-4-methylphenol (500 mg, 0.79 mmol) was weighed into a Schlenk flask and dissolved in dry THF (10 mL) in the glove box. $Mg(HMDS)_2$ (540.6 mg, 1.58 mmol) was added to the ligand solution and additional 2 mL of THF were added. The resulting mixture was stirred for 1 h at ambient temperature under an argon atmosphere in the glove box. THF was subsequently removed *in vacuo*, resulting in a pale orange powder (0.65 g, 55%). ^{1}H NMR (601 MHz, THF) δ 7.95 (d, 4 H), 7.70 (d, 4 H), 7.13 (t, 4 H), 7.07 (t, 4 H), 6.95 (t, 2 H), 6.90 (t, 2 H), 6.68 (s, 2 H), 4.01 (d, 2 H), 3.86-3.89 (m, 2 H), 3.61-3.63 (m, 10 H), 2.72 (d, 2 H), 2.63 (t, 2 H), 2.32 (q, 2 H),

2.07 (s, 3 H), 1.76-1.78 (m, 10 H), 1.55-1.60 (m, 2 H), 1.43-1.49 (m, 6 H), 0.29 (s, 18 H). ^{13}C NMR (126 MHz, THF, for assignment, see Fig. S12) δ 156.04 (C13), 155.43 (C14), 155.37 (C14), 131.97 (C2), 127.70 (C9), 127.40 (C9), 127.12 (C8), 126.72 (C8), 125.52 (C10), 124.90 (C10), 77.81 (C15), 73.86 (C4), 60.85 (C3), 55.04 (C7), 29.75 (C5 + C6), 20.27 (C5 + C6), 19.94 (C1), 6.74 (C11), 2.48 (HMDSH).

Elemental analysis: Calculated for **[LMg$_2$HMDS(THF)(HMDSH)]**: C, 65.72; H, 8.23; N, 5.20%. Found: C, 66.10; H, 7.82; N, 4.80%

m/z (APPI-MS): 1385.60 $[(LMg_2OH)(LMg_2)]^+$ (calc: 1384.60).

Synthesis and characterisation of complex 7

(*S,S*)-(+)-2,6-bis[2-(hydroxydiphenylmethyl)-1-pyrrolidinyl-methyl]-4-methylphenol (300 mg, 0.47 mmol) was weighed into a Schlenk flask and dissolved in dry THF (4 mL) in the glove box. $Ca(HMDS)_2(THF)_2$ (472 mg, 0.94 mmol) was added to the ligand solution and additional 2 mL of THF were added. The resulting mixture was stirred for 16 h at ambient temperature under an argon atmosphere in the glove box. THF was subsequently removed *in vacuo*, resulting in a pale orange powder (0.44 g, 75%). Notably, the assignment of NMR spectra of complex **7** was not possible due to the rapid Schlenk equilibria resulting in very complicated and broad spectra in THF-d_8 and toluene-d_8 and by variable temperature ^{1}H NMR (THF-d_8) between 5-55 °C.[9]

Elemental analysis: Calculated for **[LCa$_2$HMDS(THF)$_4$(HMDSH)$_2$]**: C, 62.17; H, 8.88; N, 4.71%. Found: C, 62.25; H, 7.79; N, 4.42%

m/z (APPI-MS): 1391.55 $[(LHCa)(LCa_2)]^+$ (calc: 1391.55).

Synthesis and characterisation of complex 11

Complex **6** (250 mg, 0.18 mmol) and BnOH (18.70 µL, 0.18 mmol) were added to a Schlenk flask and dissolved in dry THF (4 mL). The resulting reaction mixture was stirred at ambient temperature for 1 h under argon atmosphere. Upon completion, THF was removed *in vacuo*, resulting in a pale orange powder (185 mg, 81%). ^{1}H NMR (500 MHz, THF) δ 8.53 (d, 2 H), 8.16 (d, 4 H), 7.85 (d, 4 H), 7.43 (t, 2 H), 7.22 (t, 1 H), 7.15 (t, 4 H), 7.08 (t, 4 H), 6.95 (t, 2 H), 6.90 (t, 2 H), 6.60 (s, 2 H), 5.63 (d, 1 H), 5.23 (d, 1 H), 3.77-3.82 (m, 4 H), 3.60-3.63 (m, 7 H), 2.54 (d, 2 H), 2.42 (t, 2 H), 2.17-2.23 (m, 2 H), 2.04 (s, 3 H), 1.77-1.79 (m, 7 H), 1.42-1.44 (m, 6 H), 1.21-1.29 (m, 2 H). ^{13}C NMR (126 MHz, THF, for assignment, see Fig. S15) δ 157.32 (C17), 156.79 (C18), 156.35 (C18), 149.42 (C16), 131.16 (C2), 129.34 (C12), 128.36 (C13), 127.61 (C9), 127.34 (C9), 126.75 (C8), 126.58 (C8), 126.30 (C14), 124.70 (C10), 124.58 (C10), 77.42 (C15), 74.65 (C4), 67.36 (C11), 60.87 (C3), 55.77 (C7), 29.83 (C5 + C6), 20.29 (C5 + C6), 20.10 (C1).

Elemental analysis: Calculated for **[LMg$_2$OBn(THF)$_2$(HMDSH)]**: C, 70.06; H, 7.81; N, 3.83%. Found: C, 70.47; H, 7.50; N, 3.53%

m/z (APPI-MS): 1385.60 $[(LMg_2OH)(LMg_2)]^+$ (calc: 1385.60).

Synthesis and characterisation of complex 12

Complex **7** (250 mg, 0.29 mmol) and BnOH (29.70 µL, 0.29 mmol) were added to a Schlenk flask and dissolved in dry THF (4 mL). The resulting reaction mixture was stirred at ambient temperature for 1 h under argon atmosphere. Upon completion, THF was removed *in vacuo*, resulting in a pale orange powder (160 mg, 48%). ^{1}H NMR (500 MHz, THF) δ 8.28 (d, 4 H), 7.85 (d, 4 H), 7.40 (d, 3 H), 7.17 (t, 2 H), 7.08 (t, 4 H), 7.02 (t, 4 H), 6.87 (t, 2 H), 6.82 (t, 2 H), 6.61 (s, 2 H), 3.94 (d, 2 H), 3.72-3.77 (m, 2 H), 3.60-3.63 (m, 7 H), 2.49 (t, 2 H), 2.35 (d, 2 H), 2.14 (q, 2 H), 2.04 (s, 3 H), 1.76-1.79 (m, 6 H), 1.55-1.59 (m, 2 H), 1.46-1.50 (m, 2 H), 1.21-1.27 (m, 2 H). ^{13}C NMR (126 MHz, THF, for assignment, see Fig. S17) δ 161.74 (C17), 158.71 (C18), 132.31 (C2), 128.33 (C13), 127.43 (C9), 127.09 (C9), 127.02 (C8), 126.89 (C8), 126.85 (C14), 124.40 (C10), 124.14 (C10), 79.79 (C15), 76.20 (C4), 60.99 (C3), 56.15 (C7), 29.47 (C5 + C6), 21.23 (C5 + C6), 20.37 (C1).

Elemental analysis: Calculated for **$[LCa_2OBn(THF)_2(HMDSH)]$**: C, 68.10; H, 7.59; N, 3.72%. Found: C, 67.70; H, 7.08; N, 3.59%

m/z (APPI-MS): 1447.50 $[(LCa_2OH)(LCa_2)]^+$ (calc: 1447.50).

General experimental procedure for the ring-opening polymerisation of LA in toluene

In the glove box, in two separate air-tight vials with magnetic stirrer bars, *rac*-LA, L-LA or D-LA (100 eq., 200 mg, 1.39 mmol) was dissolved in dry toluene (1 mL) and complex **1** or **2** (13.9 µmol) were dissolved in dry toluene (0.39 mL). To aid solubility, both solutions were stirred for 3 minutes at 60 °C using DrySyn heating blocks before the catalyst solution was added to the LA solution. The polymerisation was initiated by addition of BnOH (1.44 µL, 13.9 µmol). The reaction was subsequently stirred at the appropriate temperature for the required time. Upon completion, the reaction was quenched in excess hexane. The volatiles were removed under compressed air and an aliquot was dissolved in $CDCl_3$ for NMR spectroscopic analysis.

General experimental procedure for the ring-opening polymerisation of LA in THF

In the glove box, in an air-tight vial with a magnetic stirrer bar, *rac*-LA (100 eq., 200 mg, 1.39 mmol) and complex **1** (13.9 µmol) were dissolved in dry THF (1.39 mL). The polymerisation was initiated by addition of BnOH (1.44 µL, 13.9 µmol). The reaction was subsequently stirred using DrySyn heating blocks at the appropriate temperature for the required time. Upon completion, the reaction was quenched in excess hexane. The volatiles were removed under compressed air and an aliquot was dissolved in $CDCl_3$ for NMR spectroscopic analysis.

General experimental procedure for the ring-opening polymerisation of ε-CL

In the glove box, in an air-tight vial with a magnetic stirrer bar, ε-CL (100 eq., 154 µL, 1.39 mmol) and complex **1** or **2** (13.9 µmol) were dissolved in dry toluene (1.39 mL). The polymerisation was initiated by addition of BnOH (1.44 µL, 13.9 µmol). The reaction was subsequently stirred using DrySyn heating blocks at the appropriate temperature for the required time. Upon completion, the reaction was quenched in excess hexane. The volatiles were removed under compressed air and an aliquot was dissolved in $CDCl_3$ for NMR spectroscopic analysis.

General experimental procedure for the ring-opening polymerisation of δ-VL

In the glove box, in an air-tight vial with a magnetic stirrer bar, δ-VL (100 eq., 129 µL, 1.39 mmol) and complex **1** or **2** (13.9 µmol) were dissolved in dry toluene (1.39 mL). The polymerisation was initiated by addition of BnOH (1.44 µL, 13.9 µmol). The reaction was subsequently stirred using DrySyn heating blocks at the appropriate temperature for the required time. Upon completion, the reaction was quenched in excess hexane. The volatiles were removed under compressed air and an aliquot was dissolved in CDCl3 for NMR spectroscopic analysis.

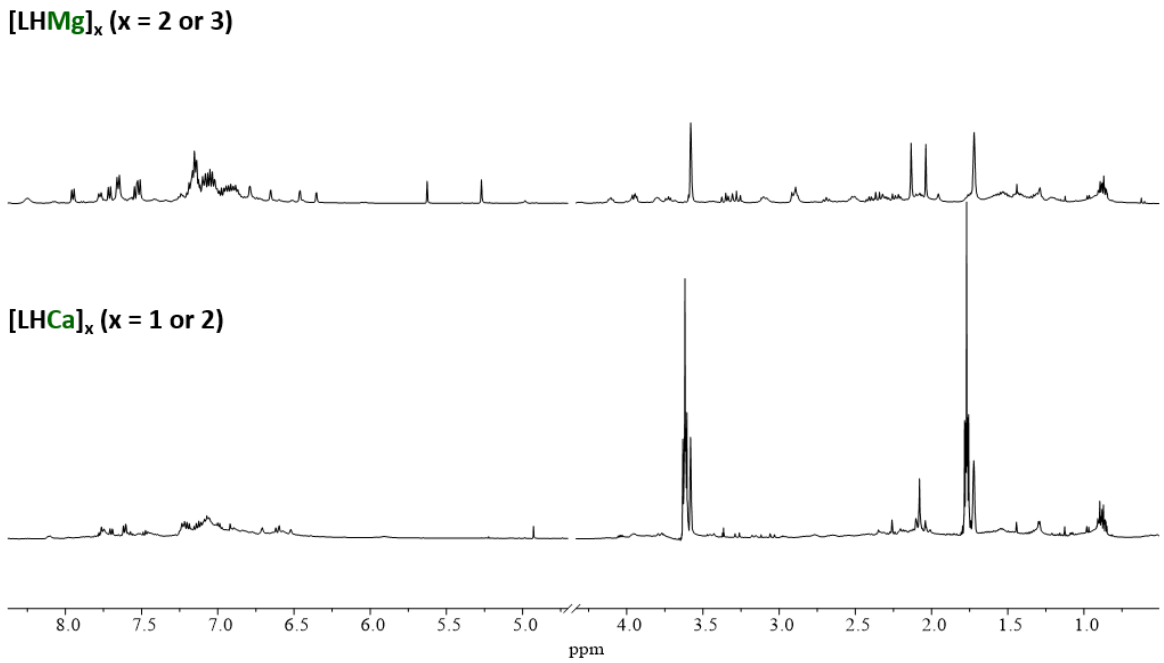

Figure S1. Overlay of ^{1}H NMR spectra of **[LHM]$_x$** (M = Mg or Ca, x = 1-3) in THF-d_8 (298 K).

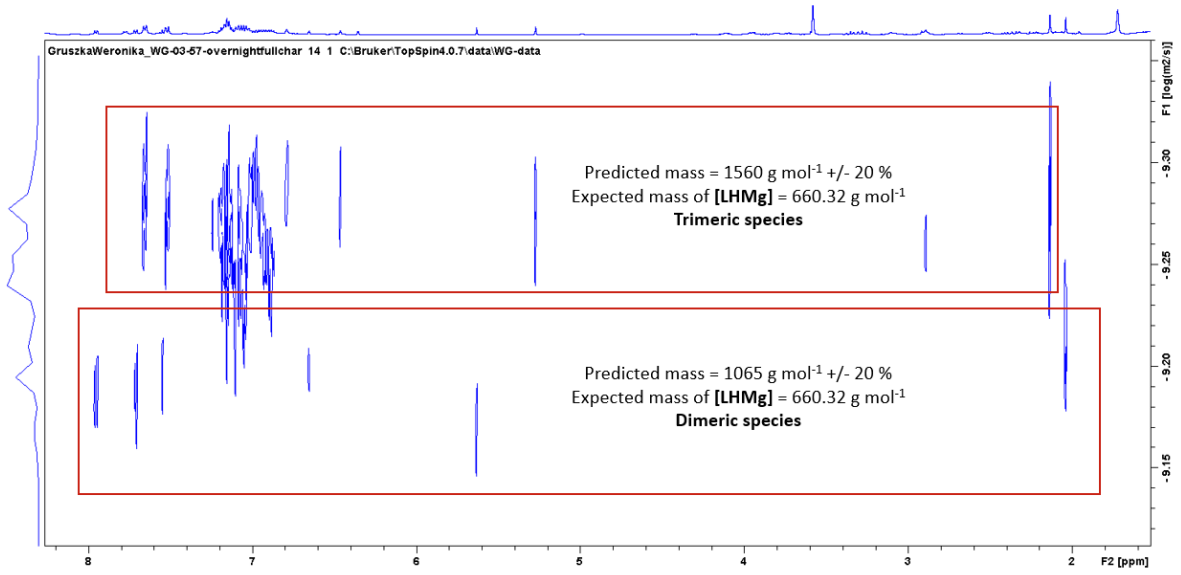

Figure S2. DOSY NMR spectrum of **[LHMg]$_x$** (x = 2-3) in THF-d_8 (298 K).

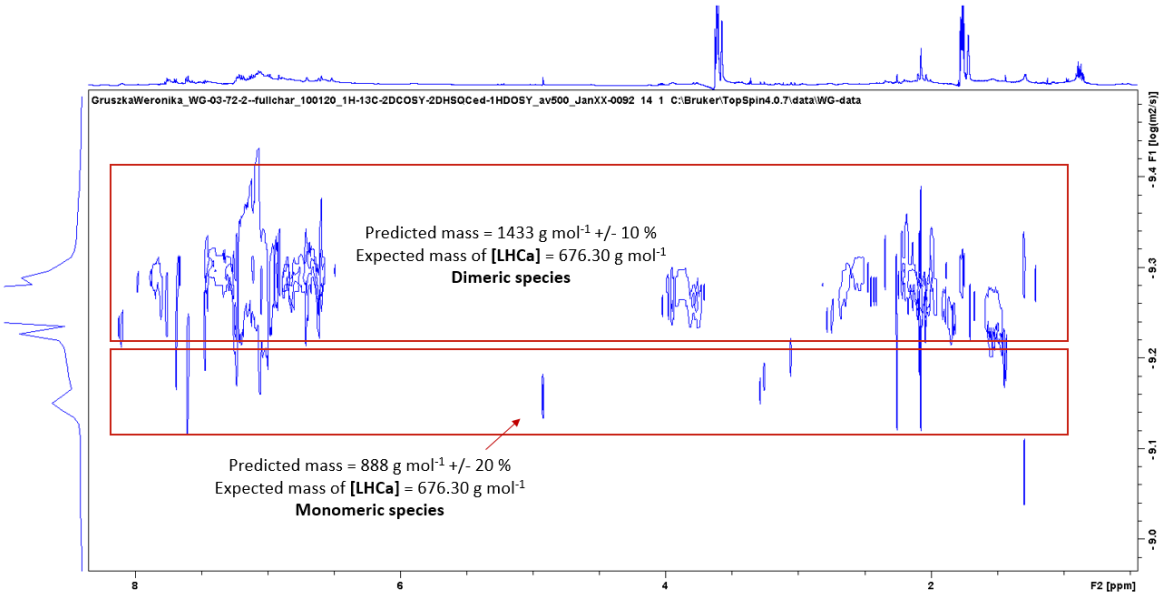

Figure S3. DOSY NMR spectrum of **[LHCa]$_x$** (x = 1-2) in THF-d_8 (298 K).

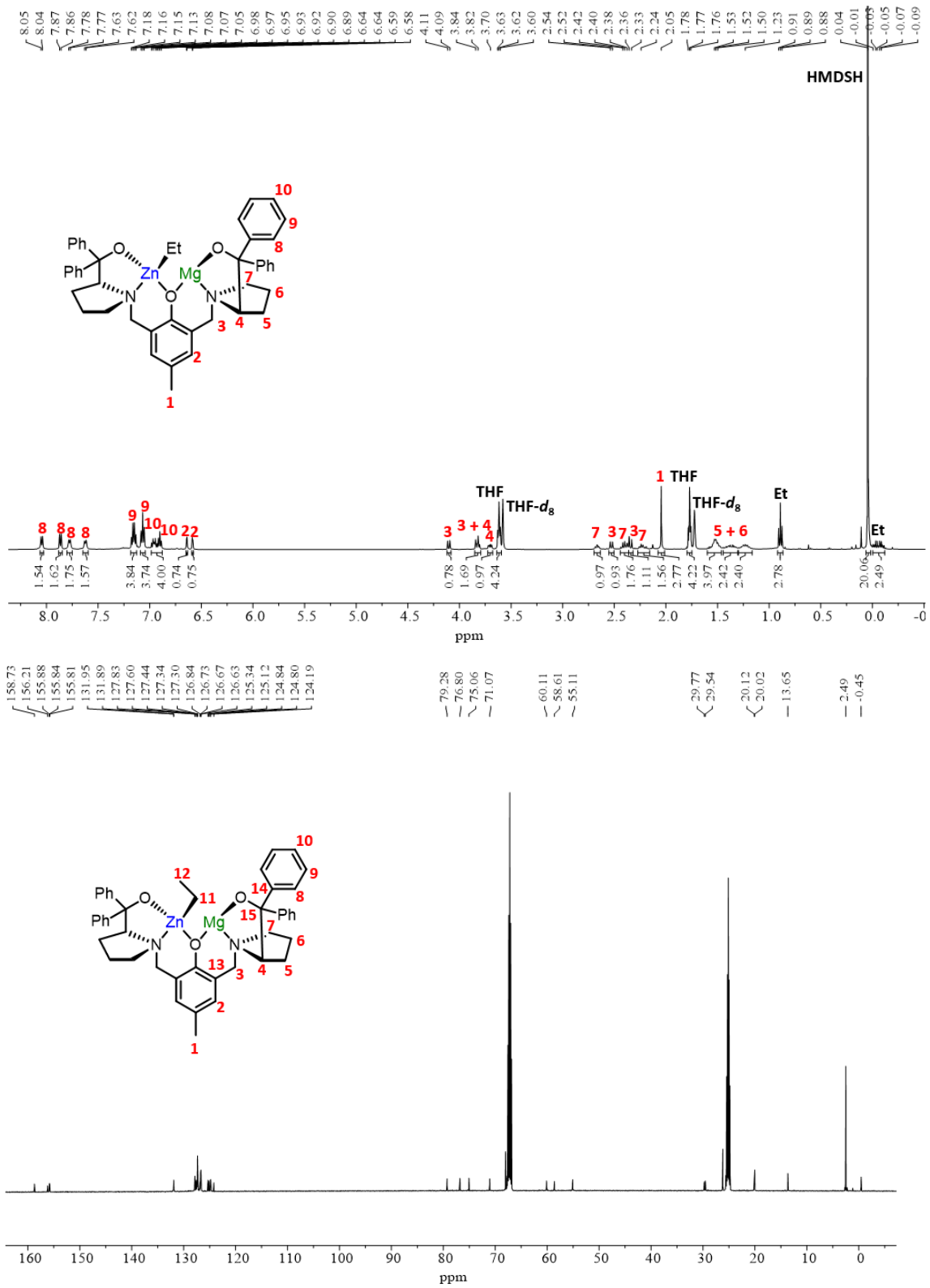

Figure S4. ^{1}H and ^{13}C NMR spectra of complex **1** in THF-d_8 (298 K). For clarity, THF and HMDSH are not shown in the chemical structure as the ^{1}H NMR chemical shifts and DOSY analysis (Fig. S5) suggest these Lewis donors are in coordinative equilibrium with THF-d_8 solvent. For assignment of the ^{13}C NMR spectrum, see above.

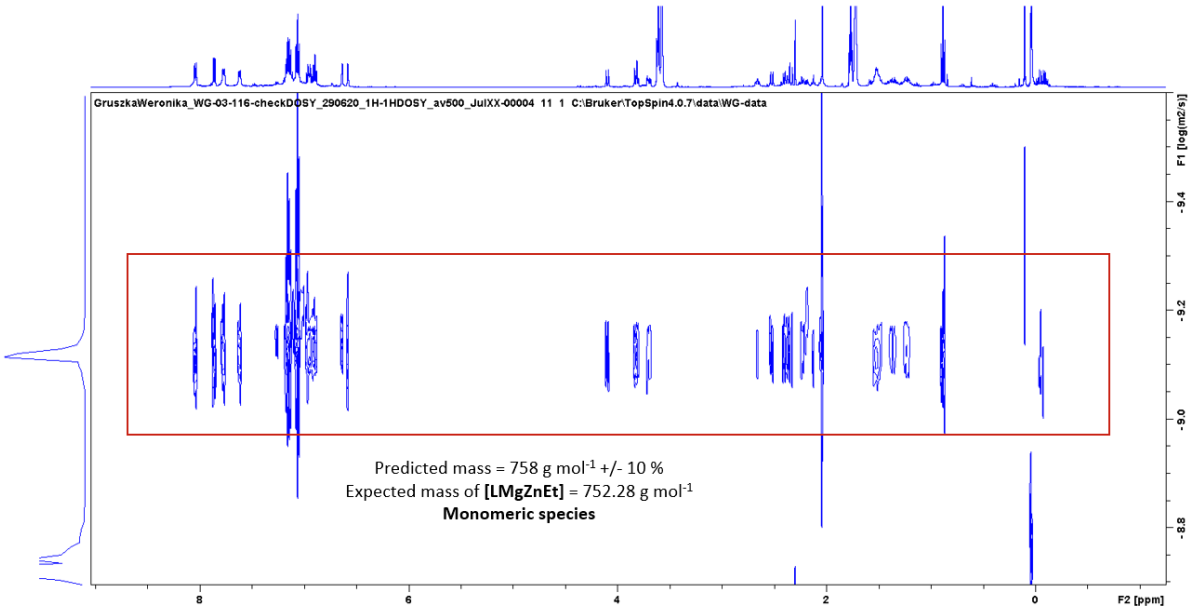

Figure S5. DOSY NMR spectrum of complex **1** in THF-d_8 (298 K).

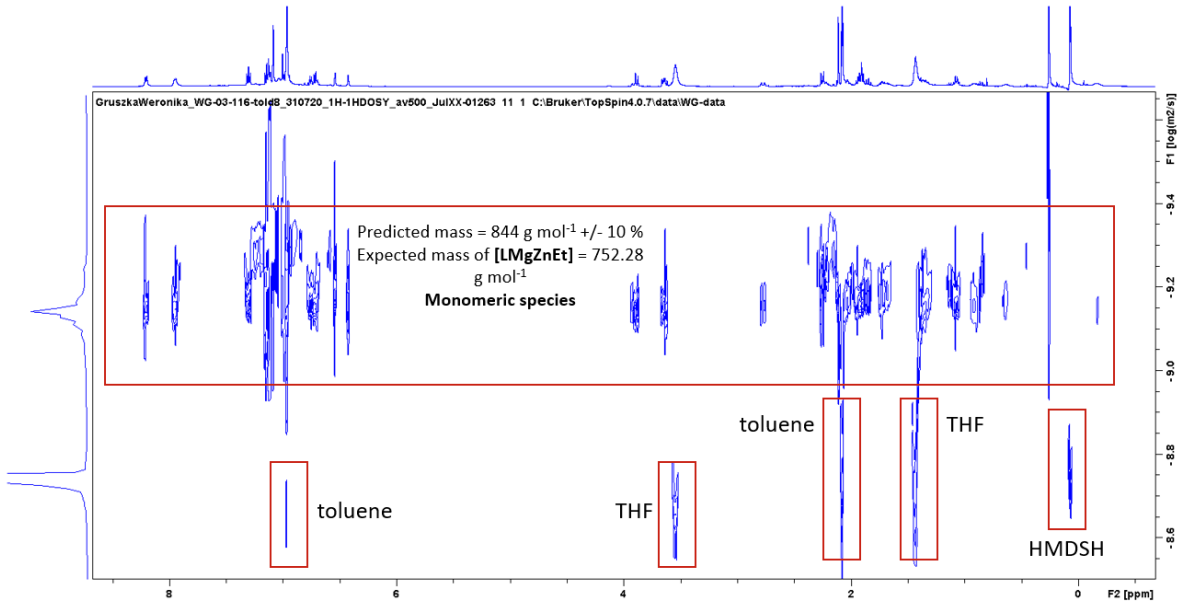

Figure S6. DOSY NMR spectrum of complex **1** in toluene-d_8 (298 K).

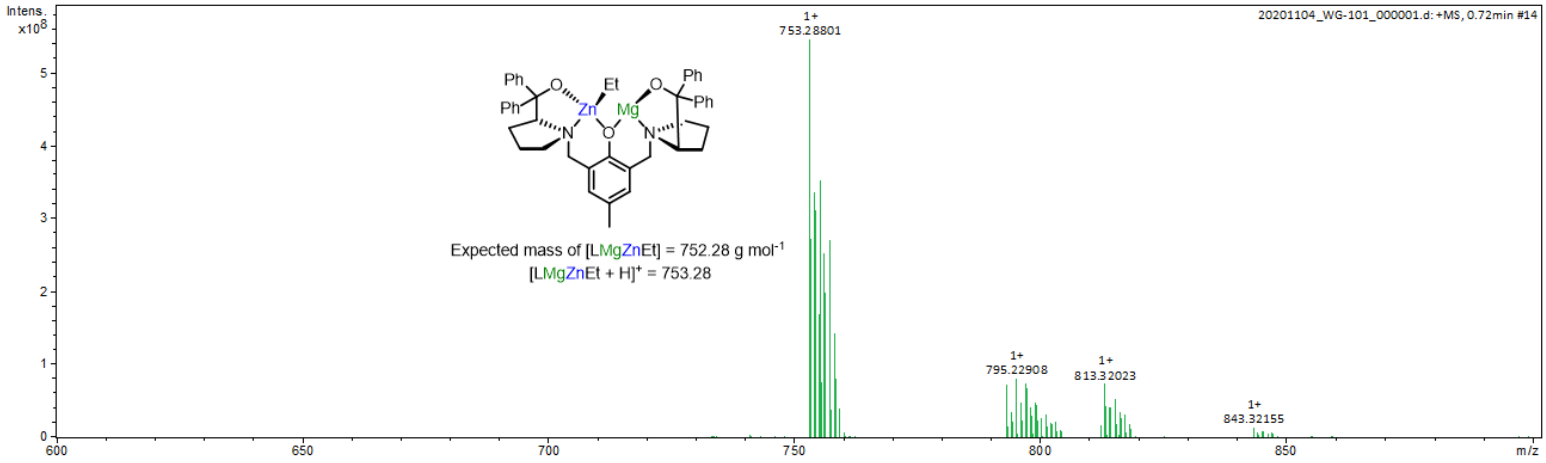

Figure S7. APPI-MS spectrum of complex **1**.

Figure S8. ^{1}H and ^{13}C NMR spectra of complex **2** in THF-d_8 (298 K). For clarity, THF and HMDSH are not shown in the chemical structure as the ^{1}H chemical shifts and DOSY analysis (Fig. S9) suggest these Lewis donors are in coordinative equilibrium with THF-d_8 solvent. For assignment of the ^{13}C NMR spectrum, see above.

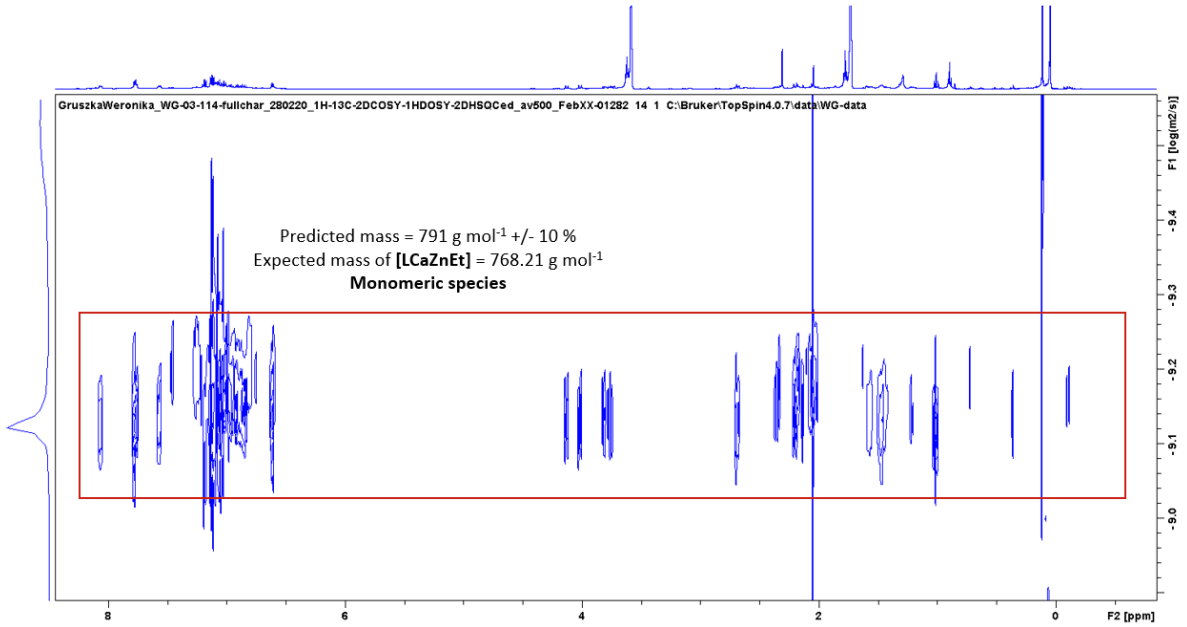

Figure S9. DOSY NMR spectrum of complex **2** in THF-d_8 (298 K).

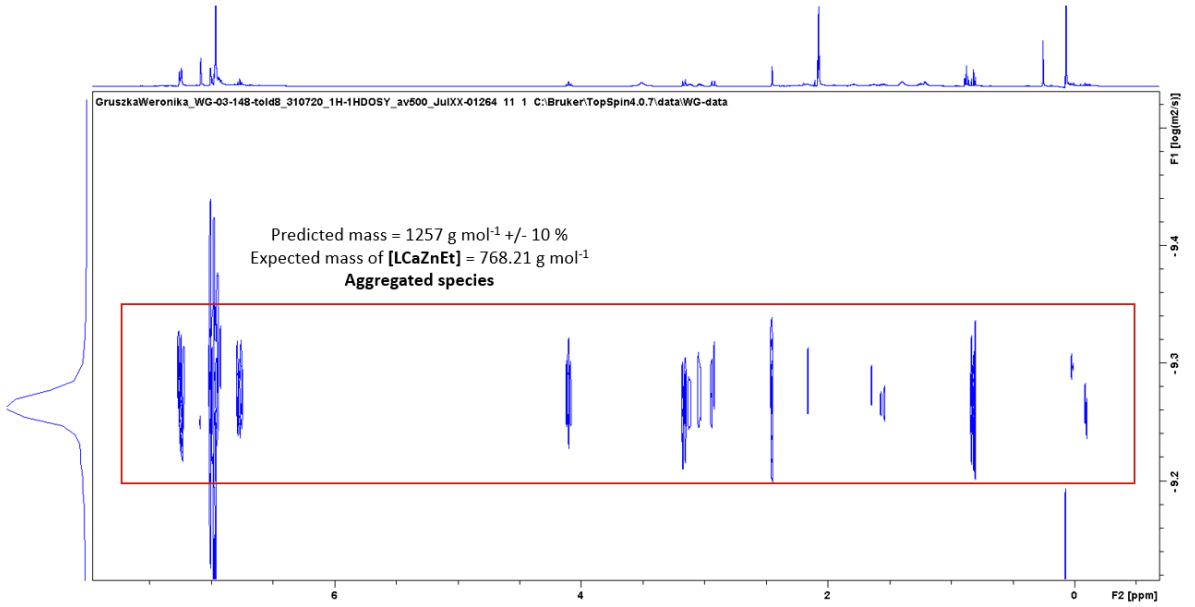

Figure S10. DOSY NMR spectrum of complex **2** in toluene-d_8 (298 K).

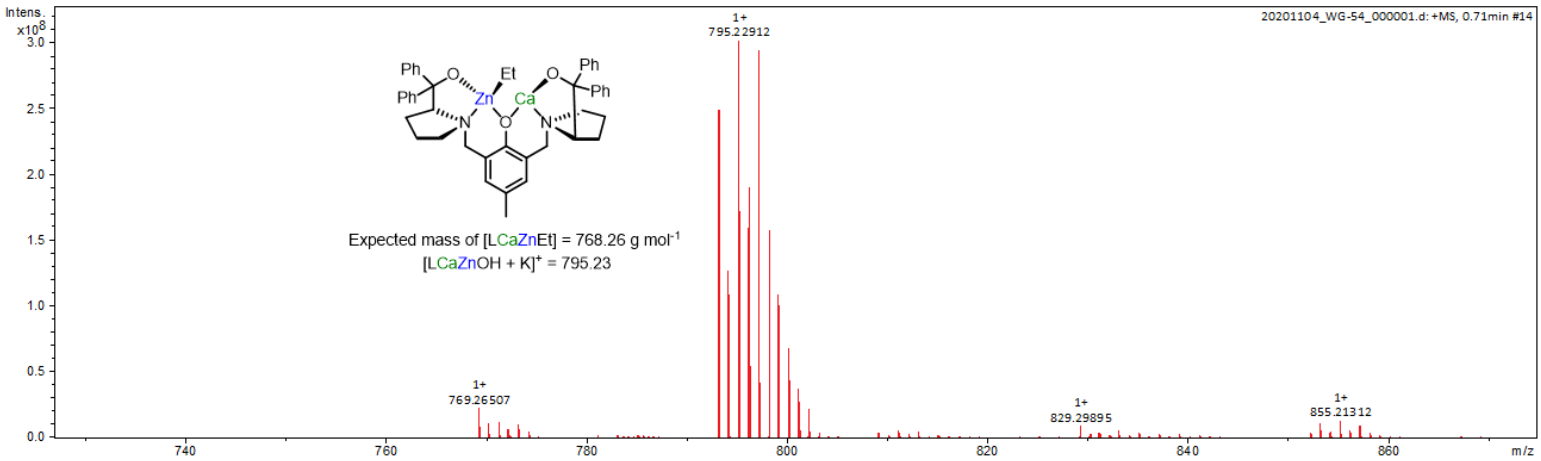

Figure S11. APPI-MS spectrum of complex **2**. Decomposition of complex **2** to [LCaZnOH + K^+] was attributed to performing the APPI-MS measurement under non-strictly air-/moisture-sensitive conditions.

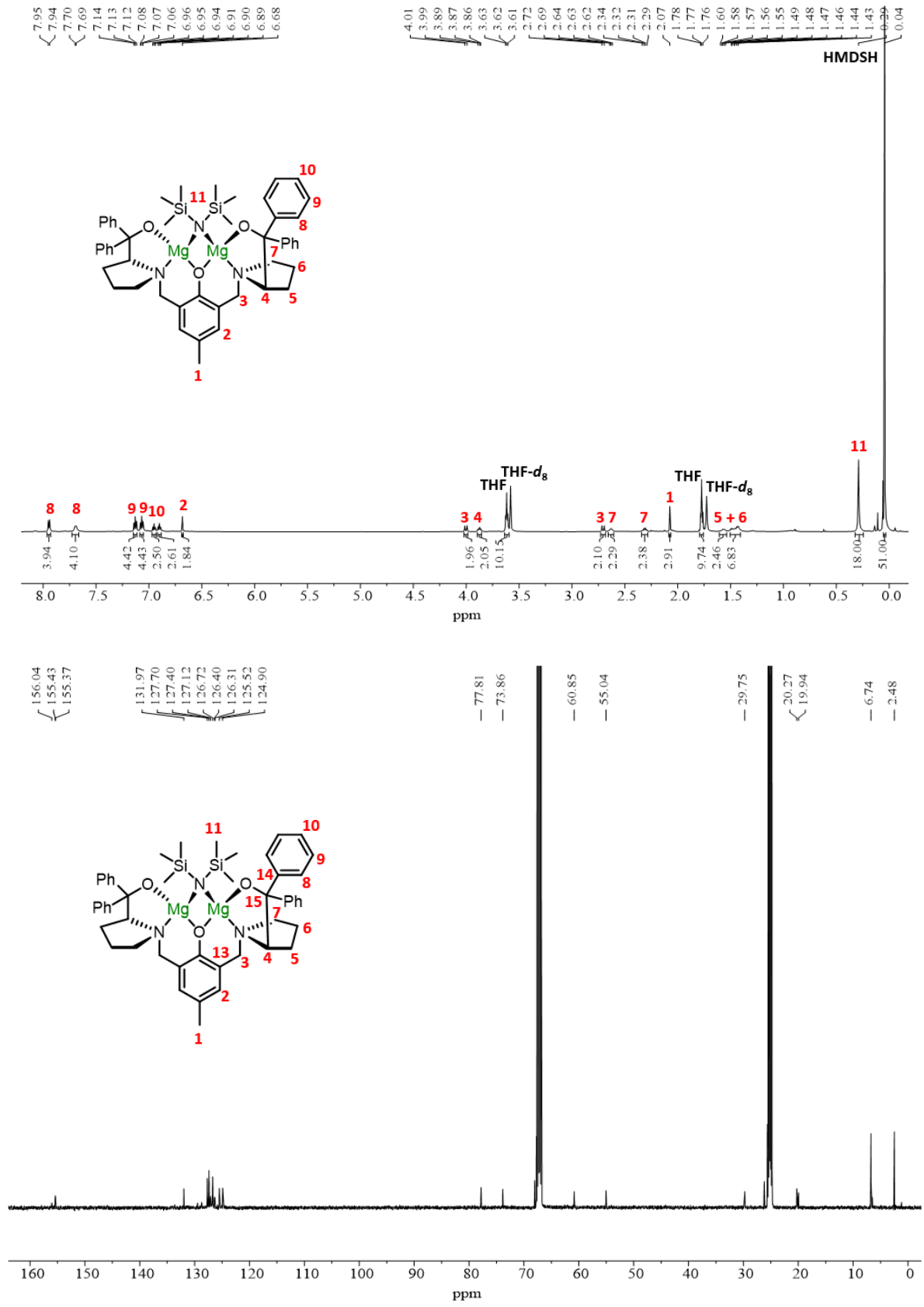

Figure S12. ^{1}H and ^{13}C NMR spectra of complex **6** in THF-d_8 (298 K). For assignment of the ^{13}C NMR spectrum, see above.

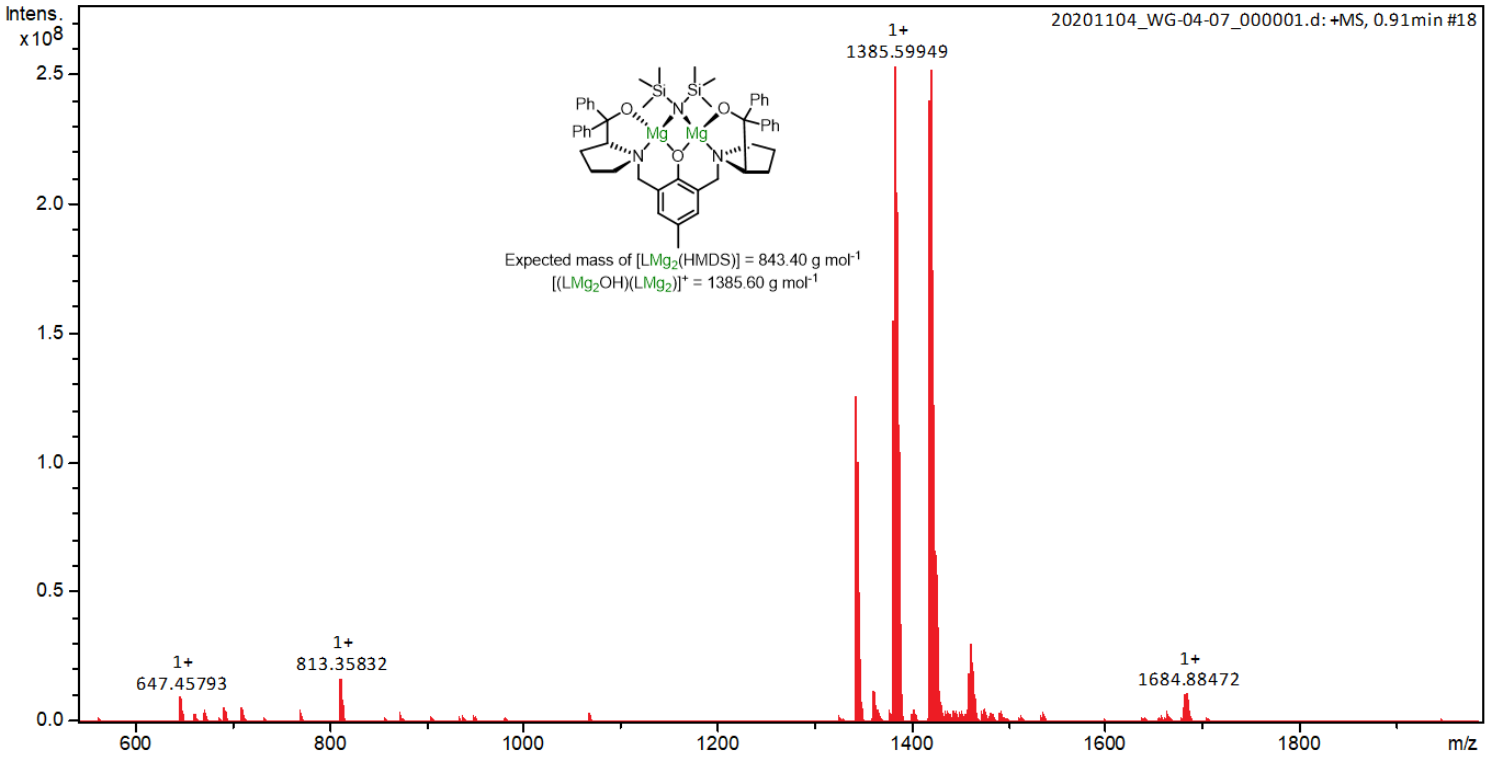

Figure S13. APPI-MS spectrum of complex **6**. Decomposition of complex **6** to $[(LMg_2OH)(LMg_2)]^+$ was attributed to performing the APPI-MS measurement under non-strictly air-/moisture-sensitive conditions.

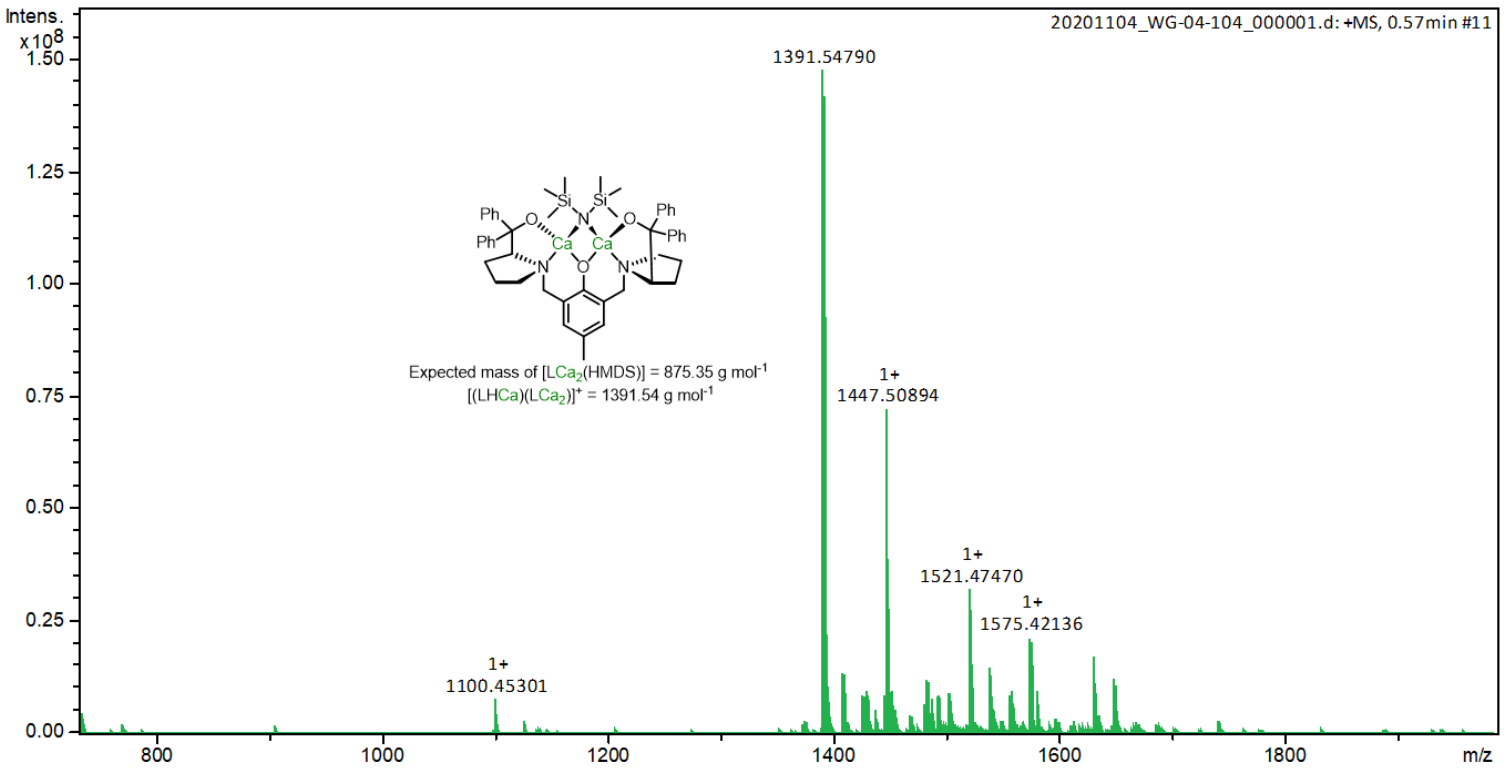

Figure S14. APPI-MS spectrum of complex **7**. Decomposition of complex **7** to $[(LHCa)(LCa_2)]^+$ was attributed to performing the APPI-MS measurement under non-strictly air-/moisture-sensitive conditions.

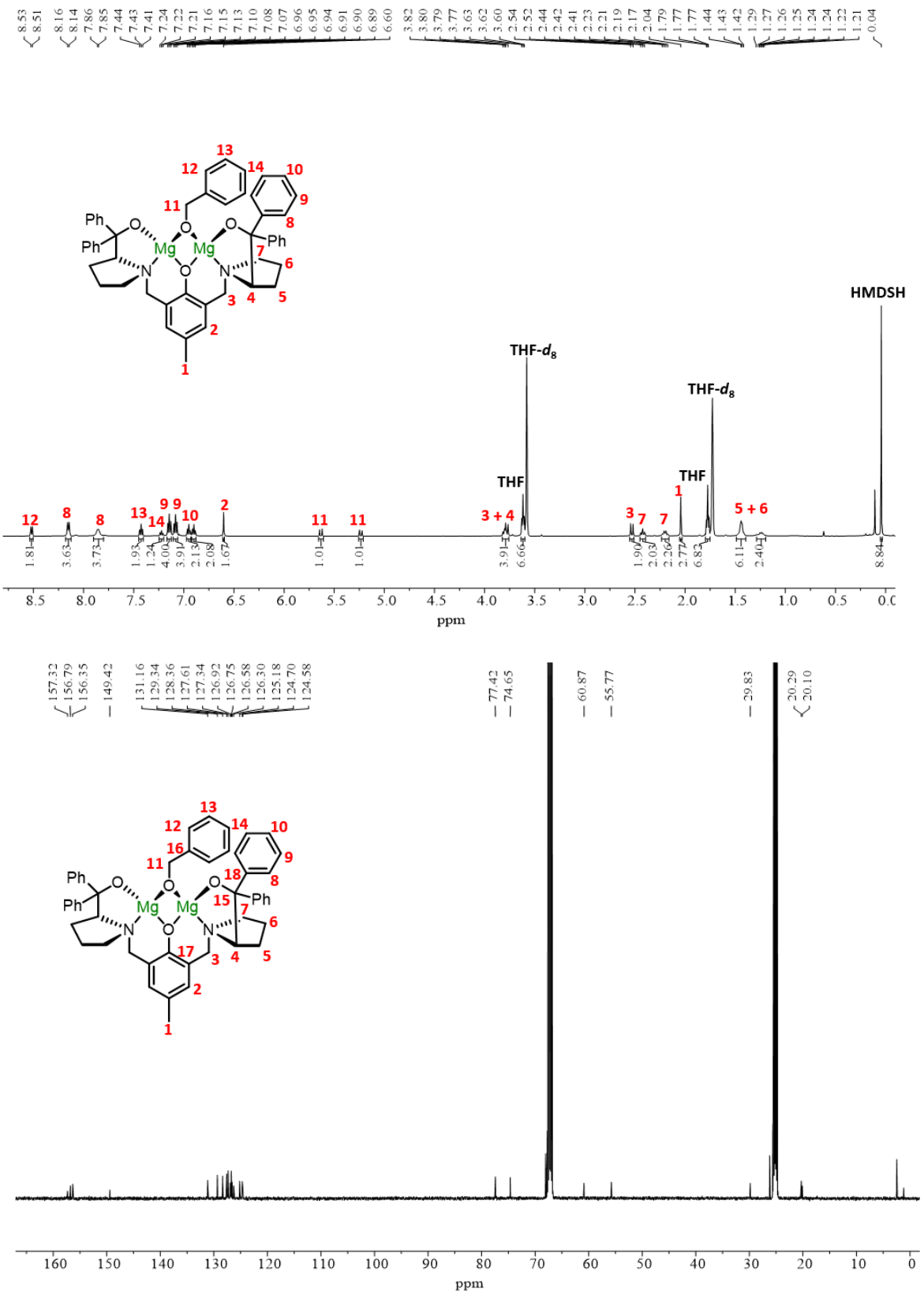

Figure S15. ^{1}H and ^{13}C NMR spectra of complex **11** in THF-d_8 (298 K). For assignment of the ^{13}C NMR spectrum, see above.

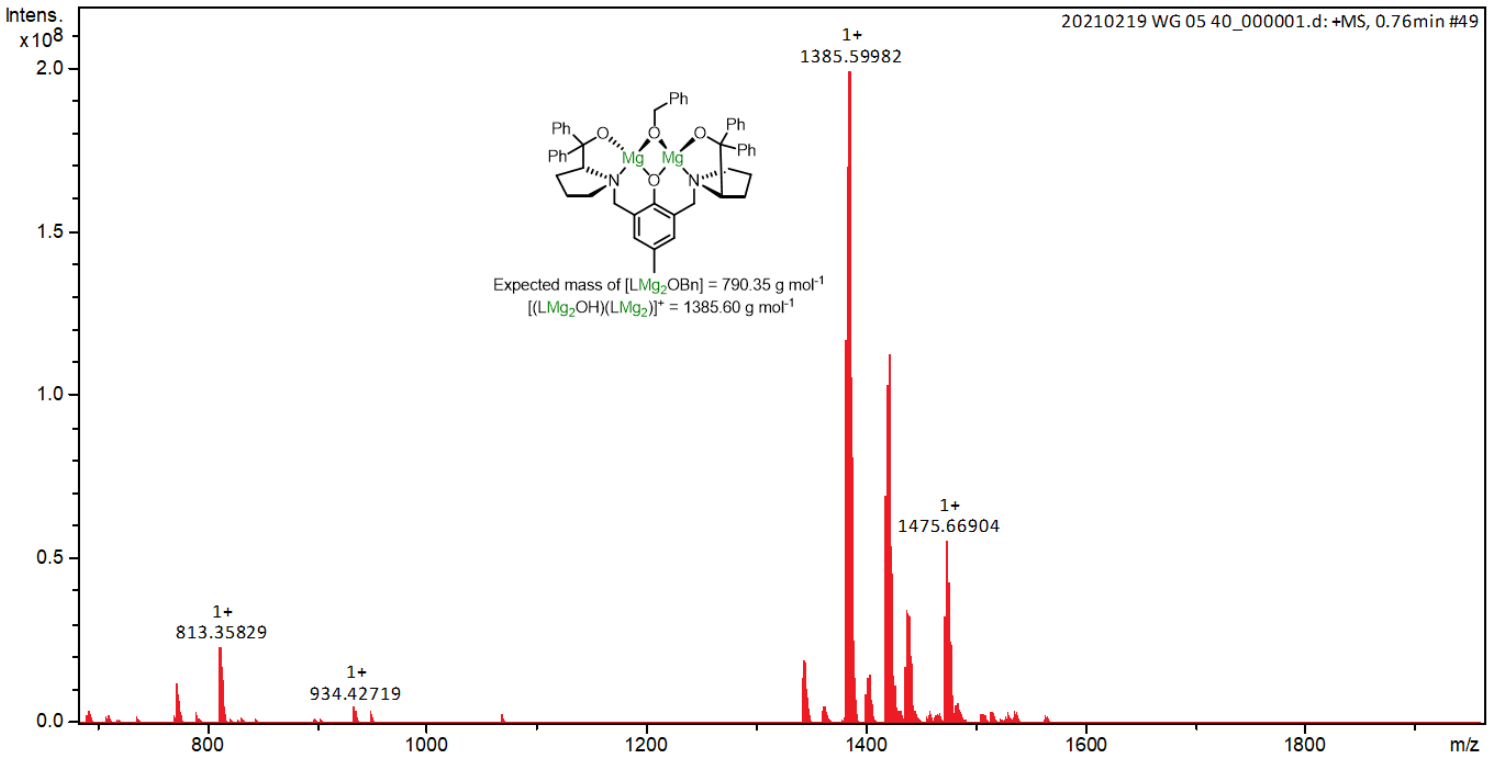

Figure S16. APPI-MS spectrum of complex **11**. Decomposition of complex **11** to $[(LMg_2OH)(LMg_2)]^+$ was attributed to performing the APPI-MS measurement under non-strictly air-/moisture-sensitive conditions.

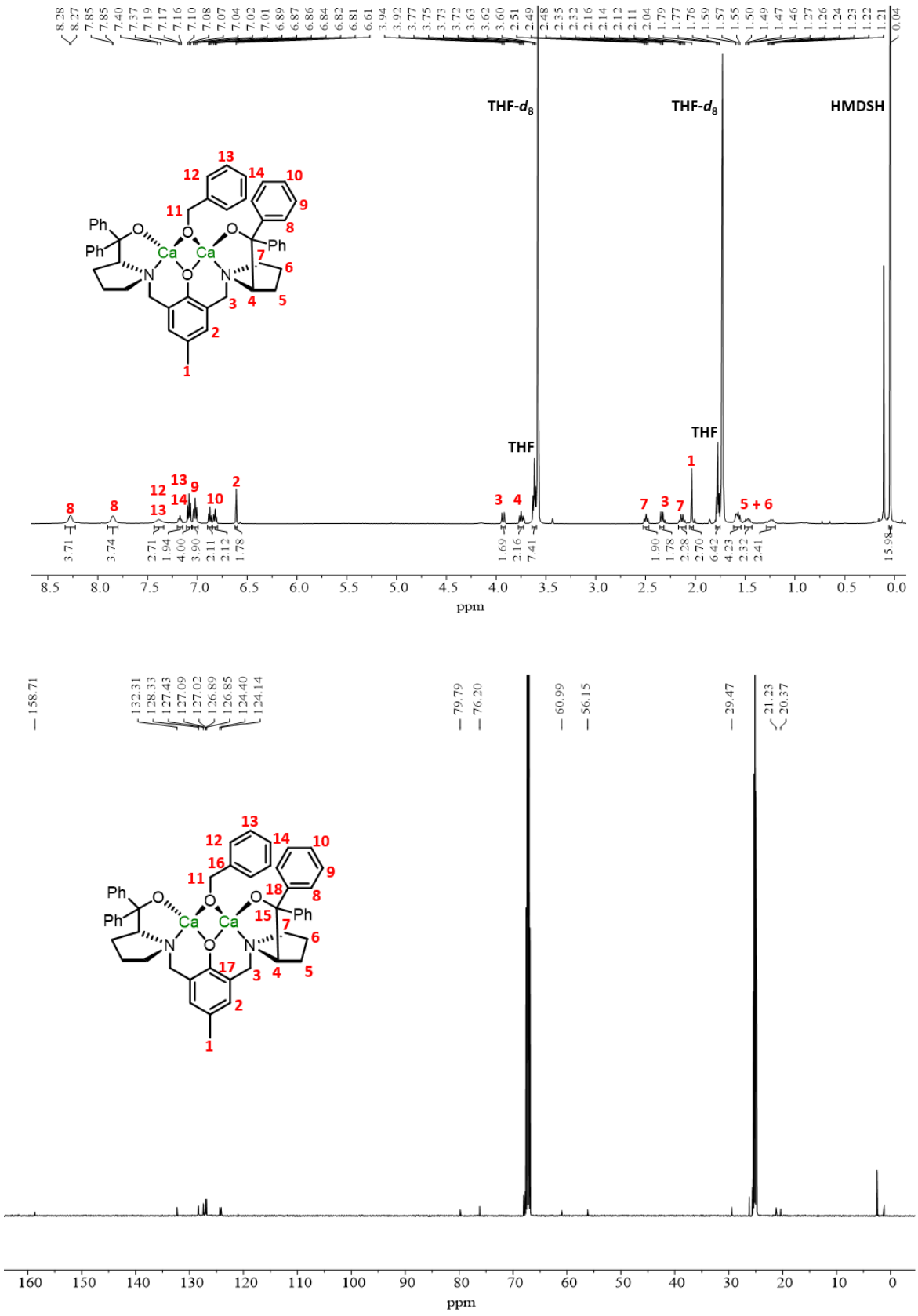

Figure S17. ^{1}H and ^{13}C NMR spectra of complex **12** in THF-d_8 (298 K). For assignment of the ^{13}C NMR spectrum, see above.

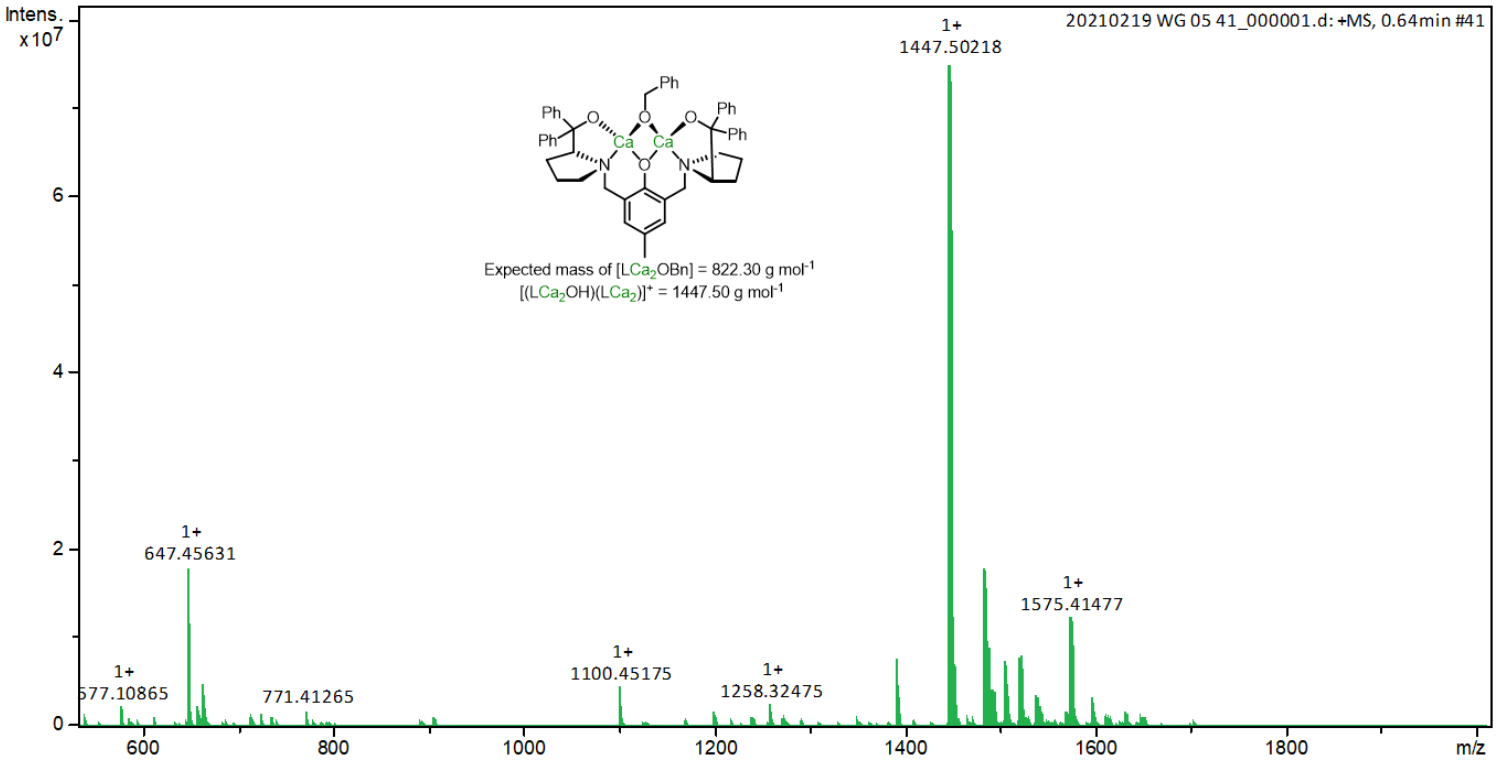

Figure S18. APPI-MS spectrum of complex **12**. Decomposition of complex **12** to $[(LCa_2OH)(LCa_2)]^+$ was attributed to performing the APPI-MS measurement under non-strictly air-/moisture-sensitive conditions.

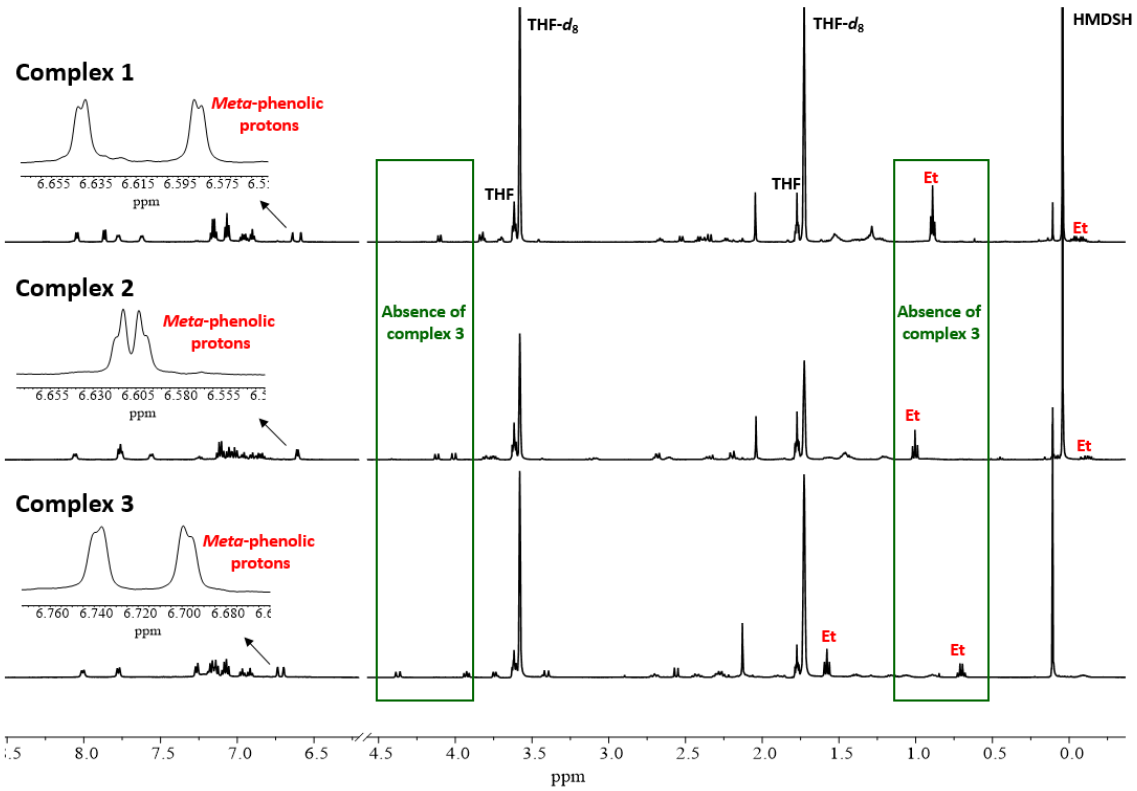

Figure S19. Overlaid ^{1}H NMR spectra of complexes **1**-**3** in THF-d_8.

Table S1. Results for the ROP of *rac*-LA catalysed by heterometallic **1**-**2** and homometallic **6**-**7** in the presence of 1 eq. BnOH in toluene at 60 °C.

Entry	Catalyst	Time (min)	Conv.[a] (%)	$M_{n,obs}$[b] (g mol^{-1})	$M_{n,calc}$[c] (g mol^{-1})	$Đ$[b]	P_i[d]
1	**1**	0.67	26	1200	3700	1.13	-
2	**1**	2.5	36	3300	5200	1.12	0.6
3	**1**	4	46	3400	6600	1.14	0.56
4	**1**	5	53	4300	7600	1.13	0.5
5	**1**	7.5	69	4700	9900	1.22	-
6	**1**	10	84	5600	12100	1.13	0.54
7	**2**	0.08	32	1300	4600	1.19	-
8	**2**	0.33	39	2300	5600	1.16	0.64
9	**2**	0.67	46	2400	6600	1.27	0.5
10	**2**	1	70	3200	10100	1.26	0.51
11	**2**	1.25	82	4700	11800	1.26	0.46
12	**6**	1.25	25	2000	3600	1.16	-
13	**6**	2.5	34	2200	4900	1.19	-
14	**6**	5	46	2600	6600	1.12	0.45
15	**6**	10	66	4600	9500	1.21	0.43
16	**6**	20	87	8100	12500	1.15	0.49
17	**7**	0.08	39	2000	5600	2.01	0.54
18	**7**	0.33	49	1900	7000	1.78	-
19	**7**	0.67	56	3500	8000	1.42	0.49
20	**7**	1.25	64	4800	9200	1.51	-
21	**7**	2.5	75	4100	10800	1.27	-
22	**7**	5	93	5700	13400	1.58	0.47

100 eq. *rac*-LA, [LA] = 1 M in toluene. LA and pre-catalyst pre-stirred separately for 3 min in toluene at 60 °C before mixing and initiation with BnOH. [a] Conversion calculated using ^{1}H NMR spectroscopy.[b] $M_{n,obs}$ and $Đ$ determined by SEC using polystyrene standards in THF. Values corrected by Mark-Houwink factor (0.58).[10] [c] $M_{n,calc}$ of polymers calculated from the monomer conversion $M_{n,calc}$ = M_0 x ([M]/[I]) x conversion assuming 1 chain per catalyst. [d] Determined by homodecoupled ^{1}H NMR spectroscopy.

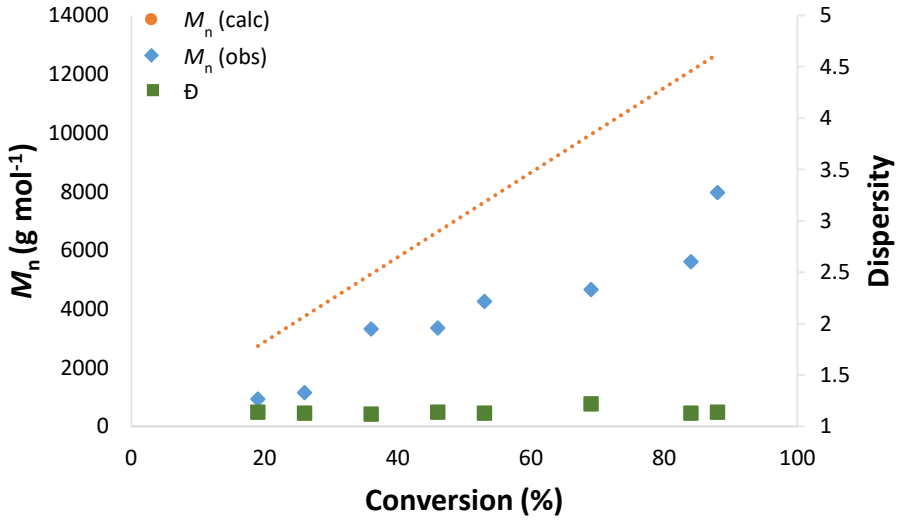

Figure S20. Comparison between experimental and calculated M_n values and dispersity values at increasing conversions of *rac*-LA in presence of complex **1** + 1 eq. BnOH in toluene at 60 °C.

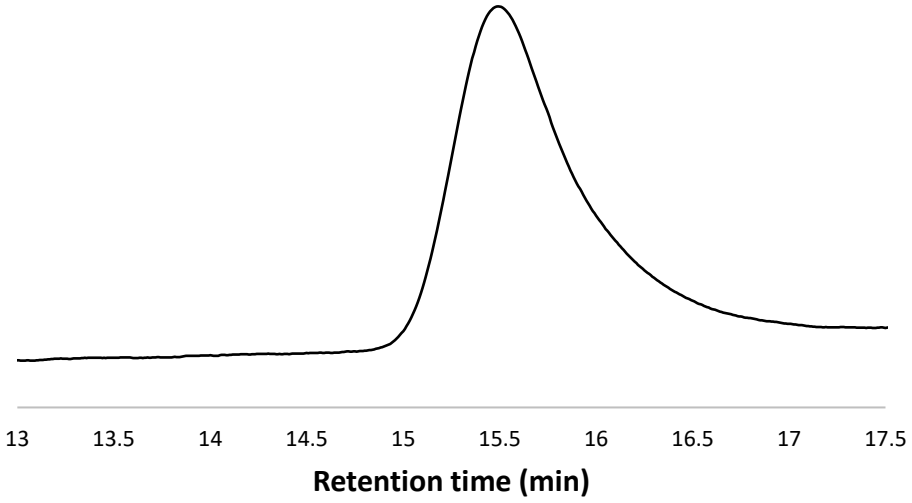

Figure S21. Example SEC trace of PLA generated in the presence of complex **1** + 1 eq. BnOH in toluene at 60 °C (Entry 5, Table S1).

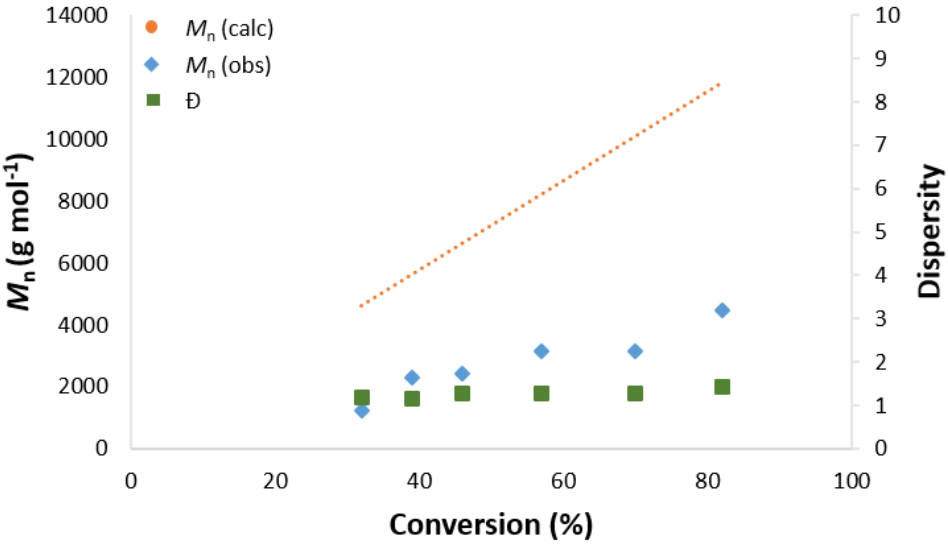

Figure S22. Comparison between experimental and calculated M_n values and dispersity values at increasing conversions of *rac*-LA in presence of complex **2** + 1 eq. BnOH in toluene at 60 °C.

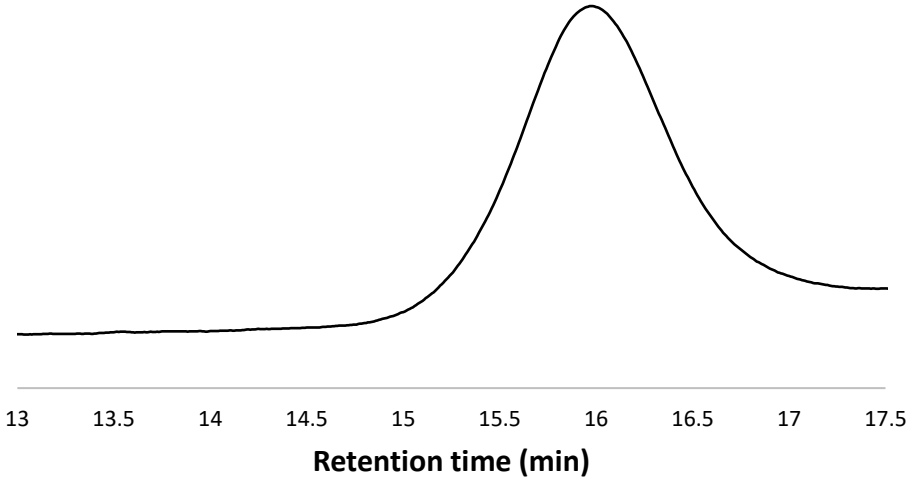

Figure S23. Example SEC trace of PLA generated in the presence of complex **2** + 1 eq. BnOH in toluene at 60 °C (Entry 10, Table S1).

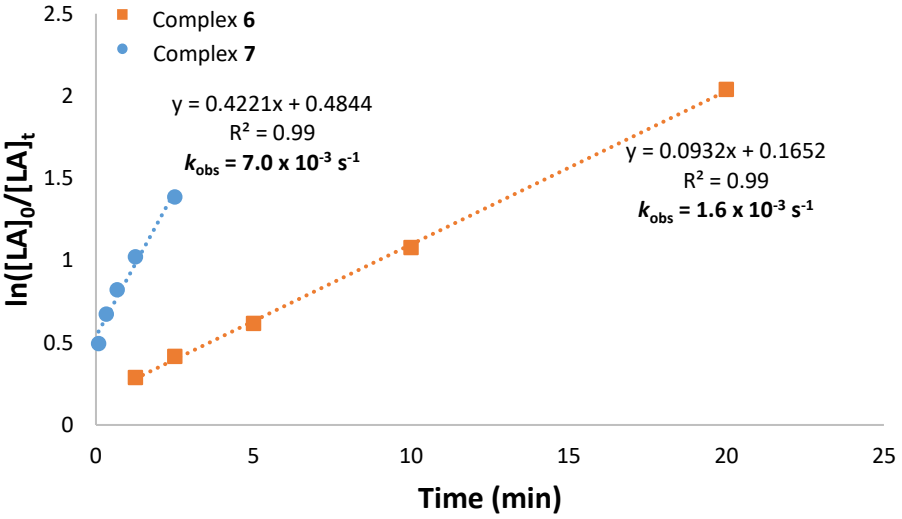

Figure S24. Plot of ln([*rac*-LA]$_0$/[*rac*-LA]$_t$) *vs*. time (min) for *rac*-LA ROP with **6** and **7** in the presence of 1 eq. BnOH (100 eq. *rac*-LA, [*rac*-LA] = 1 M, toluene, 60 °C).

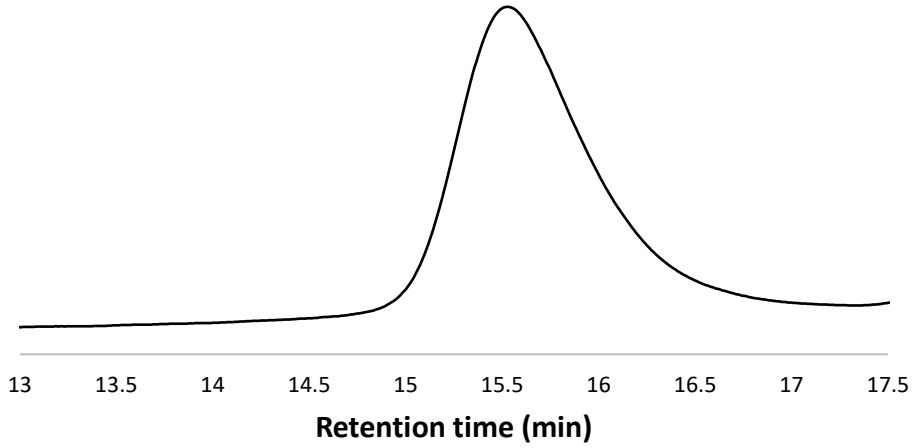

Figure S25. Example SEC trace of PLA generated in the presence of complex **6** + 1 eq. BnOH in toluene at 60 °C (Entry 15, Table S1).

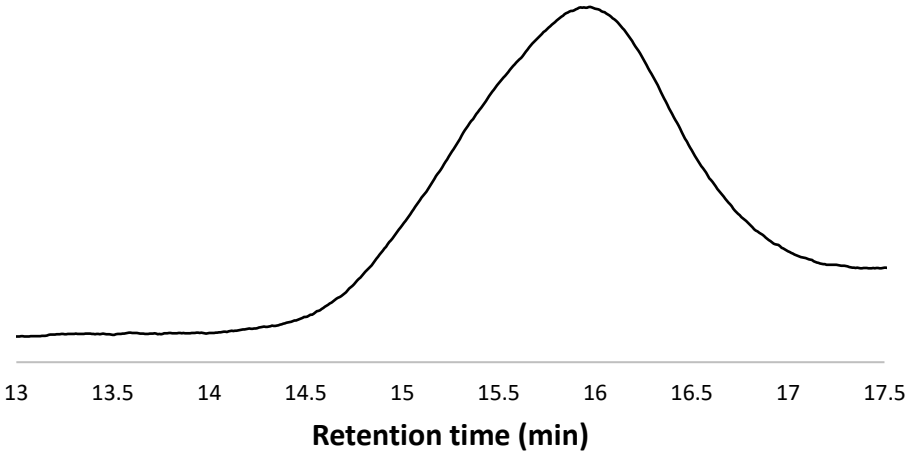

Figure S26. Example SEC trace of PLA generated in the presence of complex **7** + 1 eq. BnOH in toluene at 60 °C (Entry 19, Table S1).

Table S2. Results for the ROP of *rac*-LA catalysed by **1**-**2** in the presence of 1 eq. BnOH in THF at 60 °C and R.T.

Entry	Cat.	Temp.	Time (min)	Conv.[a] (%)	$M_{n,obs}$[b] (g mol^{-1})	$M_{n,calc}$[c] (g mol^{-1})	$Đ$[b]	P_i[d]
1	**2**	60 °C	0.08	42	2300	6100	1.34	0.47
2	**2**	60 °C	0.33	58	3200	8400	1.39	-
3	**2**	60 °C	0.67	64	4300	9200	1.5	0.48
4	**2**	60 °C	1.25	80	5800	11500	1.55	0.54
5	**2**	60 °C	2.5	92	6300	13300	1.81	0.49
6	**2**	R.T.	0.08	48	2100	6900	1.3	0.54
7	**2**	R.T.	0.67	53	3800	7600	1.45	-
8	**2**	R.T.	1.25	65	4100	9400	1.45	0.5
9	**2**	R.T.	2.5	80	5100	11500	1.49	0.49
10	**2**	R.T.	4	84	6200	12100	1.66	0.49
11[e]	**2**	R.T.	0.67	54	3300	7800	1.48	0.53
12	**2**	-36 °C	1.25	26	1800	3700	1.32	0.51
13[f]	**2**	R.T.	0.33	40	-	-	-	0.53
14[g]	**2**	60 °C	0.33	44	-	-	-	0.52
15	**1**	60 °C	10	16	-	-	-	-
16	**1**	60 °C	120	54	5300	7800	1.09	0.5

[LA] = 1 M in THF. [a] Conversion calculated using ^{1}H NMR spectroscopy.[b] $M_{n,obs}$ and $Đ$ determined by SEC using polystyrene standards in THF. Values corrected by Mark-Houwink factor (0.58).[10] [c] $M_{n,calc}$ of polymers calculated from the monomer conversion $M_{n,calc}$ = M_0 x ([M]/[I]) x conversion assuming 1 chain per catalyst. [d] Determined by homodecoupled ^{1}H NMR spectroscopy. [e] THF used was pre-chilled to -36 °C. [f] [LA] = 0.5 M in THF. [g] [LA] = 0.5 M in toluene.

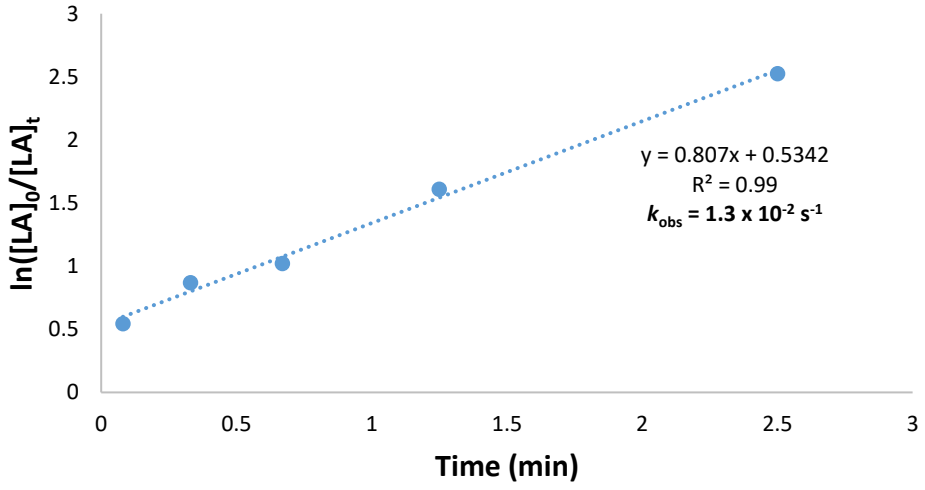

Figure S27. Plot of ln([*rac*-LA]0/[*rac*-LA]$_t$) *vs*. time (min) for *rac*-LA ROP with **2** in the presence of 1 eq. BnOH (100 eq. *rac*-LA, [*rac*-LA] = 1 M, THF, 60 °C).

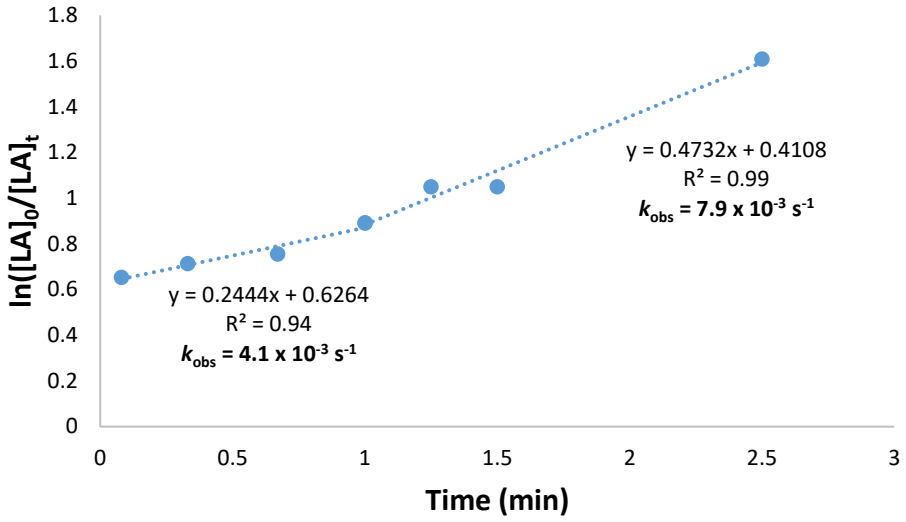

Figure S28. Plot of ln([*rac*-LA]$_0$/[*rac*-LA]$_t$) *vs*. time (min) for *rac*-LA ROP with **2** in the presence of 1 eq. BnOH (100 eq. *rac*-LA, [*rac*-LA] = 1 M, THF, R.T.).

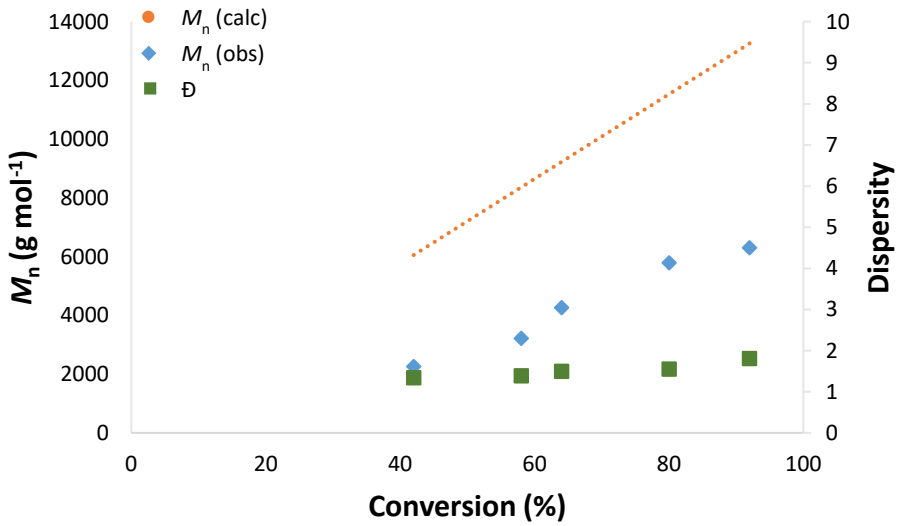

Figure S29. Comparison between experimental and calculated M_n values and dispersity values at increasing conversions of *rac*-LA in presence of complex **2** + 1 eq. BnOH in THF at 60 °C.

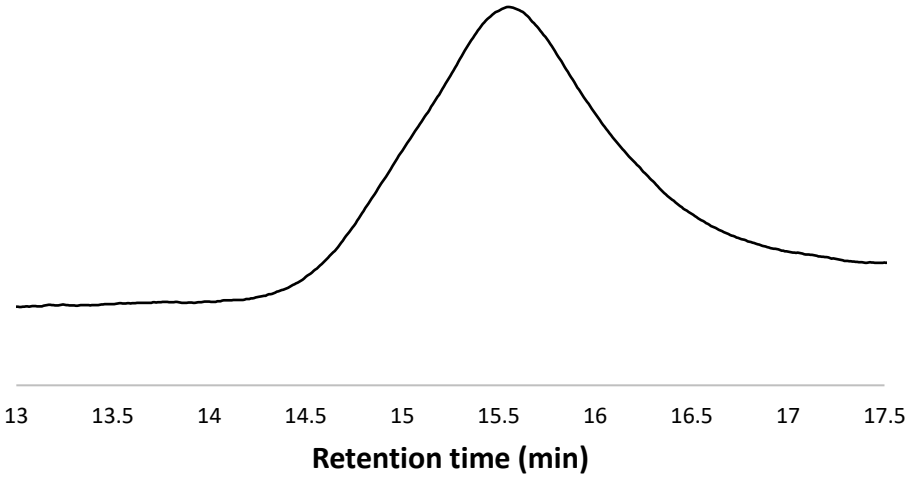

Figure S30. Example SEC trace of PLA generated in the presence of complex **2** + 1 eq. BnOH in THF at 60 °C (Entry 3, Table S2).

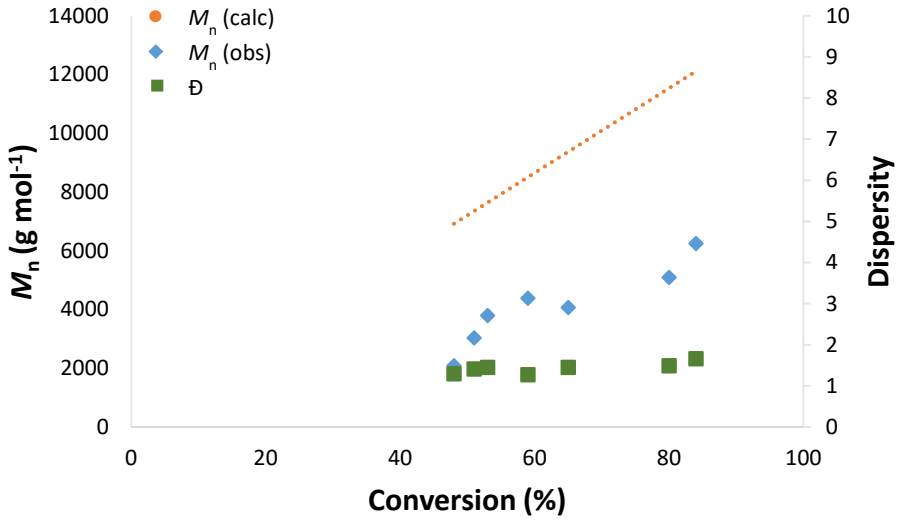

Figure S31. Comparison between experimental and calculated M_n values and dispersity values at increasing conversions of *rac*-LA in presence of complex **2** + 1 eq. BnOH in THF at R.T.

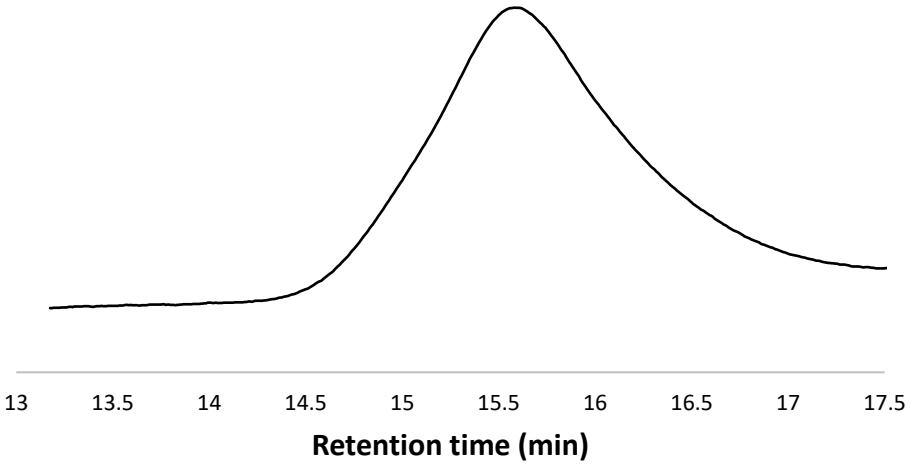

Figure S32. Example SEC trace of PLA generated in the presence of complex **2** + 1 eq. BnOH in THF at R.T. (Entry 8, Table S2).

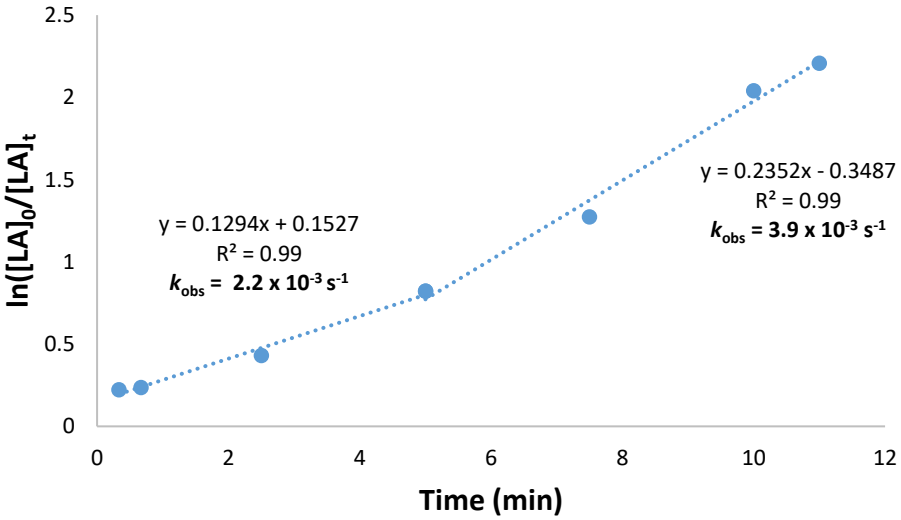

Figure S33. Plot of ln([*rac*-LA]0/[*rac*-LA]$_t$) *vs*. time (min) for *rac*-LA ROP with **3** in the presence of 1 eq. BnOH (100 eq. *rac*-LA, [*rac*-LA] = 1 M, toluene, 60 °C).

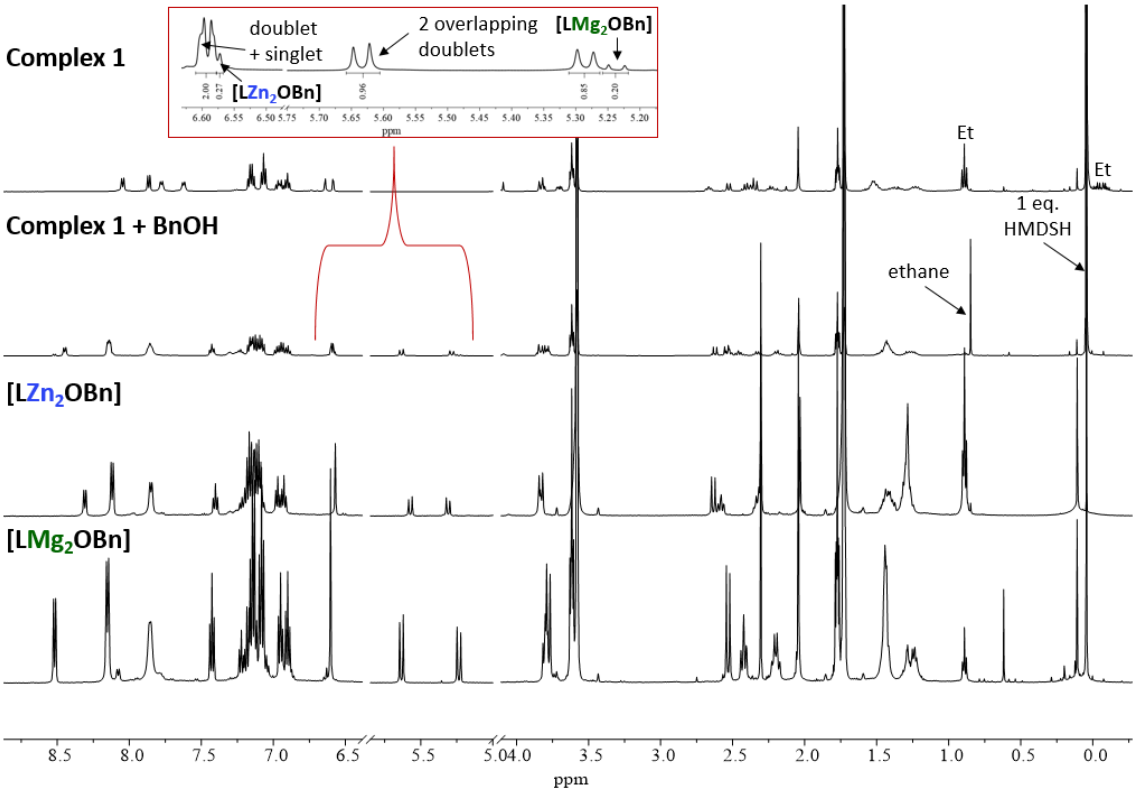

Figure S34. Overlaid ^{1}H NMR spectra (in THF-d_8, R.T.) of complex **1**, product mixture generated upon reaction of **1** with 1 eq. BnOH, **[LZn$_2$OBn]** (**10**) and **[LMg$_2$OBn]** (**11**).

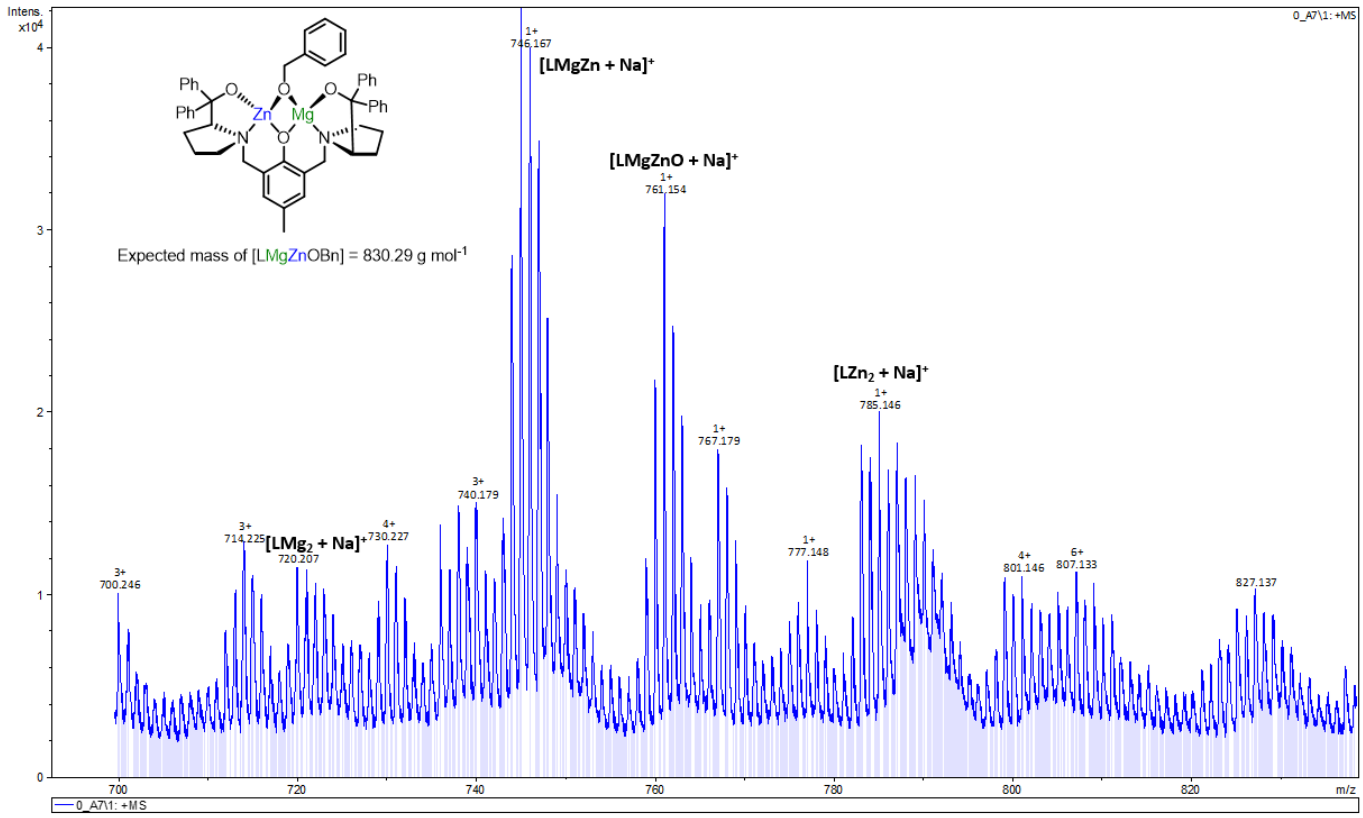

Figure S35. MALDI-ToF spectrum of product mixture generated upon reaction of **1** with 1 eq. BnOH.

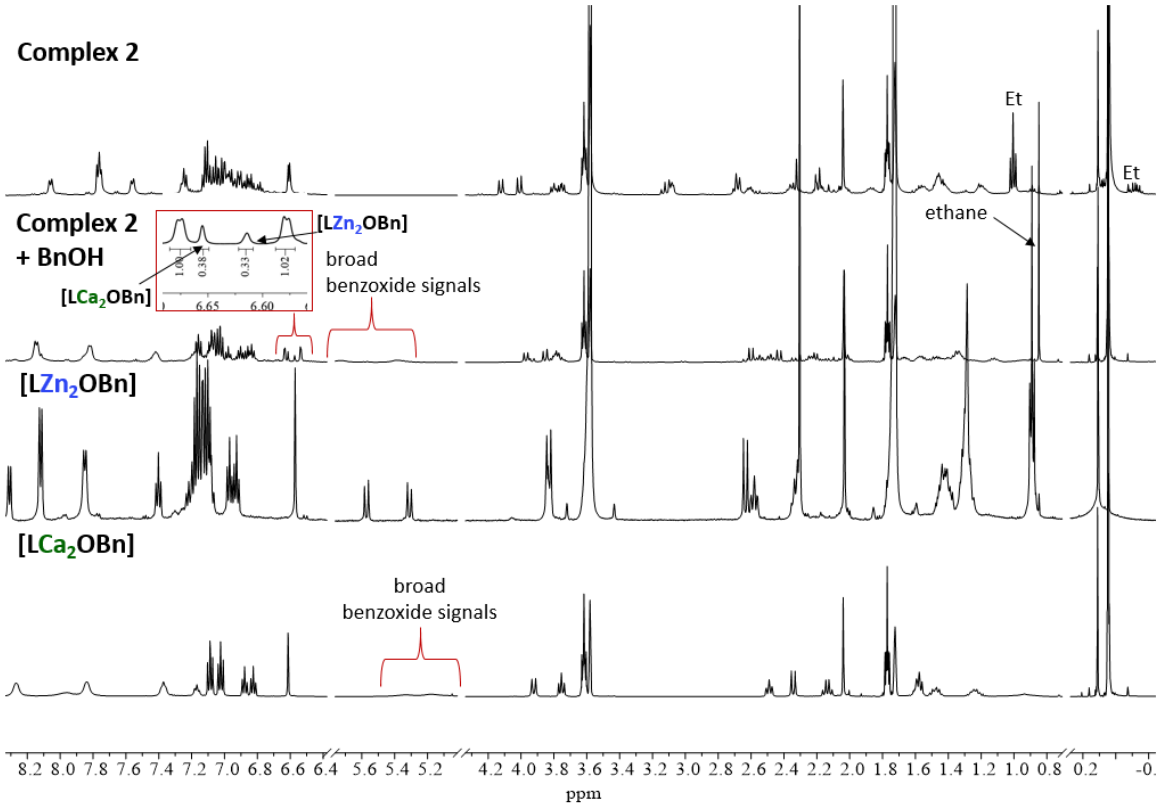

Figure S36. Overlaid ^{1}H NMR spectra (in THF-d_8, R.T.) of complex **2**, product mixture generated upon reaction of **1** with 1 eq. BnOH, **[LZn$_2$OBn]** (**10**) and **[LCa$_2$OBn]** (**12**).

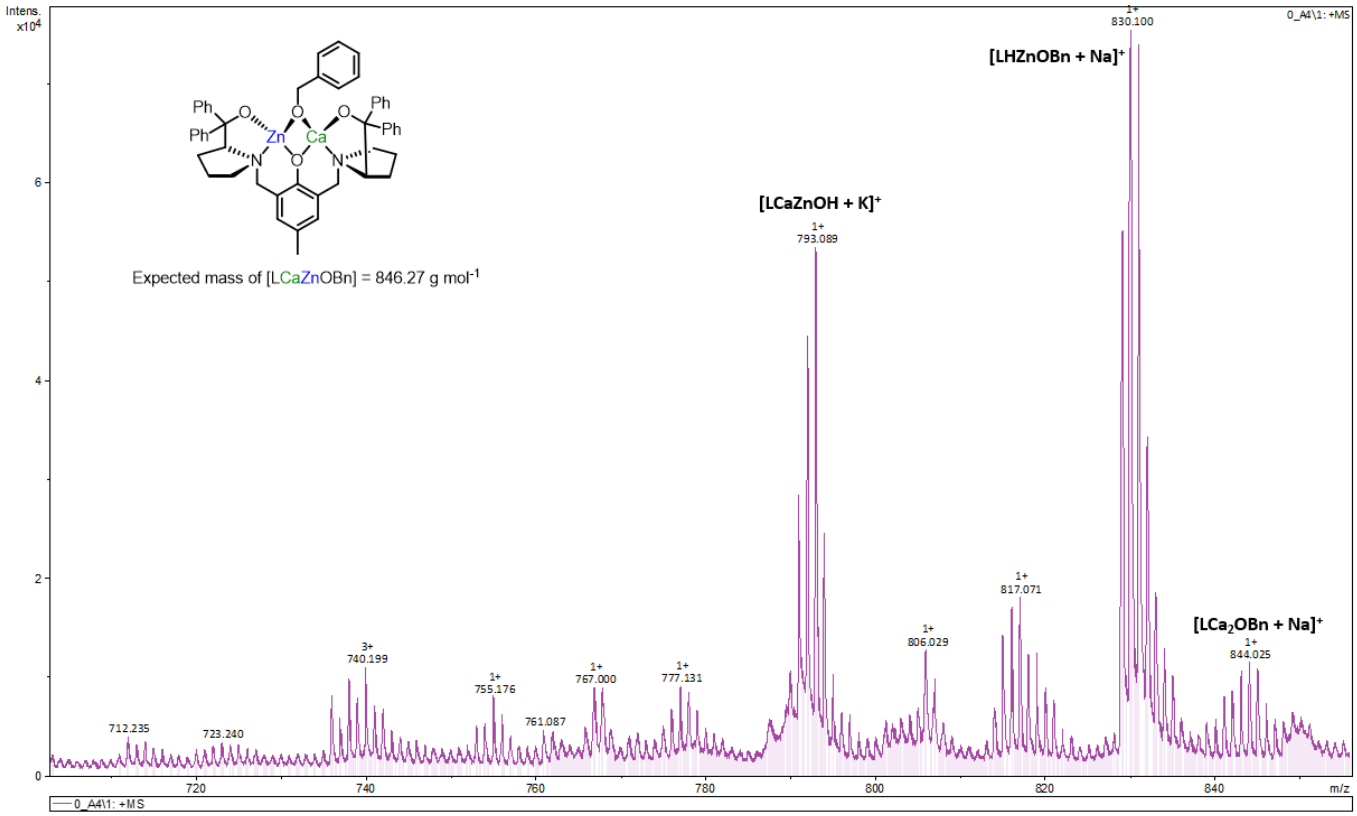

Figure S37. MALDI-ToF spectrum of product mixture generated upon reaction of **2** with 1 eq. BnOH. Decomposition was attributed to performing the MALDI-ToF measurement under non air-/moisture-sensitive conditions.

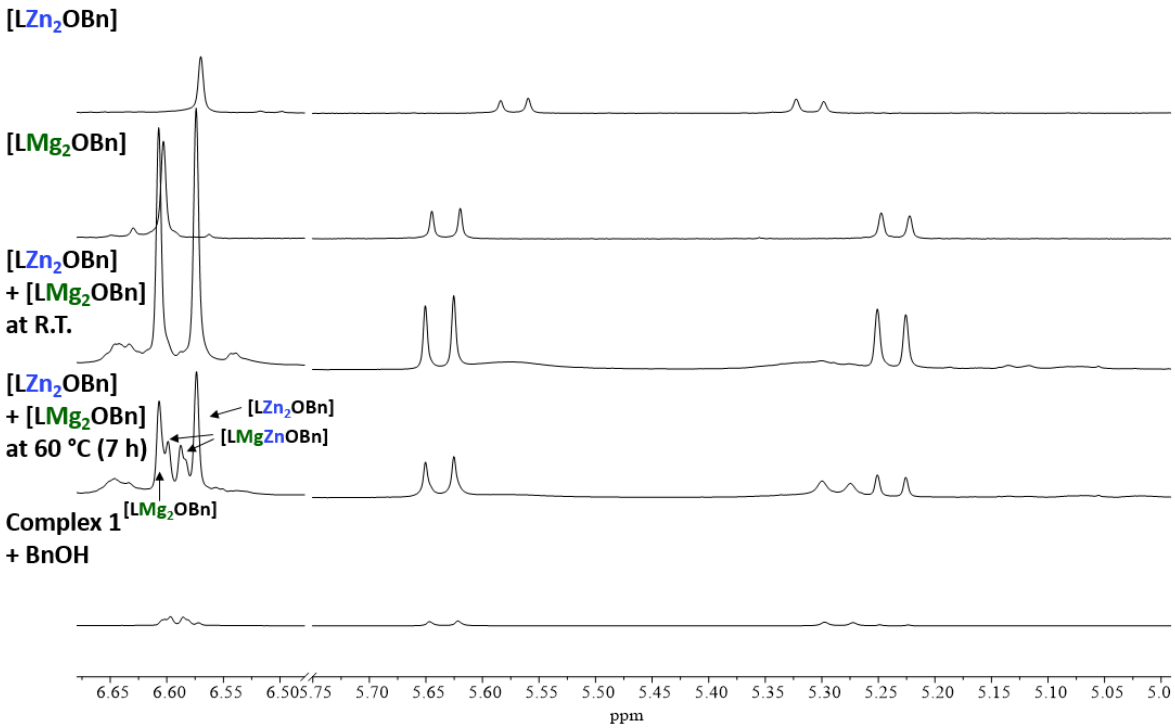

Figure S38. Overlaid ^{1}H NMR region (in THF-d_8), corresponding to the *meta*-phenolic protons on the ligand backbone and the benzylic PhCH_2-O(complex) protons, of **[LZn$_2$OBn]** (**10**), **[LMg$_2$OBn]** (**11**), 1:1 mixture of **10** and **11** at R.T., 1:1 mixture of **10** and **11** after 7 h at 60 °C and product mixture generated upon reaction of **1** with 1 eq. BnOH.

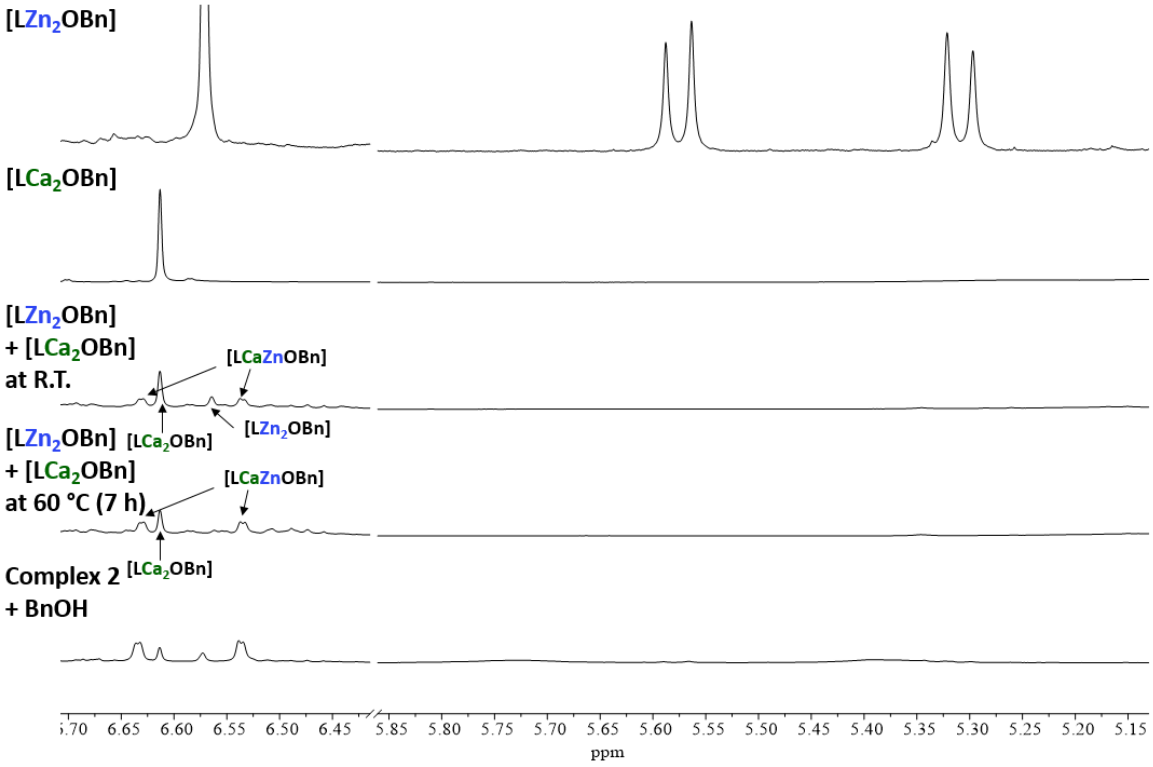

Figure S39. Overlaid ^{1}H NMR region (in THF-d_8), corresponding to the *meta*-phenolic protons on the ligand backbone and the benzylic PhCH_2-O(complex) protons, of **[LZn$_2$OBn]** (**10**), **[LCa$_2$OBn]** (**12**), 1:1 mixture of **10** and **12** at R.T., 1:1 mixture of **10** and **12** after 7 h at 60 °C and product mixture generated upon reaction of **2** with 1 eq. BnOH.

Table S3. ROP of L- and D-LA with **1** in the presence of 1 eq. BnOH in toluene at 60 °C.

Entry	Monomer	Time (min)	Conv.[a] (%)	$M_{n,obs}$[b] (g mol^{-1})	$M_{n,calc}$[c] (g mol^{-1})	$Đ$[b]	P_i[d]
1	L-LA	0.67	25	1500	3600	1.19	0.99
2	L-LA	2.5	30	2800	4300	1.18	0.48
3	L-LA	5	53	4100	7600	1.11	0.56
4	L-LA	7.5	76	5400	11000	1.09	0.47
5	L-LA	10	86	6400	12400	1.07	0.49
6	D-LA	0.67	21	1300	3000	1.21	0.99
7	D-LA	2.5	31	2300	4500	1.17	0.99
8	D-LA	5	41	5100	5900	1.16	0.99
9	D-LA	10	64	4900	9200	1.15	0.70
10	D-LA	12.5	72	5100	10400	1.09	0.76

100 eq. LA; [LA] = 1 M in toluene. LA and pre-catalyst pre-stirred separately for 3 min in toluene at 60 °C before mixing and initiation with BnOH. [a] Conversion calculated using ^{1}H NMR spectroscopy.[b] $M_{n,obs}$ and $Đ$ determined by SEC using polystyrene standards in THF. Values corrected by Mark-Houwink factor (0.58).[10] [c] $M_{n,calc}$ of polymers calculated from the monomer conversion $M_{n,calc}$ = M_0 x ([M]/[I]) x conversion assuming 1 chain per catalyst. [d] Determined by homodecoupled ^{1}H NMR spectroscopy.

Table S4. ROP of L- and D-LA with **2** in the presence of 1 eq. BnOH in toluene at 60 °C.

Entry	Monomer	Time (min)	Conv.[a] (%)	$M_{n,obs}$[b] (g mol^{-1})	$M_{n,calc}$[c] (g mol^{-1})	$Đ$[b]	P_i[d]
1	L-LA	0.08	30	1800	4300	1.21	0.99
2	L-LA	0.33	35	3600	5000	1.18	0.99
3	L-LA	0.5	65	5000	9400	1.15	0.99
4	L-LA	0.58	79	7500	11400	1.43	-
5	L-LA	0.67	91	7200	13100	1.37	-
6	D-LA	0.08	28	1700	4000	1.23	0.99
7	D-LA	0.33	35	3100	5000	1.42	-
8	D-LA	0.67	60	7400	8600	1.3	0.99
9	D-LA	1.08	77	8700	11100	1.2	0.99
10	D-LA	1.25	81	8300	11700	1.21	0.99

100 eq. LA; [LA] = 1 M in toluene. LA and pre-catalyst pre-stirred separately for 3 min in toluene at 60 °C before mixing and initiation with BnOH. [a] Conversion calculated using ^{1}H NMR spectroscopy.[b] $M_{n,obs}$ and $Đ$ determined by SEC using polystyrene standards in THF. Values corrected by Mark-Houwink factor (0.58).[10] [c] $M_{n,calc}$ of polymers calculated from the monomer conversion $M_{n,calc}$ = M_0 x ([M]/[I]) x conversion assuming 1 chain per catalyst. [d] Determined by homodecoupled ^{1}H NMR spectroscopy.

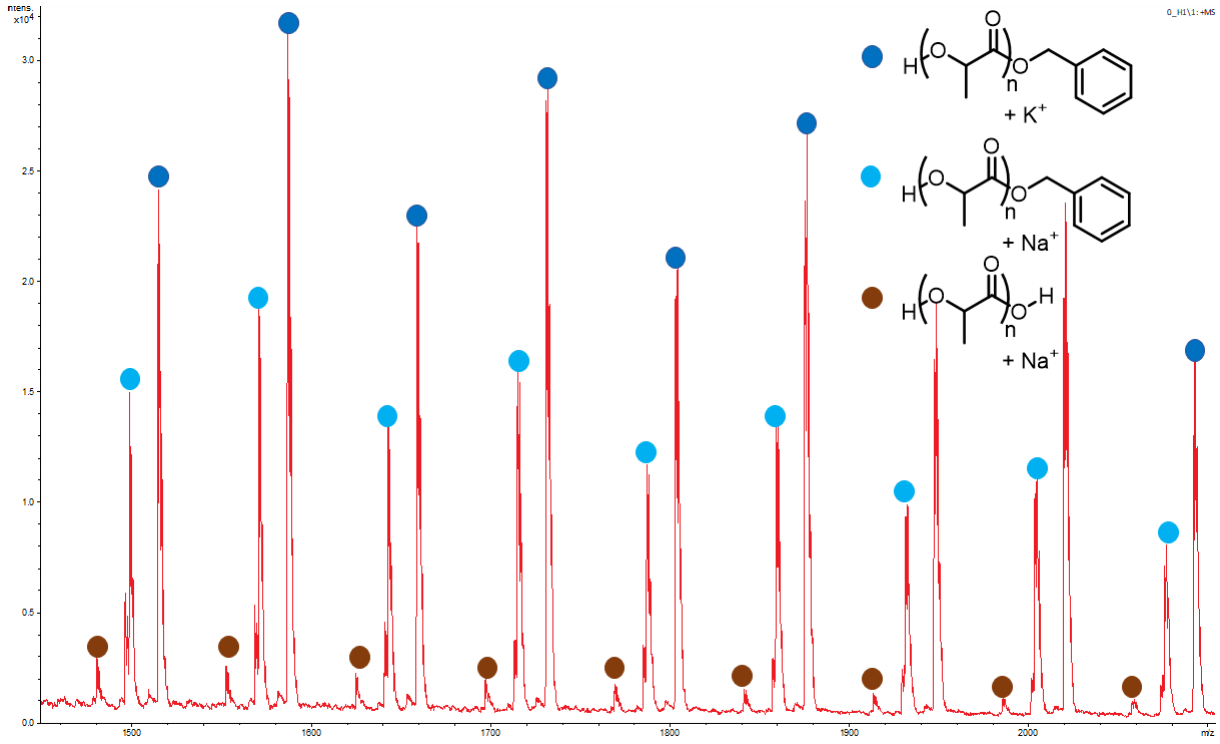

Figure S40. MALDI-ToF spectrum of PLA resulting from 26% conversion of *rac*-LA in the presence of complex **1** + 1 eq. BnOH (toluene, 60 °C).

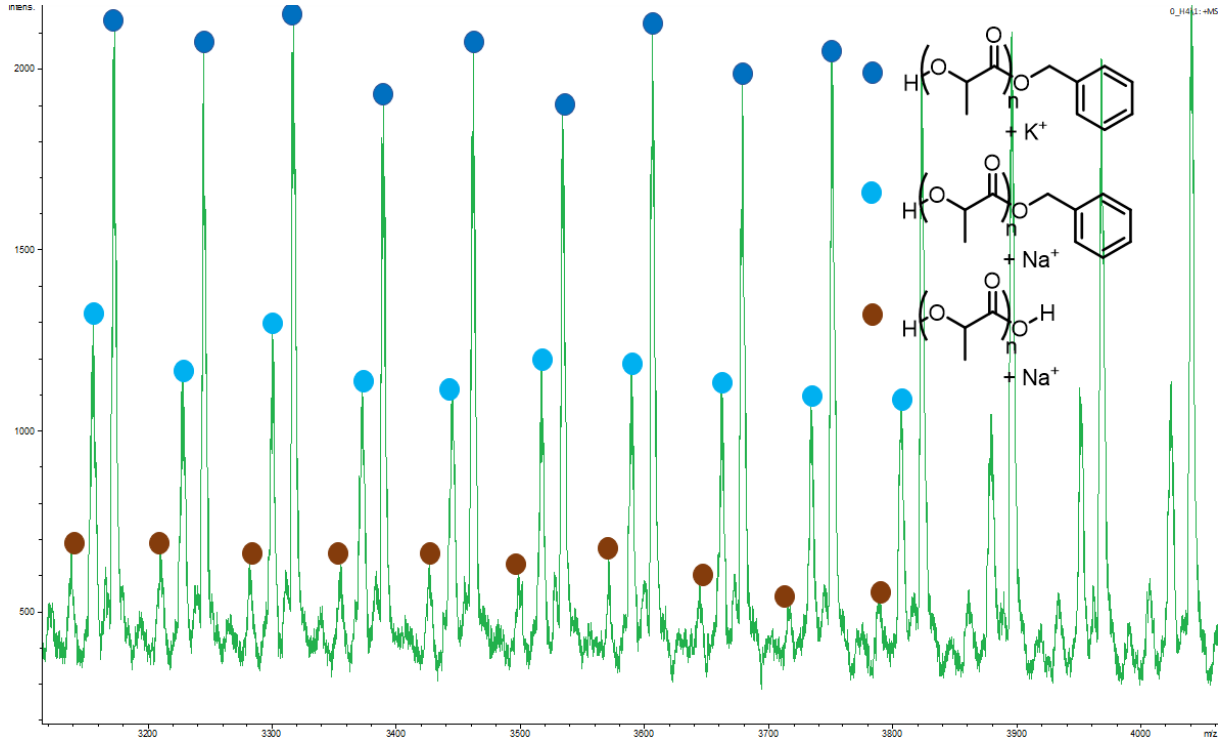

Figure S41. MALDI-ToF spectrum of PLA resulting from 53% conversion of *rac*-LA in the presence of complex **1** + 1 eq. BnOH (toluene, 60 °C).

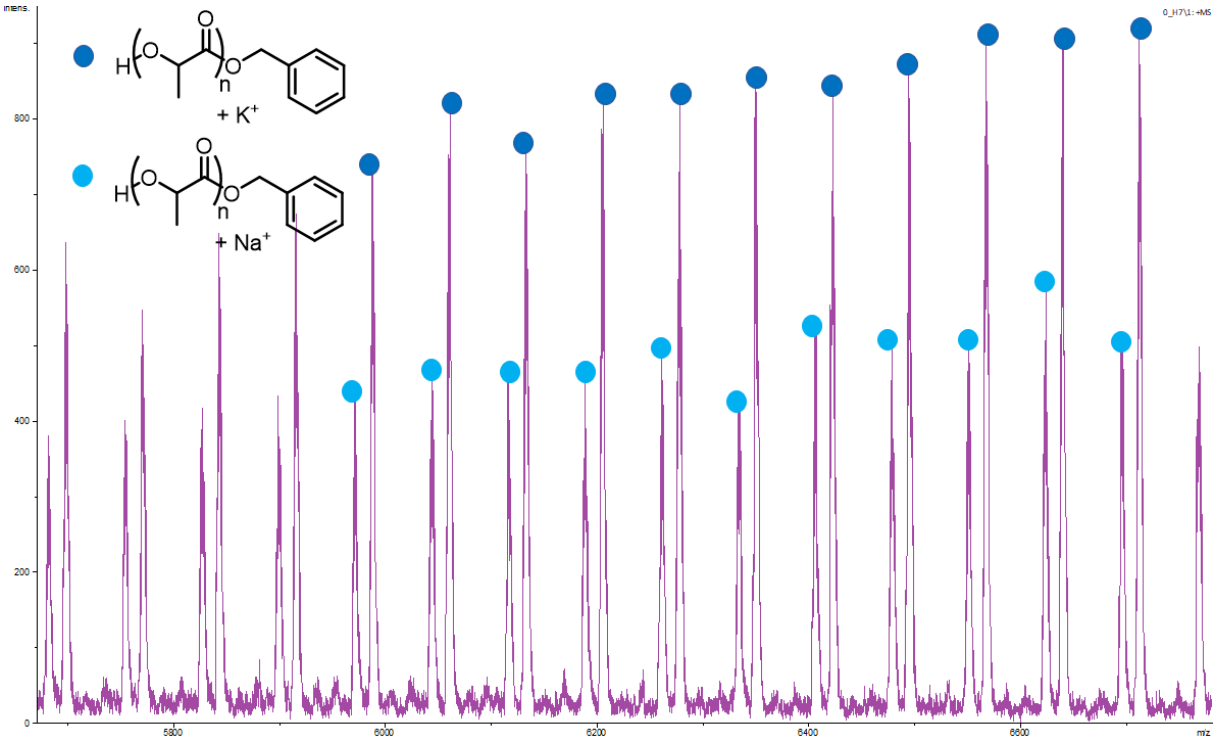

Figure S42. MALDI-ToF spectrum of PLA resulting from 91% conversion of *rac*-LA in the presence of complex **1** + 1 eq. BnOH (toluene, 60 °C).

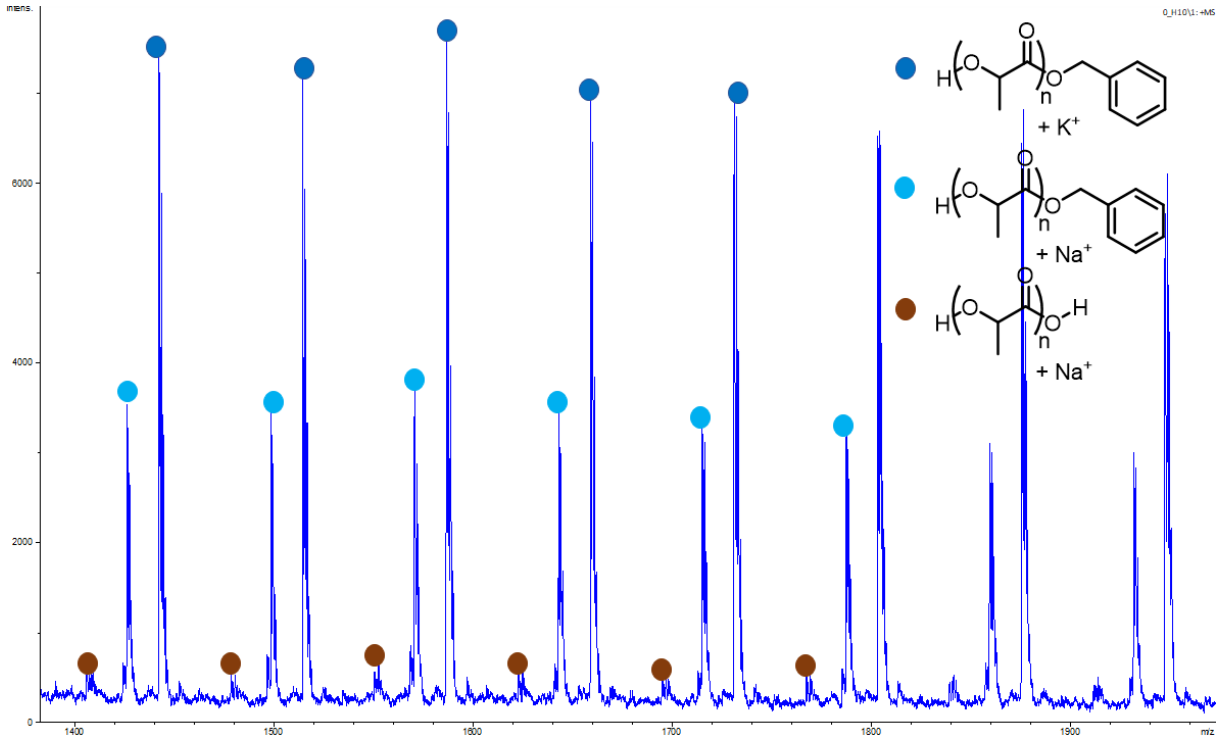

Figure S43. MALDI-ToF spectrum of PLA resulting from 32% conversion of *rac*-LA in the presence of complex **2** + 1 eq. BnOH (toluene, 60 °C).

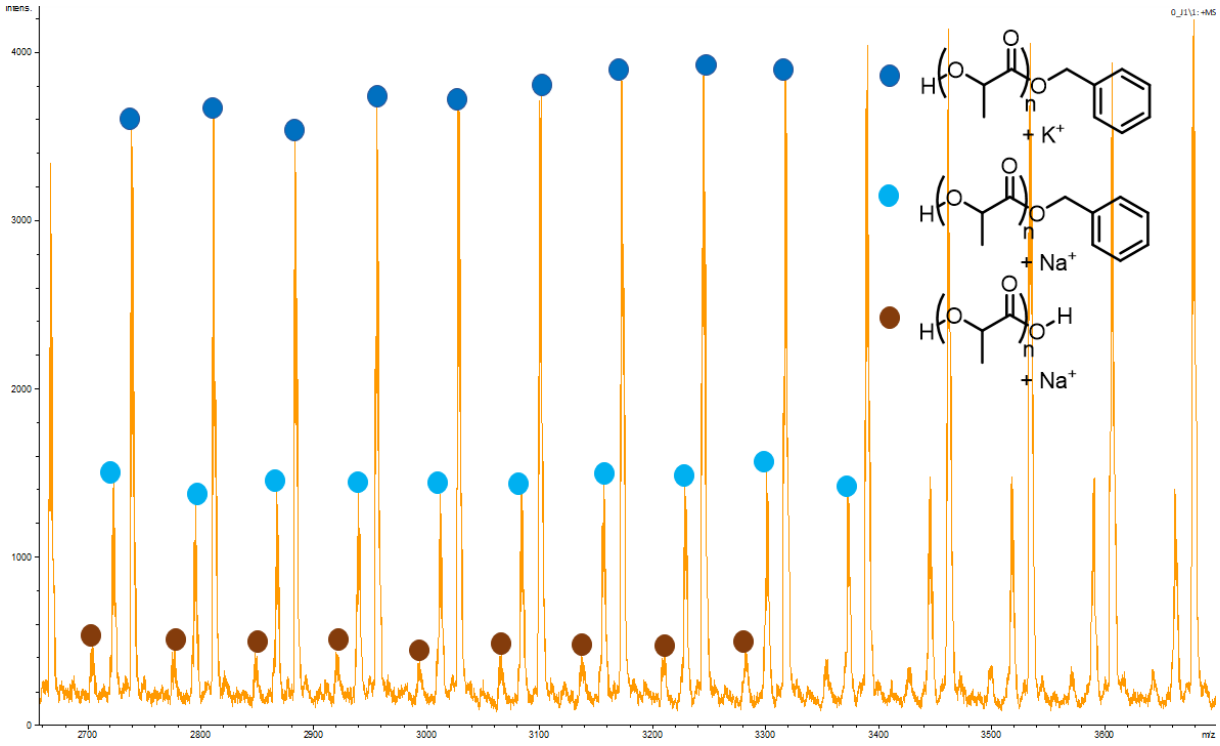

Figure S44. MALDI-ToF spectrum of PLA resulting from 70% conversion of *rac*-LA in the presence of complex **2** + 1 eq. BnOH (toluene, 60 °C).

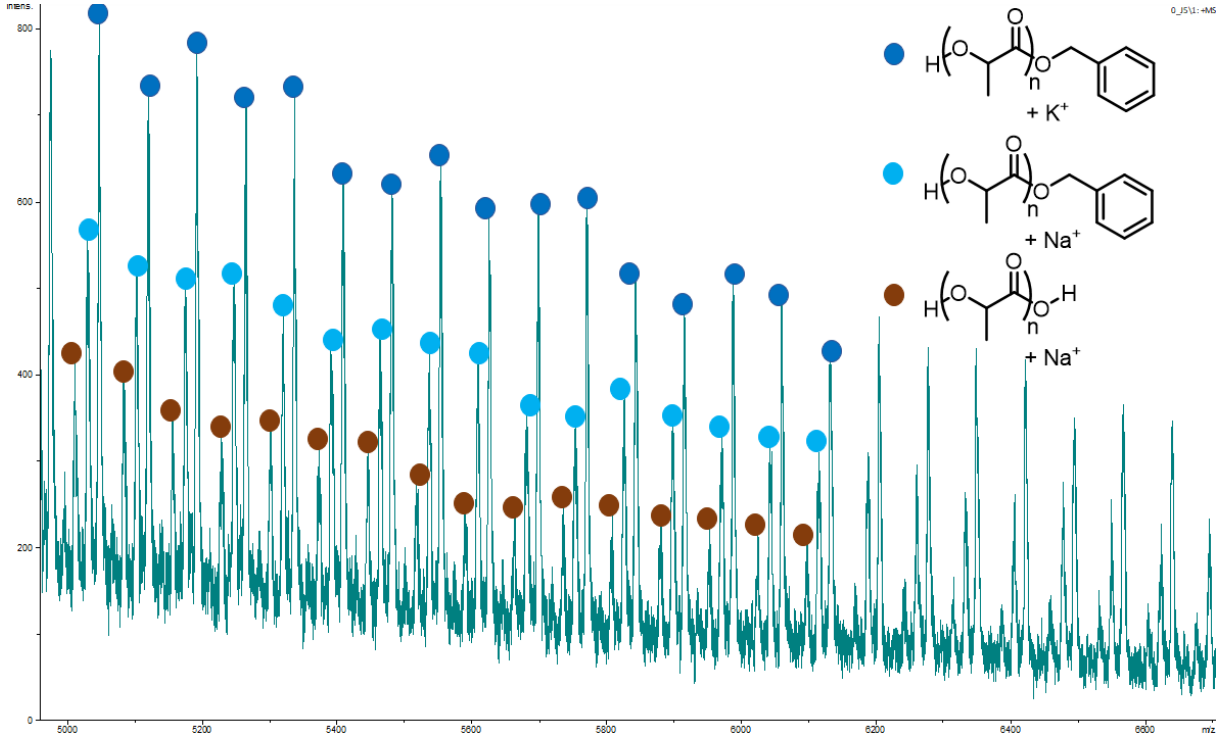

Figure S45. MALDI-ToF spectrum of PLA resulting from 99% conversion of *rac*-LA in the presence of complex **2** + 1 eq. BnOH (toluene, 60 °C).

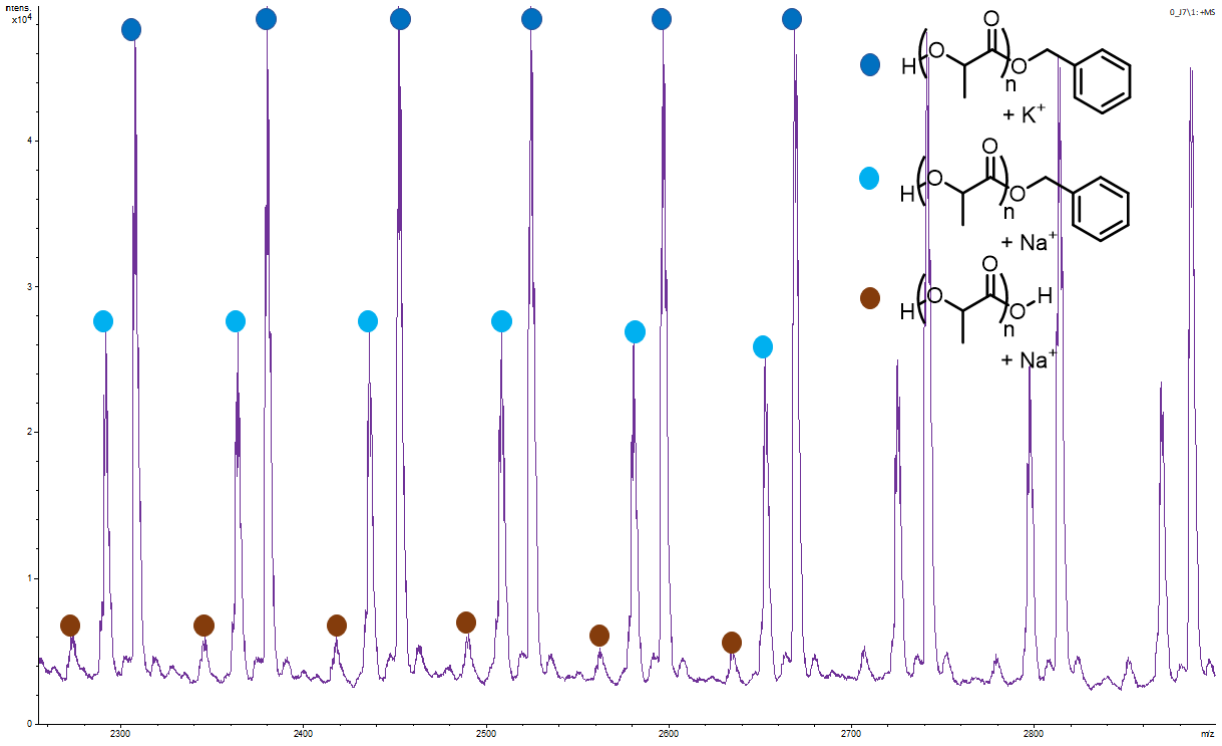

Figure S46. MALDI-ToF spectrum of PLA resulting from 48% conversion of *rac*-LA in the presence of complex **2** + 1 eq. BnOH (THF, R.T.).

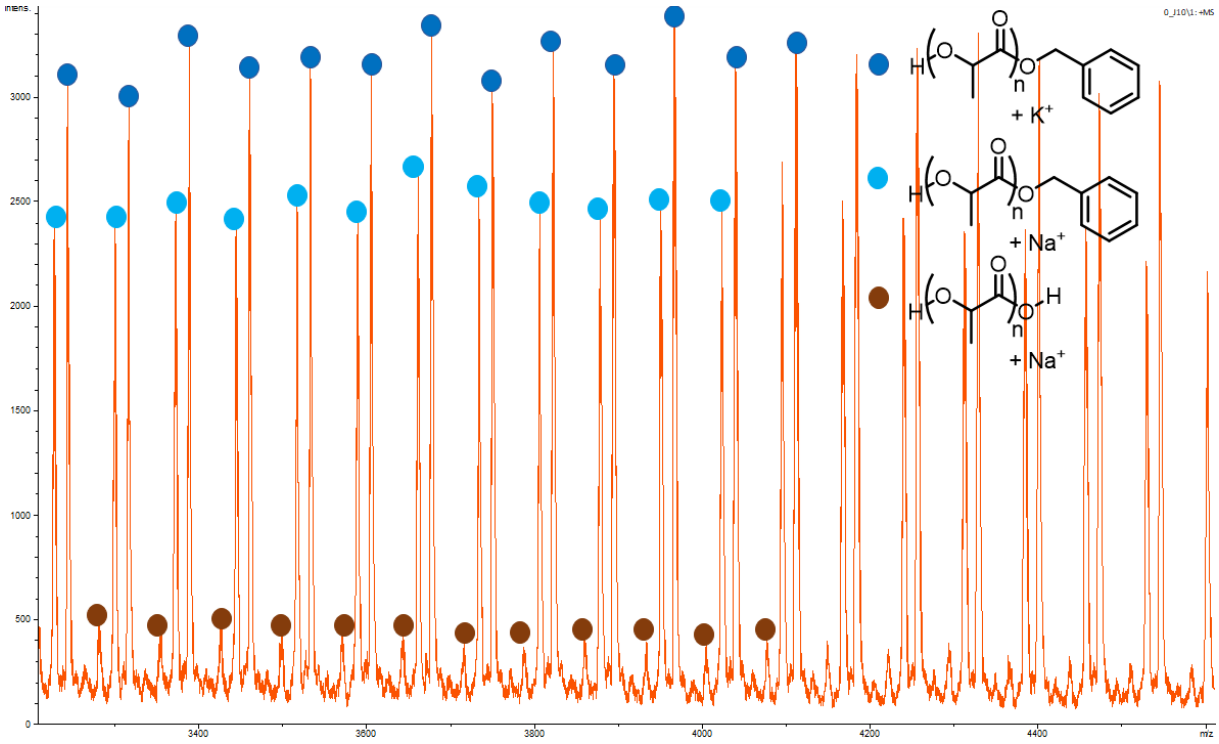

Figure S47. MALDI-ToF spectrum of PLA resulting from 68% conversion of *rac*-LA in the presence of complex **2** + 1 eq. BnOH (THF, R.T.).

Table S5. ROP of *rac*-LA with **1** and **2** in the presence of 1 eq. BnOH and 1-5 eq. of exogenous HMDSH in toluene at 60 °C.

Entry	Cat.	Exogenous HMDSH	Time (min)	Conv.[a] (%)	$M_{n,obs}$[b] (g mol^{-1})	$M_{n,calc}$[c] (g mol^{-1})	$Đ$[b]
1	**1**	1 eq.	0.67	15	1000	2200	1.16
2	**1**	1 eq.	2.5	33	2900	4800	1.13
3	**1**	1 eq.	4	43	3600	6200	1.13
4	**1**	1 eq.	6.25	51	5200	7400	1.12
5	**1**	1 eq.	7.5	62	6500	8900	1.16
6	**1**	1 eq.	10	79	7200	11400	1.12
7	**1**	3 eq.	10	76	7000	11000	1.15
8	**1**	5 eq.	10	70	7500	10100	1.16
9	**2**	1 eq.	0.33	33	1700	4800	1.31
10	**2**	1 eq.	0.5	57	4700	8200	1.3
11	**2**	1 eq.	0.67	71	4700	10200	1.33
12	**2**	1 eq.	1.25	76	5500	11000	1.31
13	**2**	1 eq.	2	83	6400	12000	1.47
14	**2**	3 eq.	1.25	77	6300	11100	1.38
15	**2**	5 eq.	1.25	72	5100	10400	1.43

100 eq. LA; [LA] = 1 M in toluene. LA and pre-catalyst pre-stirred separately for 3 min in toluene at 60 °C before mixing and initiation with BnOH and addition of exogenous HMDSH. [a] Conversion calculated using ^{1}H NMR spectroscopy.[b] $M_{n,obs}$ and $Đ$ determined by SEC using polystyrene standards in THF. Values corrected by Mark-Houwink factor (0.58).[10] [c] $M_{n,calc}$ of polymers calculated from the monomer conversion $M_{n,calc} = M_0 \times ([M]/[I]) \times$ conversion assuming 1 chain per catalyst.

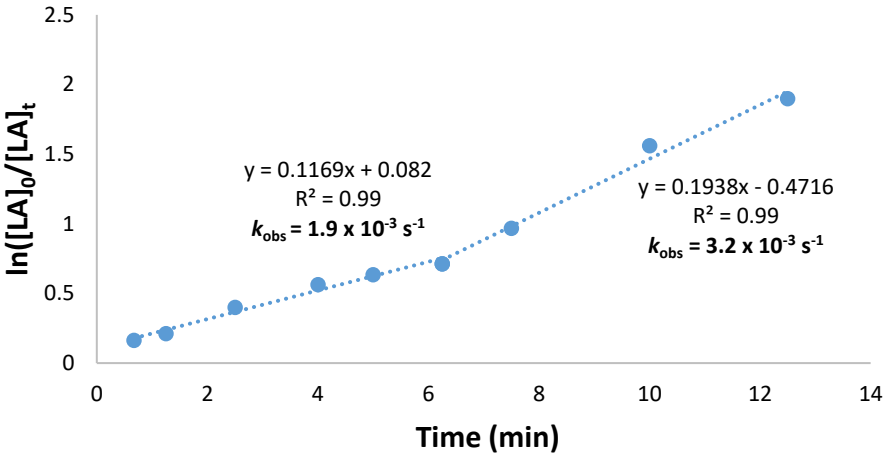

Figure S48. Plot of ln([*rac*-LA]$_0$/[*rac*-LA]$_t$) *vs*. time (min) for *rac*-LA ROP with **1** in the presence of 1 eq. BnOH and 1 eq. exogenous HMDSH (100 eq. *rac*-LA, [*rac*-LA] = 1 M, toluene, 60 °C).

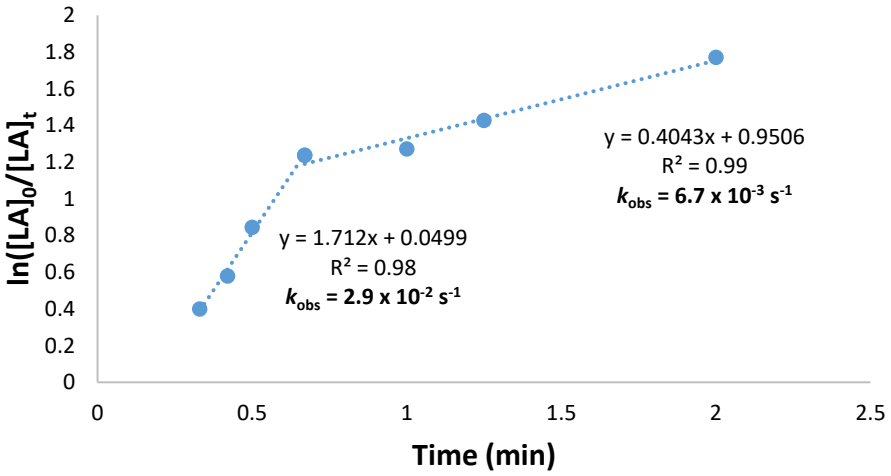

Figure S49. Plot of ln([*rac*-LA]$_0$/[*rac*-LA]$_t$) *vs*. time (min) for *rac*-LA ROP with **2** in the presence of 1 eq. BnOH and 1 eq. exogenous HMDSH (100 eq. *rac*-LA, [*rac*-LA] = 1 M, toluene, 60 °C).

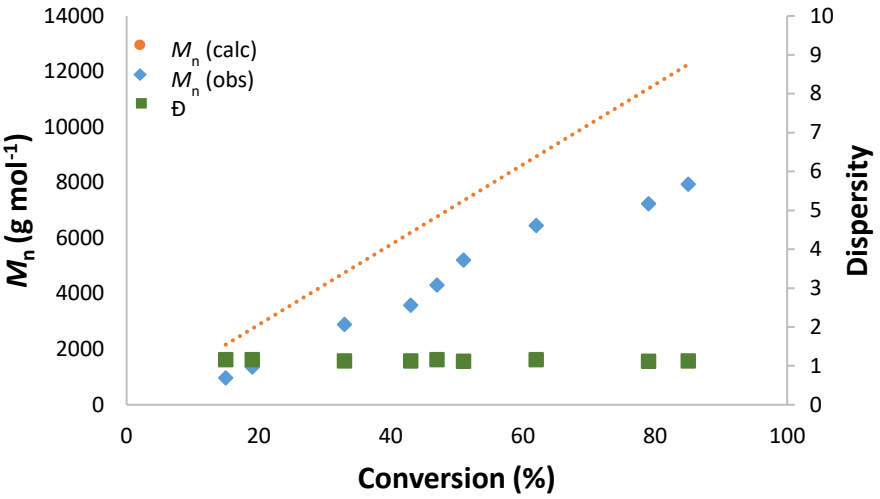

Figure S50. Comparison between experimental and calculated M_n values and dispersity values at increasing conversions of *rac*-LA in presence of complex **1** + 1 eq. BnOH and 1 eq. exogenous HMDSH in toluene at 60 °C.

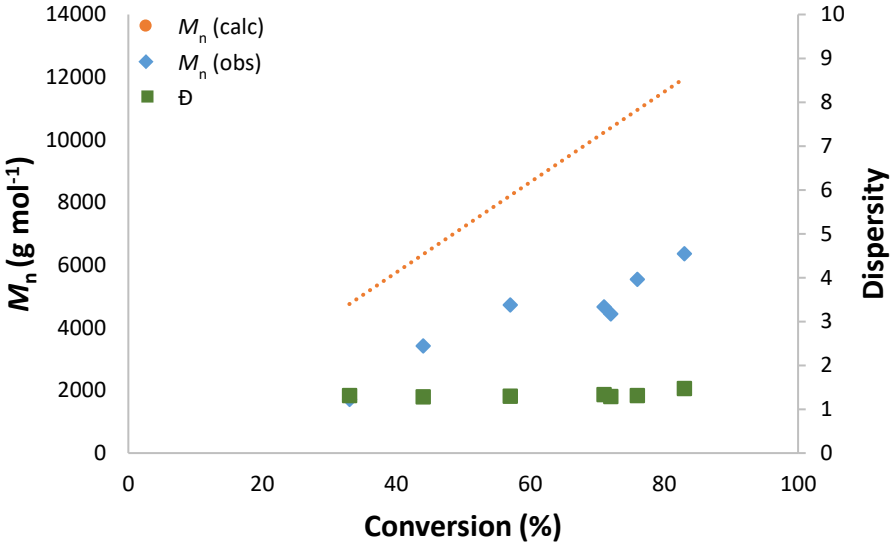

Figure S51. Comparison between experimental and calculated M_n values and dispersity values at increasing conversions of *rac*-LA in presence of complex **2** + 1 eq. BnOH and 1 eq. exogenous HMDSH in toluene at 60 °C.

Table S6. ROP of *rac*-LA with multi-component LMg/Zn-benzoxide (**8**) + **10** (bis-Zn) and **11** (bis-Mg) and LCa/Zn-benzoxide (**9**) + **10** and **12** (bis-Ca) mixtures in toluene at 60 °C.

Entry	Cat.	Time (min)	Conv.[a] (%)	$M_{n,obs}$[b] (g mol^{-1})	$M_{n,calc}$[c] (g mol^{-1})	$Đ$[b]	P_i[d]
1[e]	**8/10/11**	0.67	25	3300	3600	1.24	0.52
2[e]	**8/10/11**	1.25	49	8900	7100	1.11	-
3[e]	**8/10/11**	2.5	69	13400	10000	1.23	0.48
4[e]	**8/10/11**	5	82	15200	11800	1.2	-
5[e]	**8/10/11**	10	90	16600	13000	1.2	-
6[f]	**9/10/12**	0.33	7	-	-	-	-
7[f]	**9/10/12**	1.25	22	2900	3200	1.36	-
8[f]	**9/10/12**	5	56	11100	8100	1.28	0.5
9[f]	**9/10/12**	10	78	12100	11200	1.45	-
10[f]	**9/10/12**	12.5	85	10500	12300	1.56	0.55
11	**10**	2	99	19900	14300	1.35	-
12	**11**	10	12	-	-	-	-
13	**12**	5	84	14300	12100	1.19	-
14	**10/11**	2.5	13	1900	1900	1.15	-
15	**10/12**	5	94	12000	13400	1.48	-

100 eq. LA; [LA] = 1 M in toluene. LA and catalyst(s) pre-stirred separately for 3 min in toluene at 60 °C before mixing. [a] Conversion calculated using ^{1}H NMR spectroscopy.[b] $M_{n,obs}$ and $Đ$ determined by SEC using polystyrene standards in THF. Values corrected by Mark-Houwink factor (0.58).[10] [c] $M_{n,calc}$ of polymers calculated from the monomer conversion $M_{n,calc} = M_0$ x ([M]/[I]) x conversion assuming 1 chain per catalyst.[d] Determined by homodecoupled ^{1}H NMR spectroscopy. [e] Composition of the catalyst mixture: **8** (74%) + **10** (13%) + **11** (13%). [f] Composition of the catalyst mixture: **9** (66%) + **10** (17%) + **12** (17%).

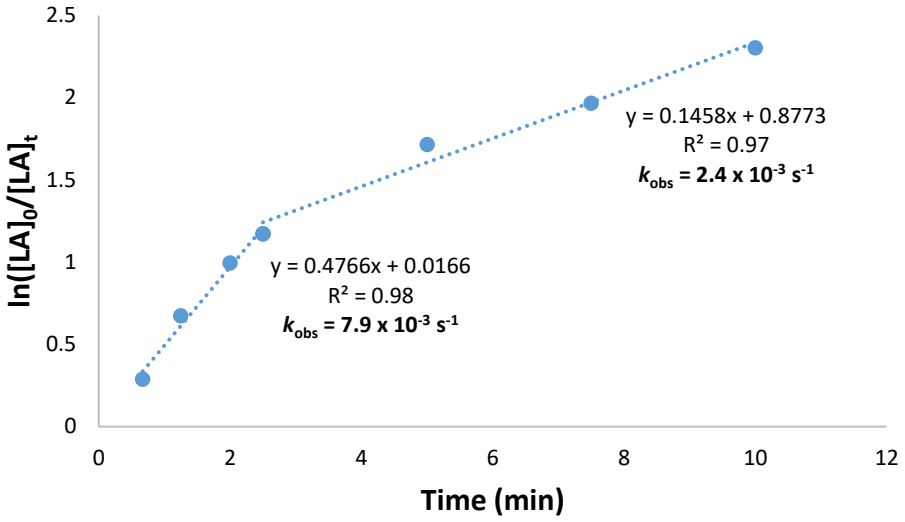

Figure S52. Plot of ln([*rac*-LA]$_0$/[*rac*-LA]$_t$) *vs*. time (min) for *rac*-LA ROP with multi-component LMg/Zn-benzoxide (**8**) + **10** (bis-Zn) and **11** (bis-Mg) mixture (100 eq. *rac*-LA, [*rac*-LA] = 1 M, toluene, 60 °C).

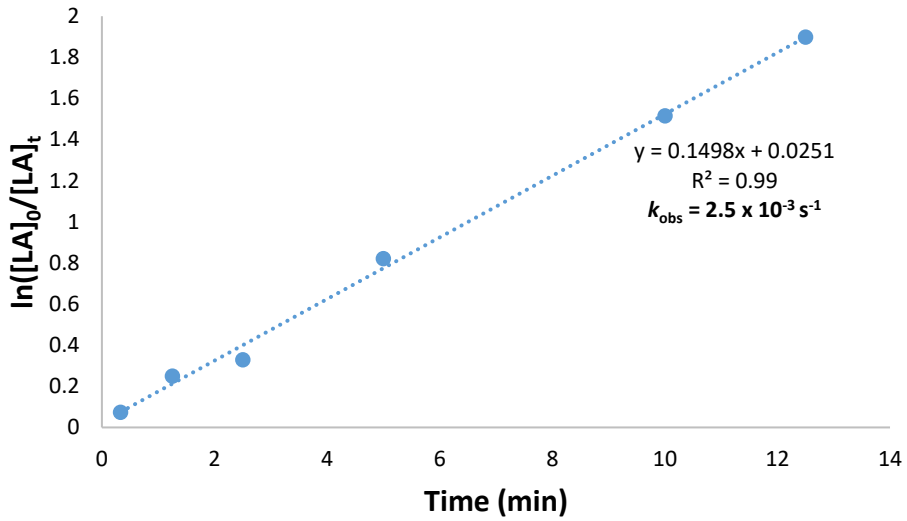

Figure S53. Plot of ln([*rac*-LA]$_0$/[*rac*-LA]$_t$) *vs*. time (min) for *rac*-LA ROP with multi-component LCa/Zn-benzoxide (**9**) + **10** (bis-Zn) and **12** (bis-Ca) mixture (100 eq. *rac*-LA, [*rac*-LA] = 1 M, toluene, 60 °C).

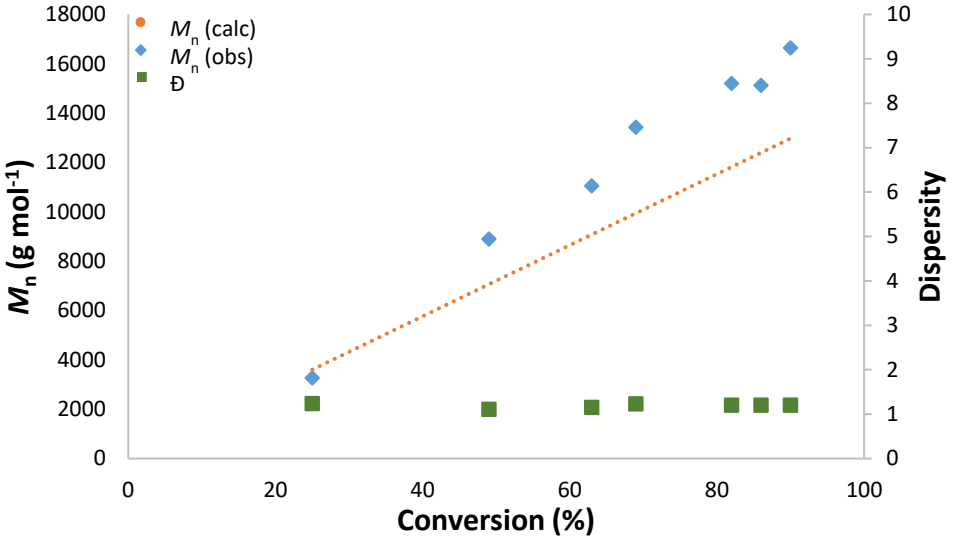

Figure S54. Comparison between experimental and calculated M_n values and dispersity values at increasing conversions of *rac*-LA in presence of multi-component LMg/Zn-benzoxide (**8**) + **10** (bis-Zn) and **11** (bis-Mg) mixture in toluene at 60 °C.

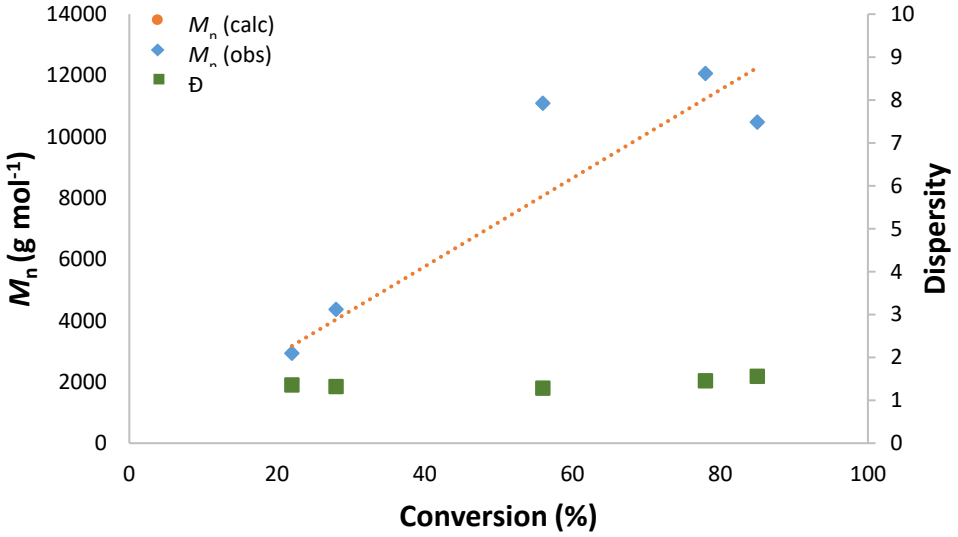

Figure S55. Comparison between experimental and calculated M_n values and dispersity values at increasing conversions of *rac*-LA in presence of multi-component LCa/Zn-benzoxide (**9**) + **10** (bis-Zn) and **12** (bis-Ca) mixture in toluene at 60 °C.

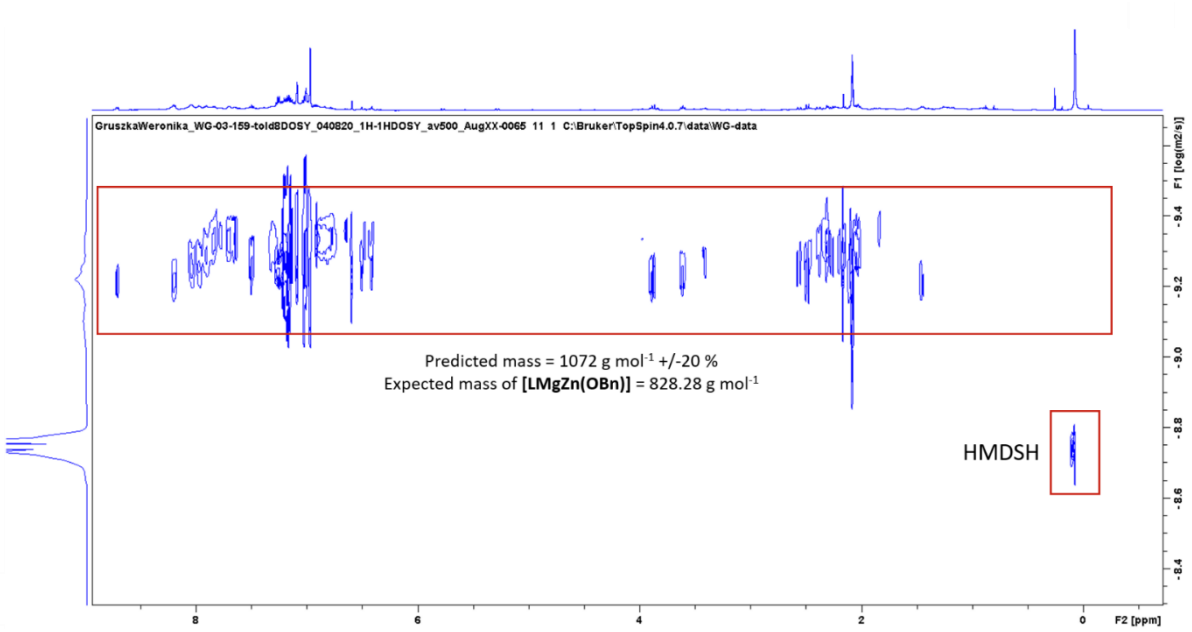

Figure S56. DOSY NMR spectrum of the multi-component **8**/**10**/**11** mixture in toluene-d_8 (298 K).

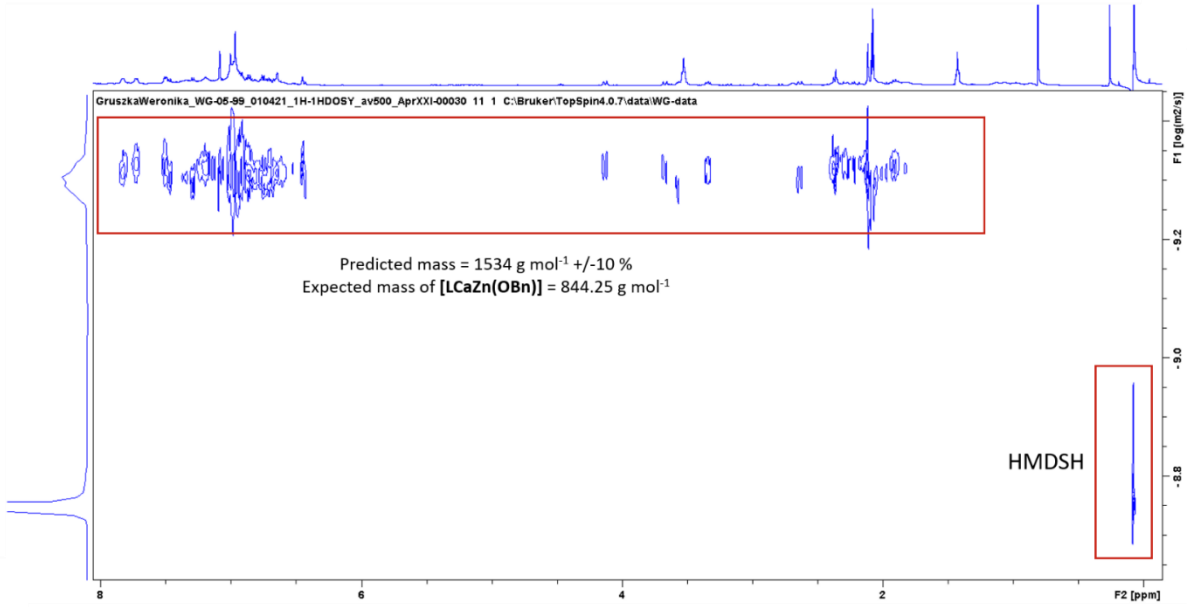

Figure S57. DOSY NMR spectrum of the multi-component **9**/**10**/**12** mixture in toluene-d_8 (298 K).

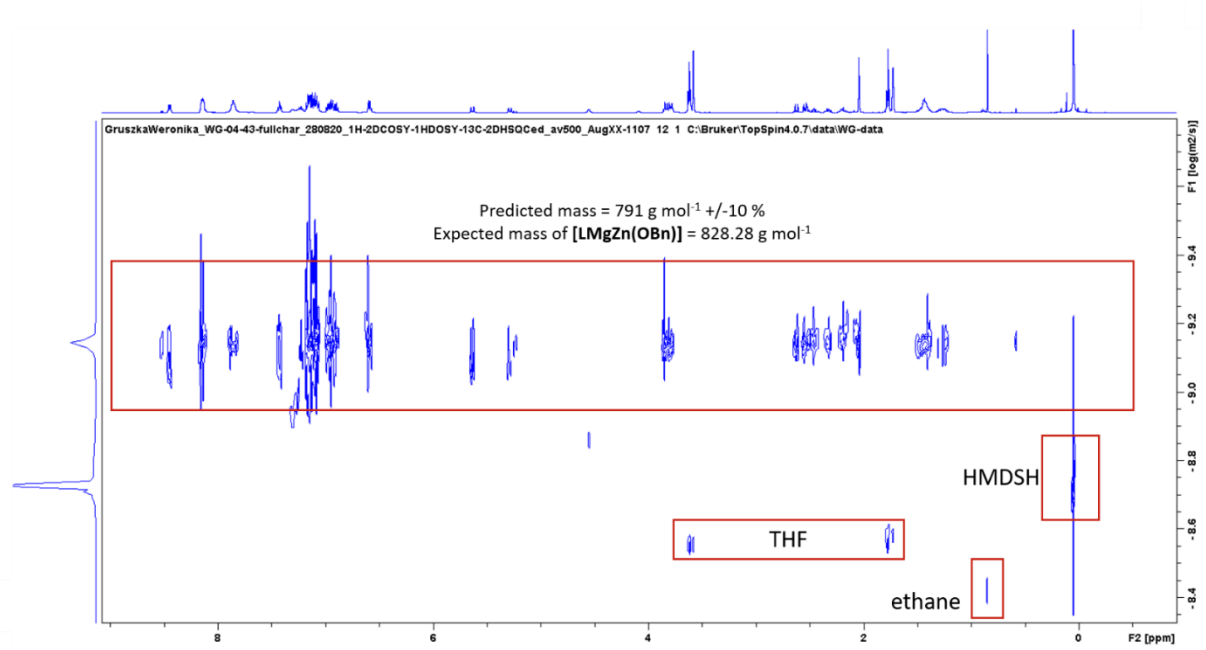

Figure S58. DOSY NMR spectrum of the multi-component **8**/**10**/**11** mixture in THF-d_8 (298 K).

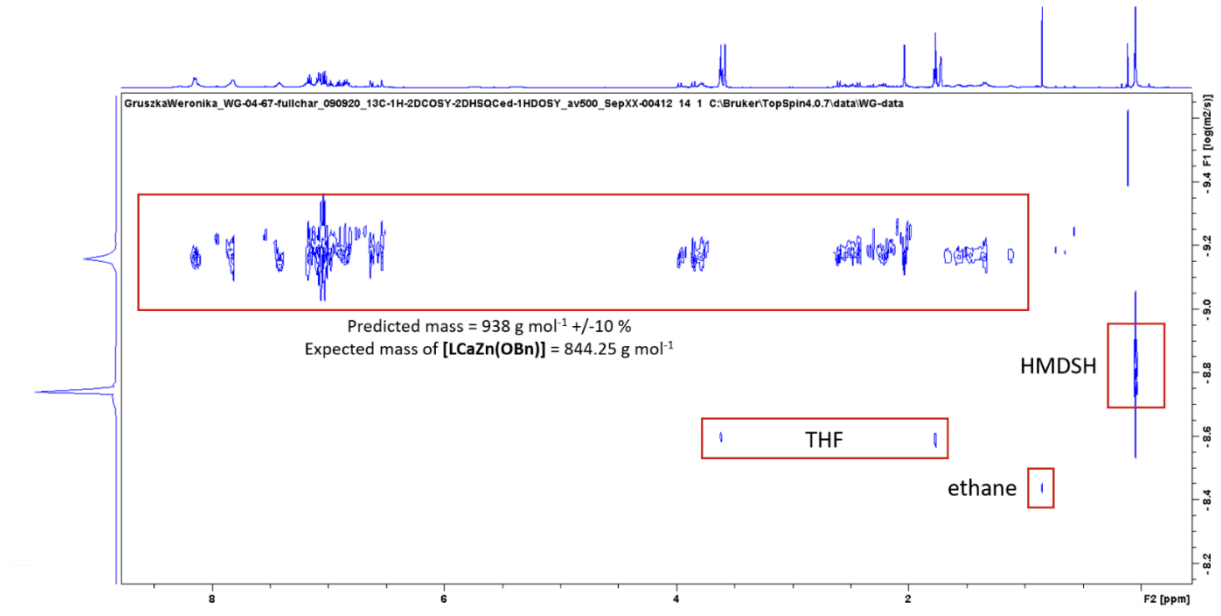

Figure S59. DOSY NMR spectrum of the multi-component **9**/**10**/**12** mixture in THF-d_8 (298 K).

Table S7. ROP of ε-CL and δ-VL with complexes **1** and **2** and 1 eq. BnOH in toluene at R.T.

Entry	Cat.	Monomer	Time (min)	Conv.[a] (%)	$M_{n,obs}$[b] (g mol^{-1})	$M_{n,calc}$[c] (g mol^{-1})	$Đ$[b]
1	**1**	ε-CL	0.08	86	7500	9800	1.76
2[e]	**1**	ε-CL	10	71	19100	40500	1.87
3[e,f]	**1**	ε-CL	10	81	42500	46200	1.54
4	**1**	δ-VL	0.08	99	24000[f]	9900	1.78
5	**2**	ε-CL	0.08	99	10600	11300	1.66
6[e]	**2**	ε-CL	0.5	81	35900	46200	1.47
7[e,f]	**2**	ε-CL	0.5	76	54200	42400	1.72
8	**2**	δ-VL	0.08	99	20400[f]	9900	1.12

100:1:1 monomer:catalyst:BnOH, [monomer] = 1 M in toluene.[a] Conversion calculated using ^{1}H NMR spectroscopy.[b] $M_{n,obs}$ and $Đ$ determined by SEC using polystyrene standards in THF. Values corrected by Mark-Houwink factor (0.56).[c] $M_{n,calc}$ of polymers calculated from the monomer conversion $M_{n,calc} = M_0 \times ([M]/[I]) \times$ conversion assuming 1 chain per catalyst. [e] 500 eq. ε-CL used. [f] Reactions were run neat. [g] $M_{n,obs}$ values reported are uncorrected.

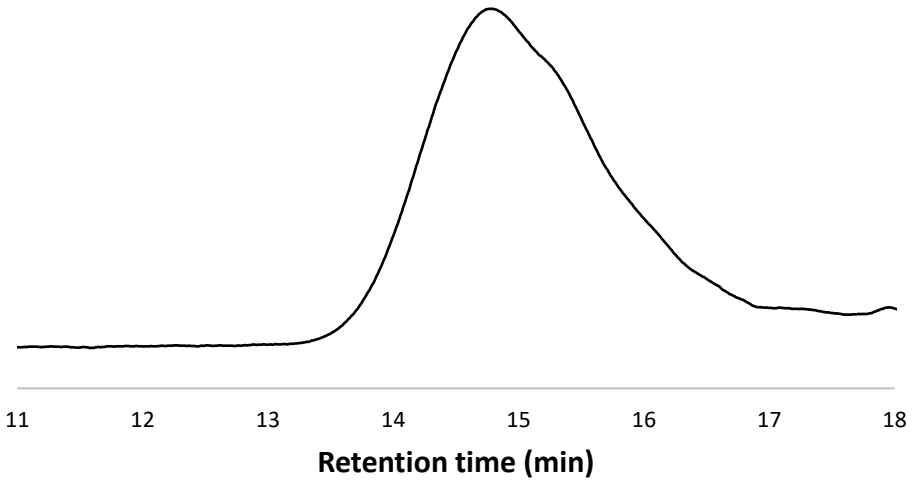

Figure S60. Example SEC trace of PCL generated in the presence of complex **1** + 1 eq. BnOH in toluene at R.T. (Entry 1, Table S7).

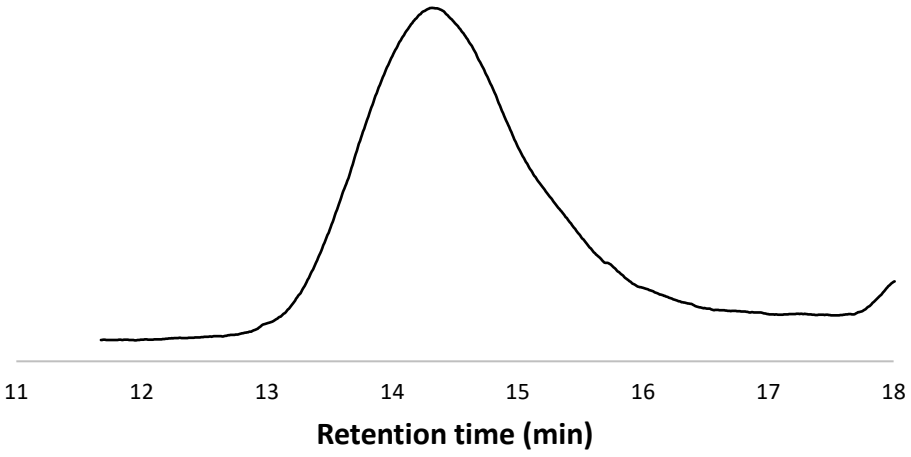

Figure S61. Example SEC trace of PVL generated in the presence of complex **1** + 1 eq. BnOH in toluene at R.T. (Entry 4, Table S7).

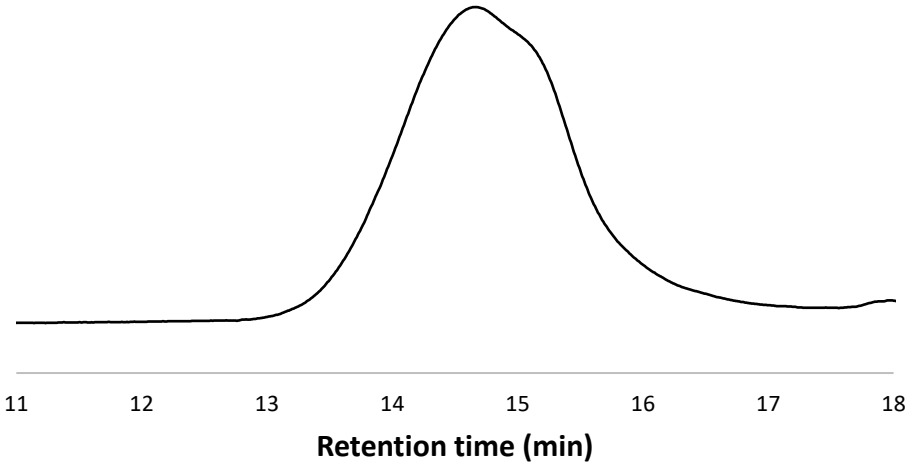

Figure S62. Example SEC trace of PCL generated in the presence of complex **2** + 1 eq. BnOH in toluene at R.T. (Entry 5, Table S7).

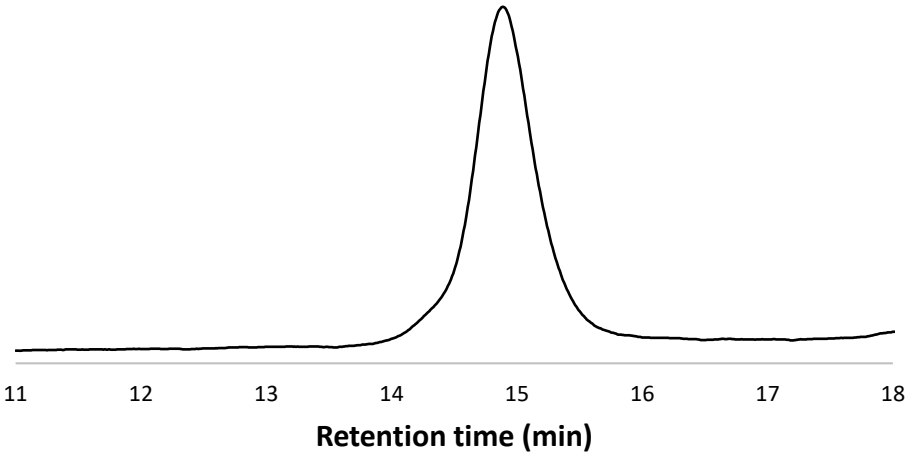

Figure S63. Example SEC trace of PVL generated in the presence of complex **2** + 1 eq. BnOH in toluene at R.T. (Entry 8, Table S7).

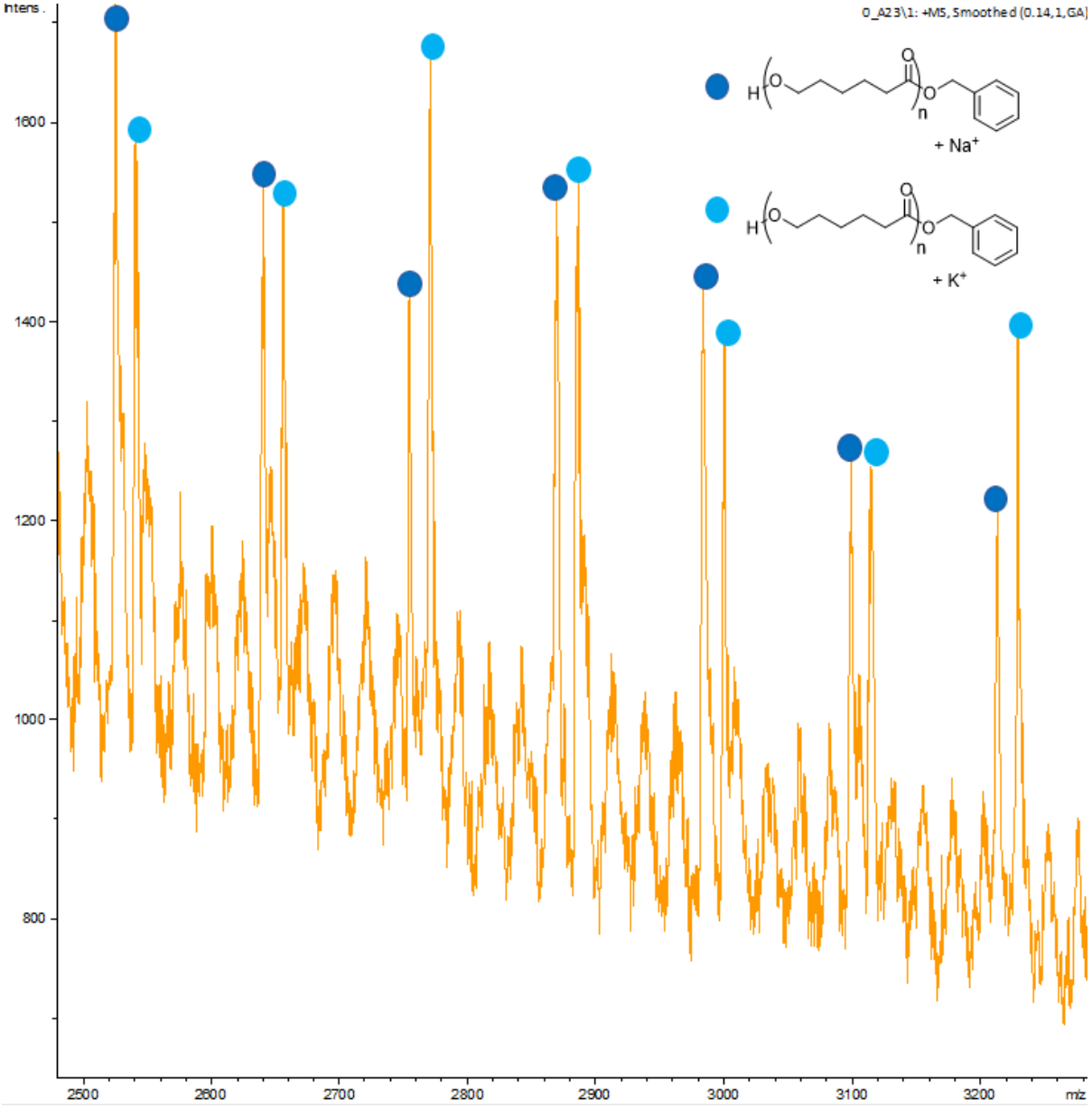

Figure S64. MALDI-ToF spectrum of PCL resulting from 86% conversion of ε-CL in the presence of complex **1** + 1 eq. BnOH (toluene, R.T.).

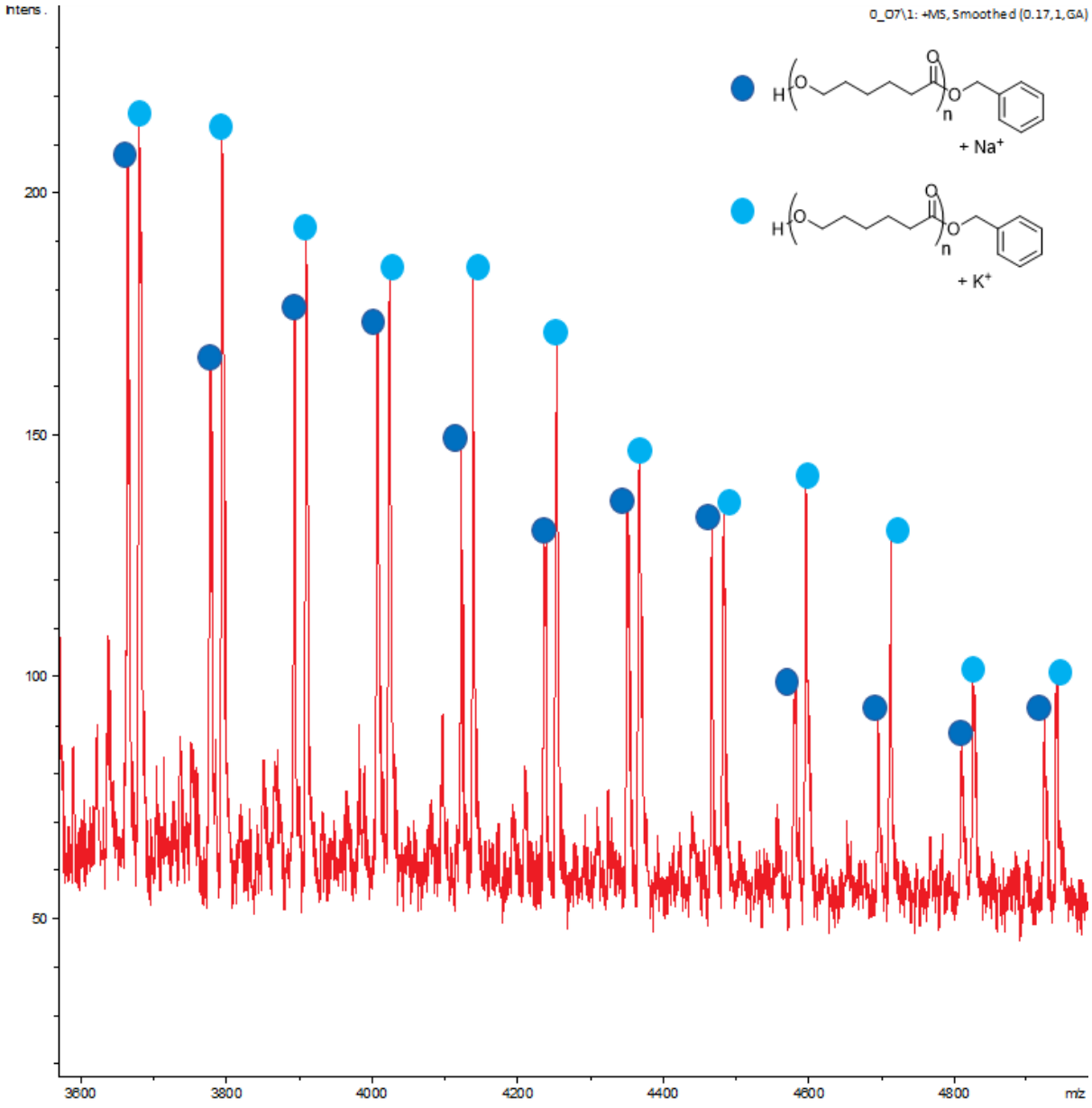

Figure S65. MALDI-ToF spectrum of PCL resulting from 91% conversion of ε-CL in the presence of complex **2** + 1 eq. BnOH (toluene, R.T.).

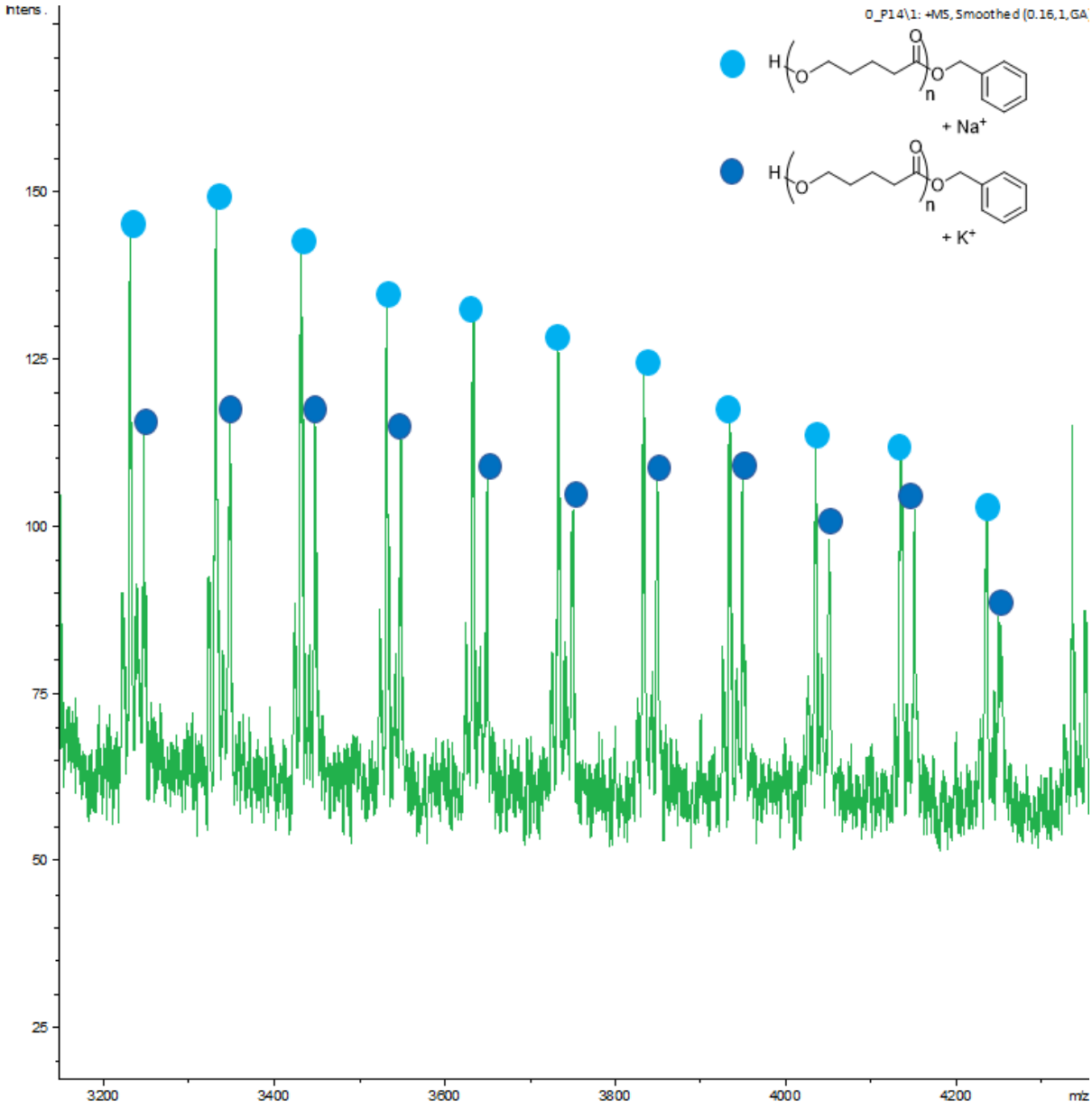

Figure S66. MALDI-ToF spectrum of PCL resulting from 96% conversion of δ-VL in the presence of complex **1** + 1 eq. BnOH (toluene, R.T.).

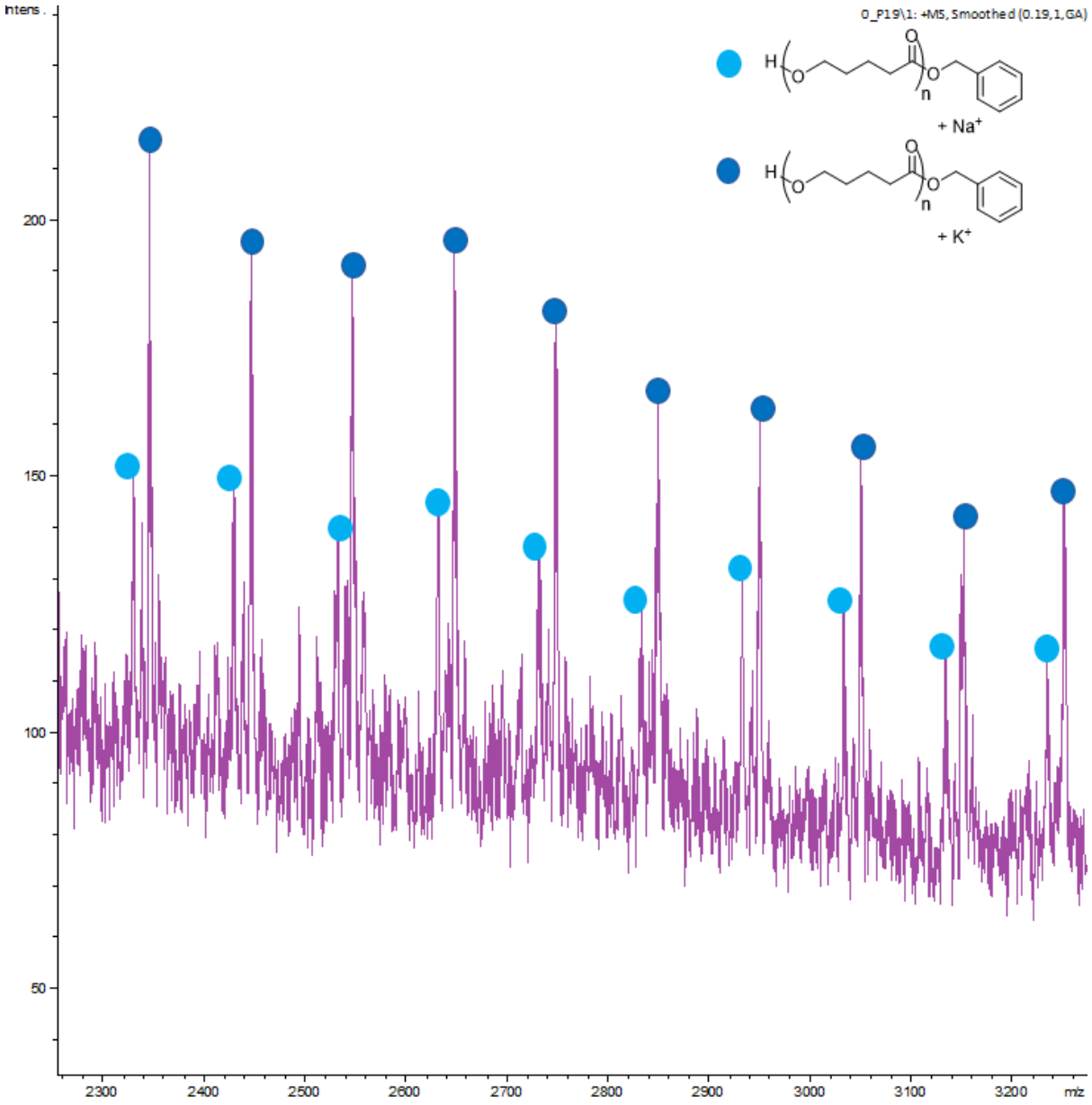

Figure S67. MALDI-ToF spectrum of PCL resulting from 97% conversion of δ-VL in the presence of complex **2** + 1 eq. BnOH (toluene, R.T.).

Computed molecular structures of complexes [LHMg]' and [LHCa]'

Potential geometries of the heterometallic precursors **[LHMg]'** and **[LHCa]'** were optimised and the molecular structures with the lowest free enthalpies computed are shown in Figures S68-69, respectively.

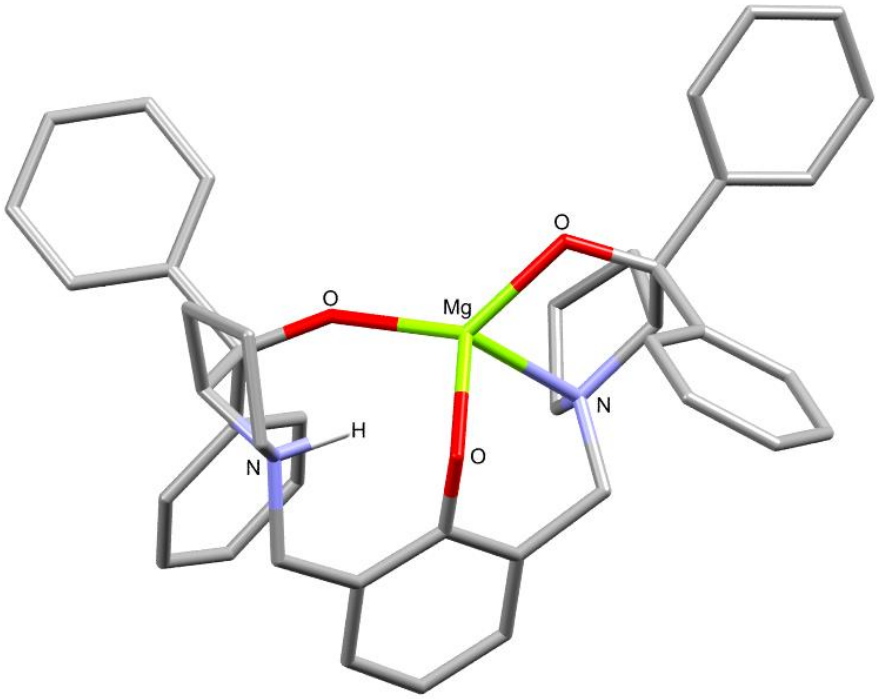

Figure S68. Molecular structure of **[LHMg]'**, computed at the rωB97XD/6-311++g(d,p)/6-31g(d)/cpcm=tetrahydrofuran/298K level of theory. DFT calculations suggest that the phenolic O*H* of **[LHMg]'** is labile, as previously demonstrated with salen-based complexes,[11] and could be on the pyrrolidine *N* or the phenolic *O*.

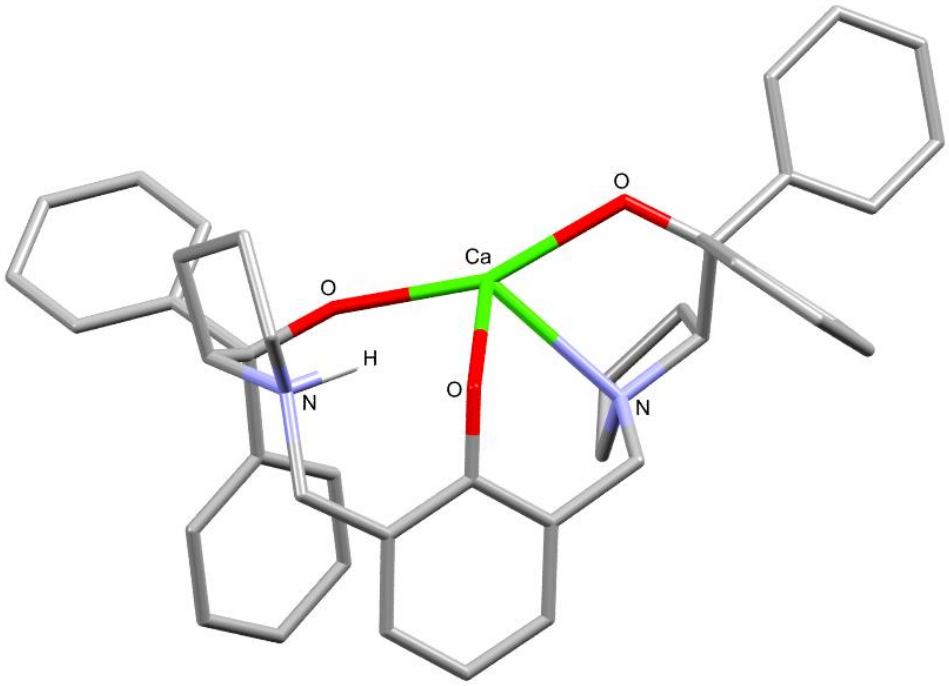

Figure S69. Molecular structure of **[LHCa]'**, computed at the rωB97XD/6-311++g(d,p)/6-31g(d)/cpcm=tetrahydrofuran/298K level of theory. DFT calculations suggest that the phenolic O*H* of **[LHCa]'** is labile, as previously demonstrated with salen-based complexes,[11] and could be on the pyrrolidine *N* or the phenolic *O*.

Computed molecular structures of complex 1'

Potential molecular structures of complex **1'** (**[LMgZnEt(THF)(HMDSH)]'**) were optimised and their relative free enthalpies were compared and referenced to a putative **[LMgZnEt]'** complex.

Table S8. Free enthalpies computed for complex **1'** at the rωB97XD/6-311++g(d,p)/6-31g(d)/cpcm=tetrahydrofuran/298K level of theory.

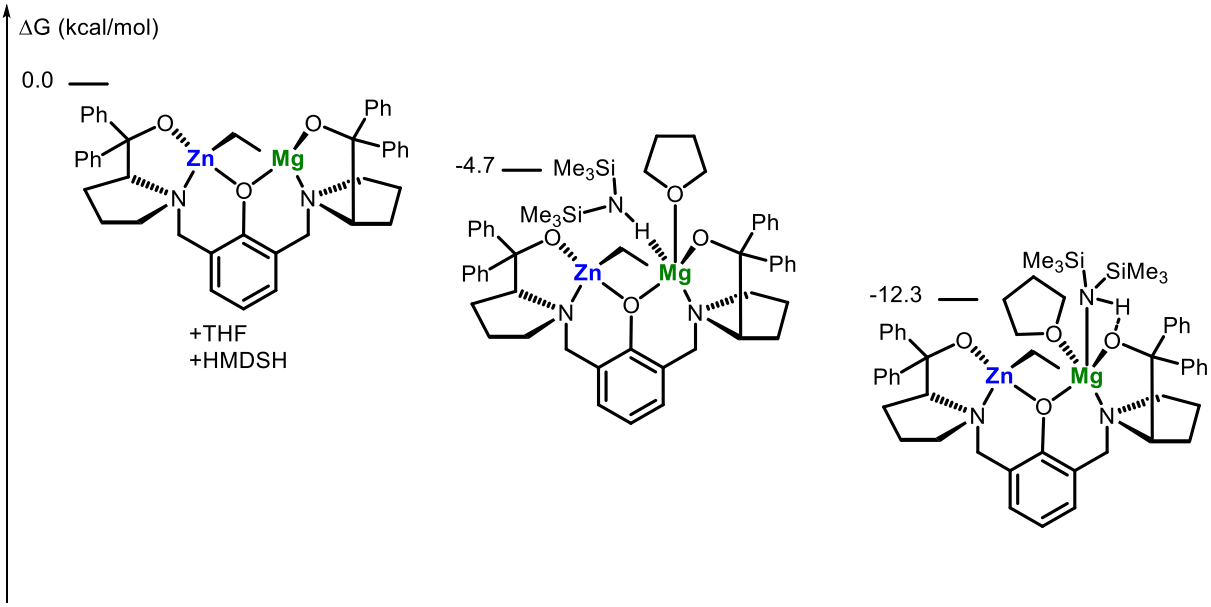

Structure	G (Hartree)	ΔG (kcal mol^{-1})
[LMgZnEt]' + THF + HMDSH	–5123.851964	+0.0 (reference)
[LMgZnEt(HMDSH)(THF)]'	–5123.888279	–4.7
[LMgZnEt(THF)(HMDSH)]'	–5123.900363	–12.3

According to the calculations detailed in Table S8, the coordination of one THF molecule and one HMDSH molecule to the magnesium atom is favoured. The molecular structure of **1'** with the lowest free enthalpy computed is shown in Figure S70. In that structure, some hydrogen bonding between the amine proton and one of the ligand's benzylic oxygen atoms can be seen, which may be a source of additional stabilisation.

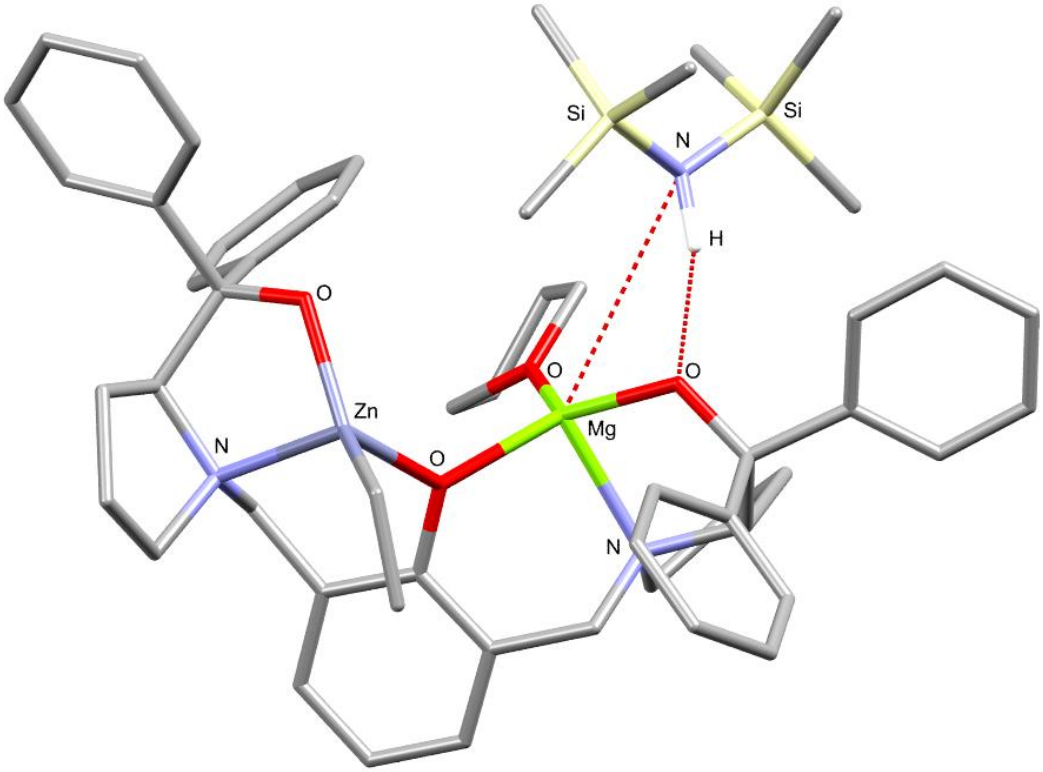

Figure S70. Molecular structure of complex **1'**, computed at the rωB97XD/6-311++g(d,p)/6-31g(d)/cpcm=tetrahydrofuran/298K level of theory.

Computed molecular structures of complex 2'

Potential molecular structures of complex **2'** (**[LCaZnEt(THF)(HMDSH)]'**) were optimised and their relative free enthalpies were compared and referenced to a putative **[LCaZnEt]'** complex.

Table S9. Free enthalpies computed for complex **2'** at the rωB97XD/6-311++g(d,p)/6-31g(d)/cpcm=tetrahydrofuran/298K level of theory.

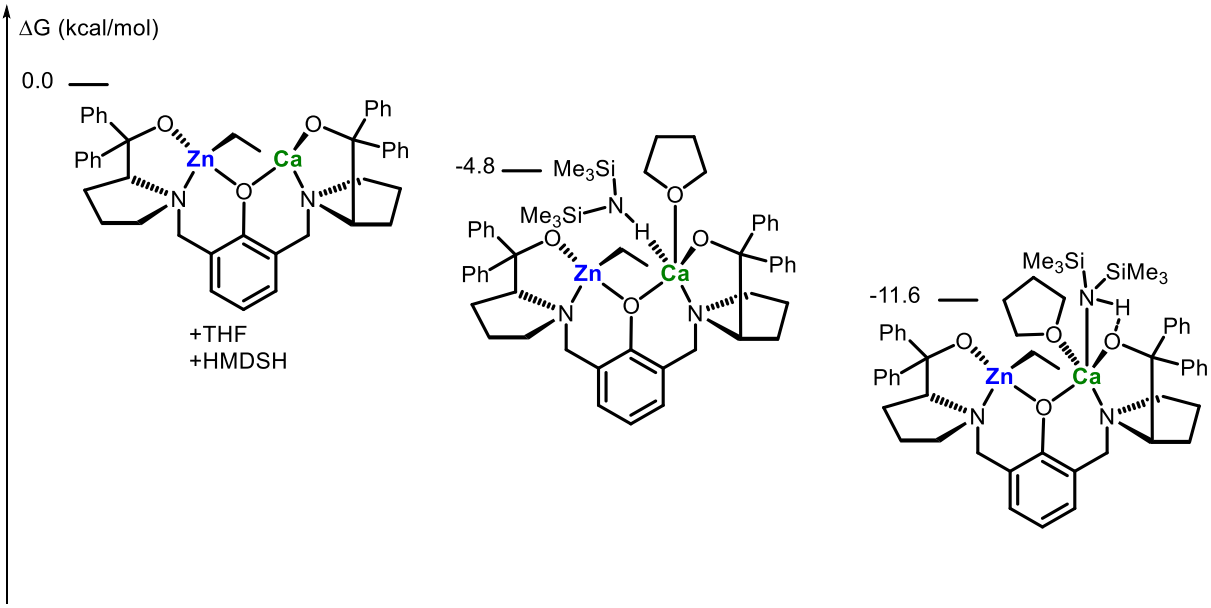

Structure	G (Hartree)	ΔG (kcal mol^{-1})
[LCaZnEt]' + THF + HMDSH	–5601.433252	+0.0 (reference)
[LCaZnEt(HMDSH)(THF)]'	–5601.440815	–4.8
[LCaZnEt(THF)(HMDSH)]'	–5601.451738	–11.6

According to the calculations detailed in Table S9, the coordination of one THF molecule and one HMDSH molecule to the calcium atom is favoured. The molecular structure of **2'** with the lowest free enthalpy computed is shown in Figure S71. In that structure, some hydrogen bonding between the amine proton and one of the ligand's benzylic oxygen atoms can be seen, which may be a source of additional stabilisation.

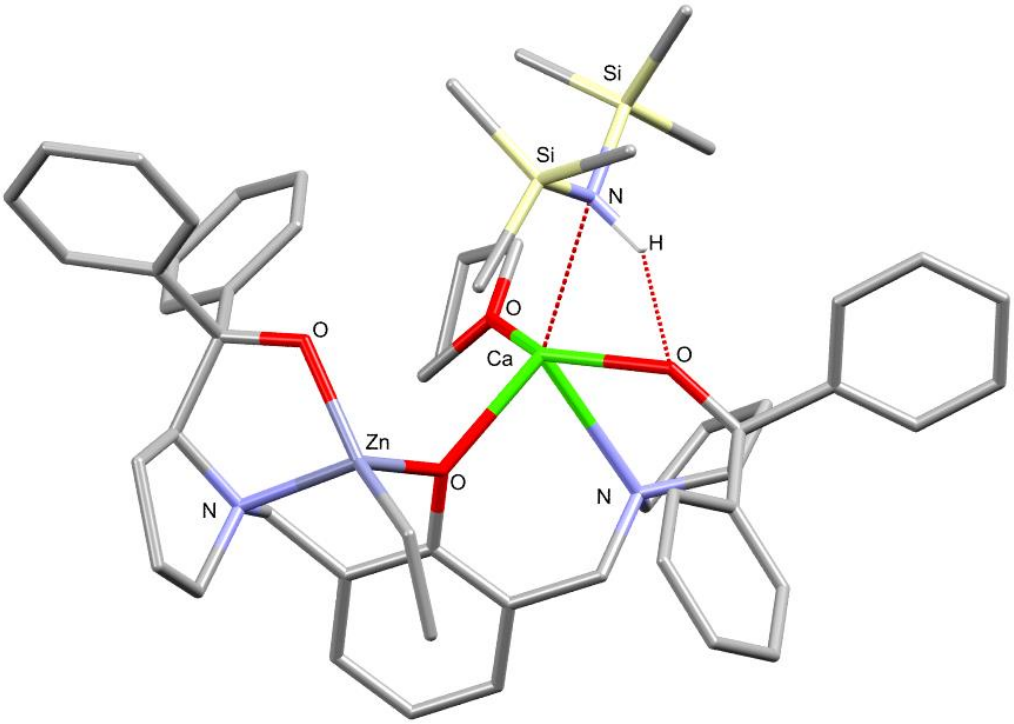

Figure S71. Molecular structure of complex **2'**, computed at the rωB97XD/6-311++g(d,p)/6-31g(d)/cpcm=tetrahydrofuran/298K level of theory.

Computed molecular structures of complex 3'

Potential molecular structures of complex **3'** (**[LZn$_2$Et]'**) **+ THF + HMDSH** were optimised and the relative free enthalpies of **[LZn$_2$Et(HMDSH)(THF)]'** and **[LZn$_2$Et(THF)(HMDSH)]'** were compared and referenced to **3' + THF + HMDSH**. N.B. **[LZn$_2$Et(HMDSH)(THF)]'** and **[LZn$_2$Et(THF)(HMDSH)]'** were computed to allow direct comparison to **1'** and **2'**.

Table S10. Free enthalpies computed for complex **3'** at the rωB97XD/6-311++g(d,p)/6-31g(d)/cpcm=tetrahydrofuran/298K level of theory.

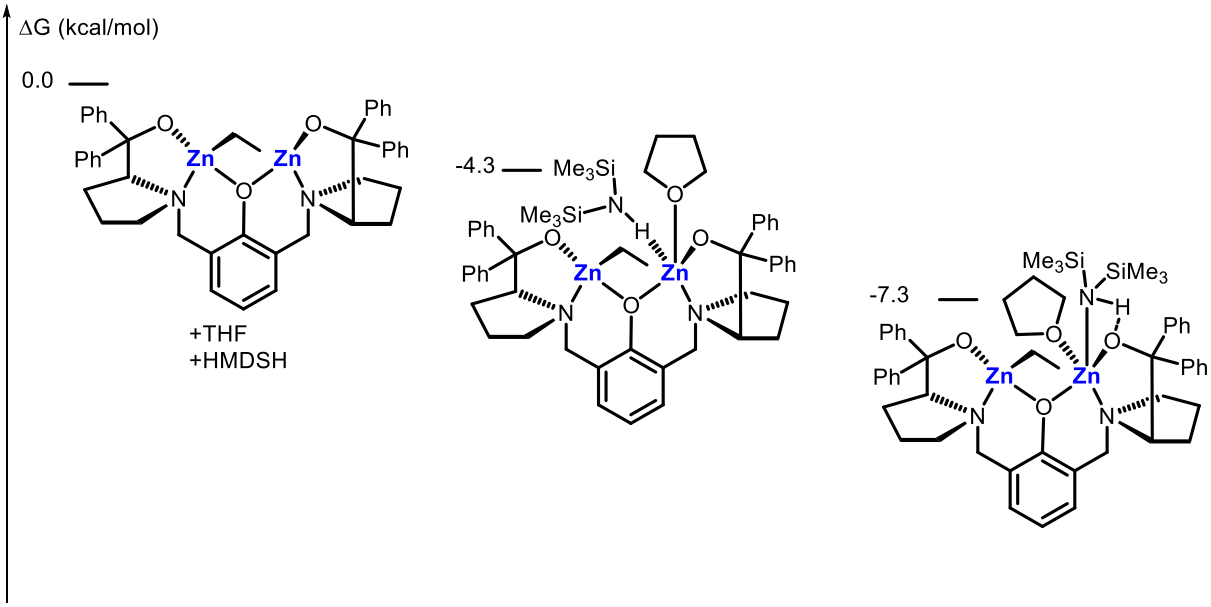

Structure	G (Hartree)	ΔG (kcal mol^{-1})
[LZn$_2$Et]' + THF + HMDSH	–5601.433252	+0.0 (reference)
[LZn$_2$Et(HMDSH)(THF)]'	–5601.440815	–4.3
[LZn$_2$Et(THF)(HMDSH)]'	–5601.451738	–7.3

According to the calculations detailed in Table S10, the coordination of one THF molecule and one HMDSH molecule to the zinc atom is favoured. The molecular structure of **3'** (**[LZn$_2$Et(THF)(HMDSH)]'**) with the lowest free enthalpy computed is shown in Figure S72. In that structure, some hydrogen bonding between the amine proton and one of the ligand's benzylic oxygen atoms can be seen, which may be a source of additional stabilisation.

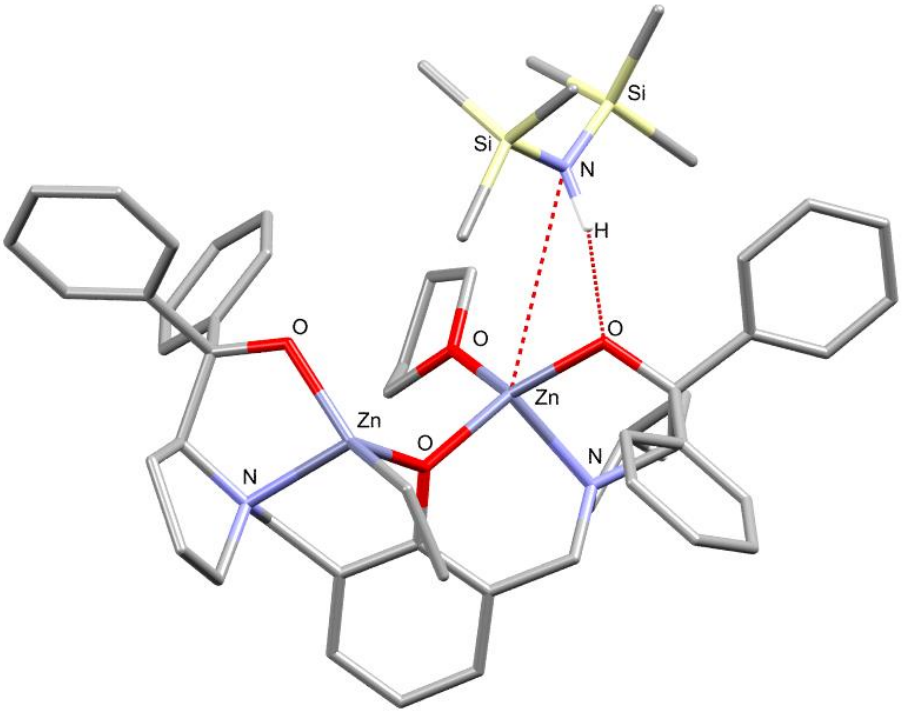

Figure S72. Molecular structure of complex **3'** (**[LZn$_2$Et(THF)(HMDSH)]'**), computed at the rωB97XD/6-311++g(d,p)/6-31g(d)/cpcm=tetrahydrofuran/298K level of theory.

Comparison of atomic charges in 1'-3'

Natural population analysis was conducted on the optimised molecular structures of **1'** (**[LMgZnEt(THF)(HMDSH)]**), **2'** (**[LCaZnEt(THF)(HMDSH)]**) and **3'** (**[LZn$_2$Et(THF)(HMDSH)]**), as shown in Figure S72.

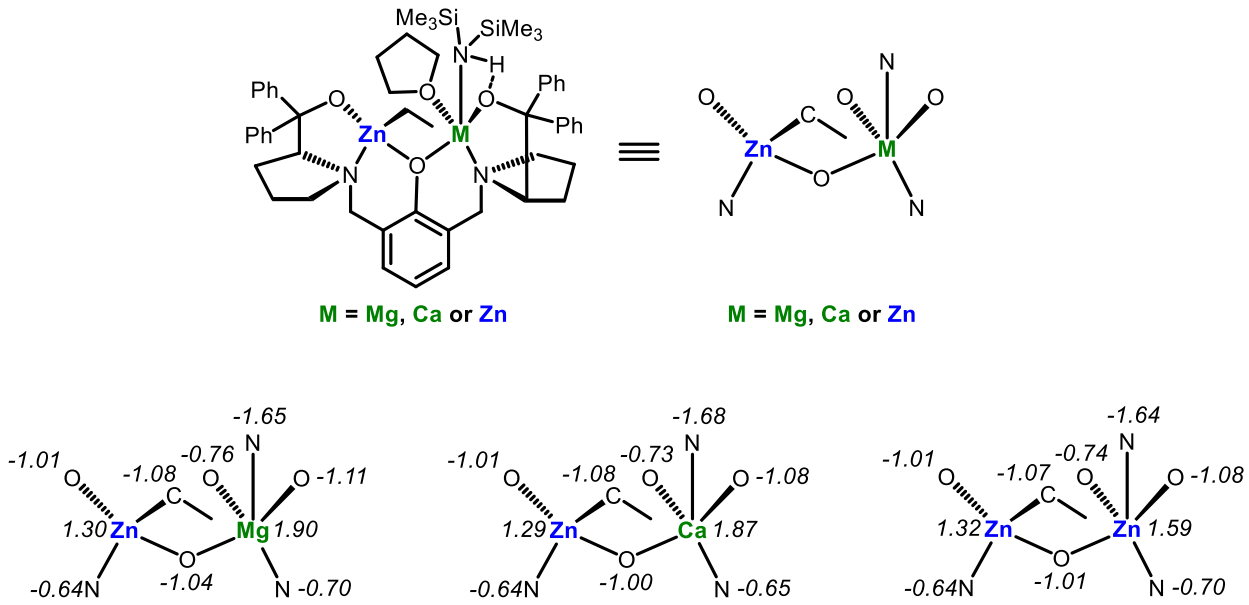

Figure S73. Selected natural population analysis charges in **1'**-**3'**.

Computed molecular structure of complex 8'

Several possible molecular structures of complex **8'** (**[LMgZnOBn]')** were optimised and their relative free enthalpies were compared. In particular, the relative position of the OBn group was investigated.

Table S11. Free enthalpies computed for complex **8'** at the rωB97XD/6-311++g(d,p)/6-31g(d)/cpcm=tetrahydrofuran/298K level of theory.

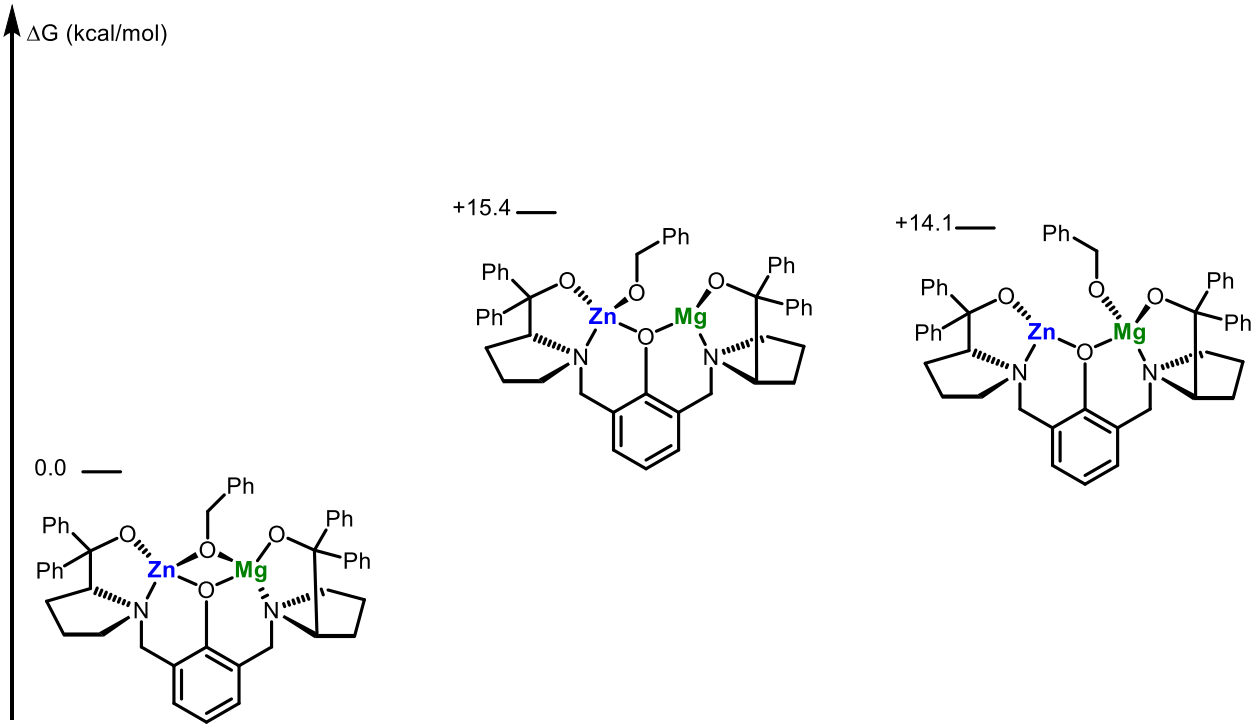

Structure	G (Hartree)	ΔG (kcal mol^{-1})
[LMgZn(OBn)]' (bridging)	–4284.826986	+0.0
[LMgZnOBn]'	–4284.802414	+15.4
[LMgOBnZn]'	–4284.804452	+14.1

According to the calculations detailed in Table S11, a bridging benzoxide group between the zinc and magnesium atoms is favoured. The molecular structure of **8'** with the lowest free enthalpy computed is shown in Figure S74.

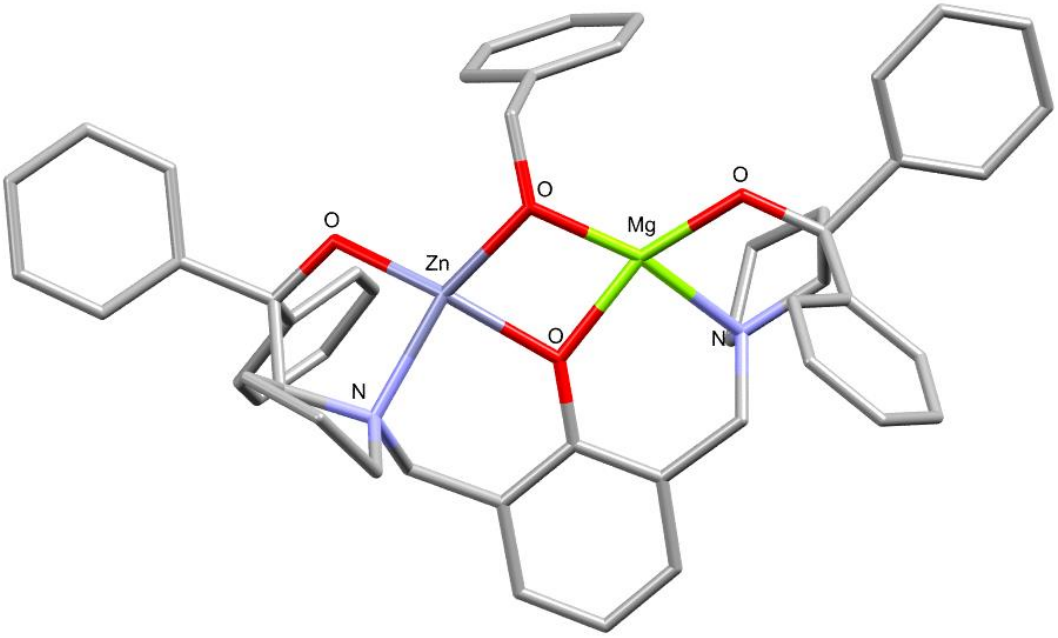

Figure S74. Molecular structure of complex **8'**, computed at the rωB97XD/6-311++g(d,p)/6-31g(d)/cpcm=tetrahydrofuran/298K level of theory.

The coordination of THF and HMDSH molecules to **8'** was also investigated. In agreement with results in Table S11, a bridging benzoxide between the zinc and magnesium atoms was also favoured in the presence of THF and HMDSH and only those structures are detailed in Table S12.

Table S12. Free enthalpies computed for complex **8'** in the presence of THF and HMDSH at the rωB97XD/6-311++g(d,p)/6-31g(d)/cpcm=tetrahydrofuran/298K level of theory.

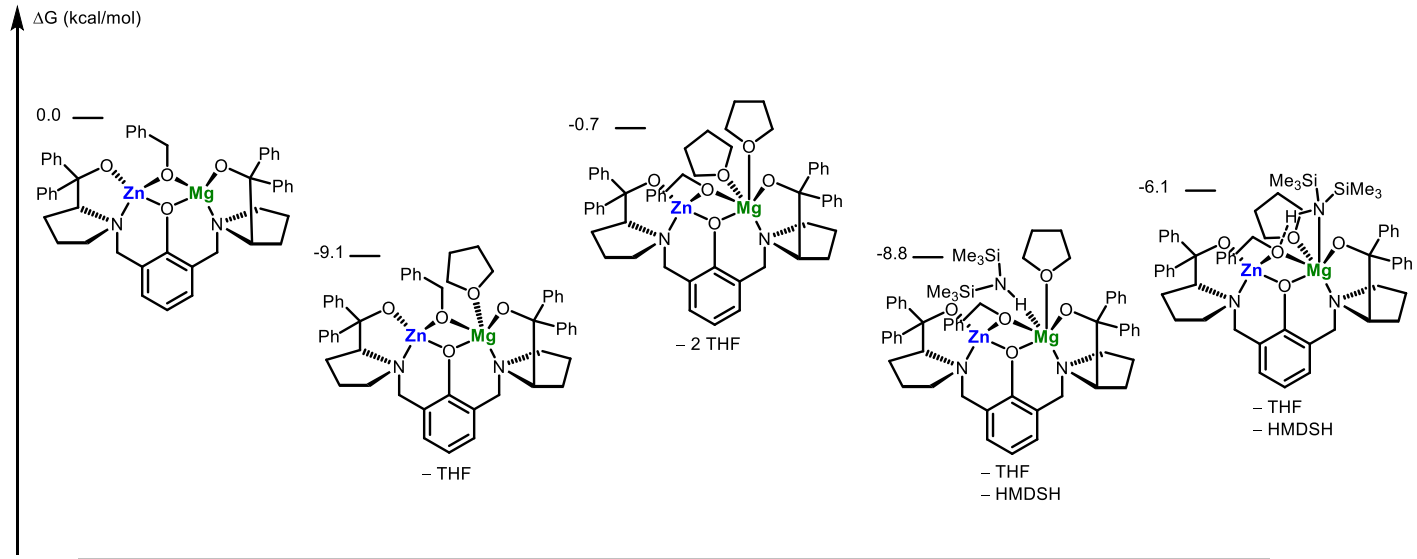

Structure	G (Hartree)	ΔG (kcal mol^{-1})
THF	–232.315175	
HMDSH	–873.63778	
[LMgZn(OBn)]' (bridging)	–4284.826986	+0.0 (reference)
[LZn(OBn)Mg(THF)]' – THF	–4284.841482	–9.1
[LZn(OBn)Mg(THF)$_2$]' – 2 THF	–4284.828086	–0.7
[LZn(OBn)Mg(THF)(HMDSH)]' – THF – HMDSH	–4284.840971	–8.8
[LZn(OBn)Mg(HMDSH)(THF)]' – THF – HMDSH	–4284.836772	–6.1

According to the calculations detailed in Table S12, a bridging benzoxide group between the zinc and magnesium atoms in **8'** is favoured, as well as the coordination of one molecule of THF, with or without an additional molecule of HMDSH. Conversely, the coordination of two molecules of HMDSH to **8'** was not found to be possible, with systematic decoordination of the second equivalent of HMDSH occurring.

Computed molecular structure of complex 9'

Several possible molecular structures of complex **9'** (**[LCaZnOBn]')** were optimised and their relative free enthalpies were compared. In particular, the relative position of the OBn group was investigated.

Table S13. Free enthalpies computed for complex **9'** at the rωB97XD/6-311++g(d,p)/6-31g(d)/cpcm=tetrahydrofuran/298K level of theory.

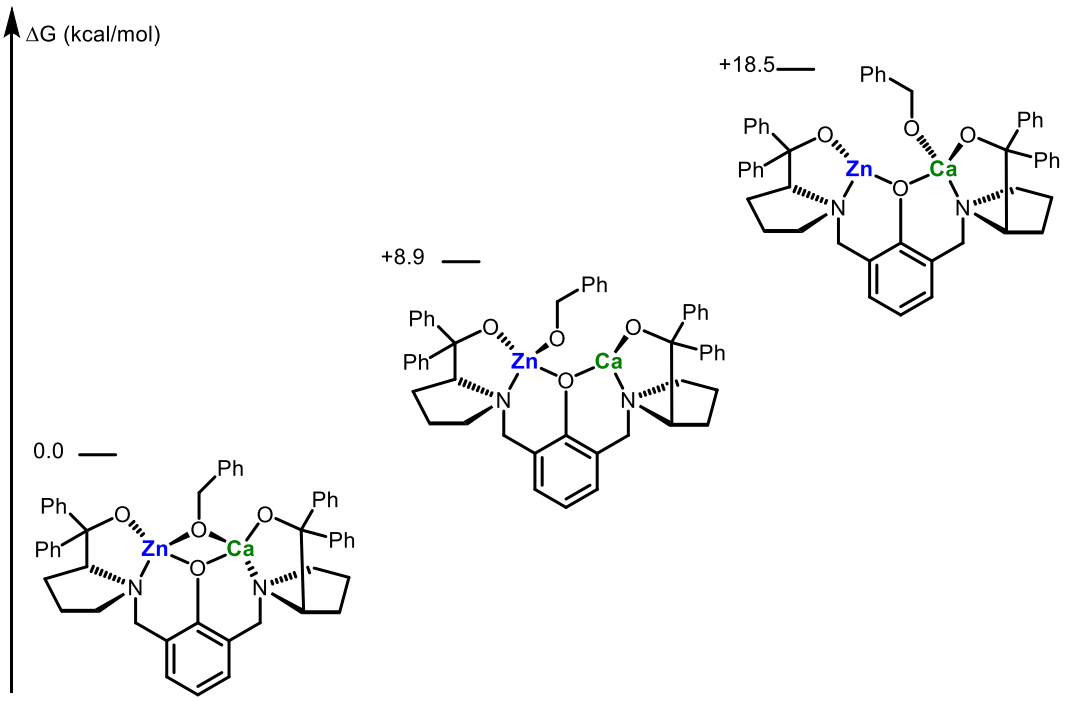

Structure	G (Hartree)	ΔG (kcal mol^{-1})
[LCaZn(OBn)]' (bridging)	–4762.370302	+0.0
[LCaZnOBn]'	–4762.356074	+8.9
[LCaOBnZn]'	–4762.340847	+18.5

According to the calculations detailed in Table S13, a bridging benzoxide between the zinc and calcium atoms is favoured. The molecular structure of **9'** with the lowest free enthalpy computed is shown in Figure S75.

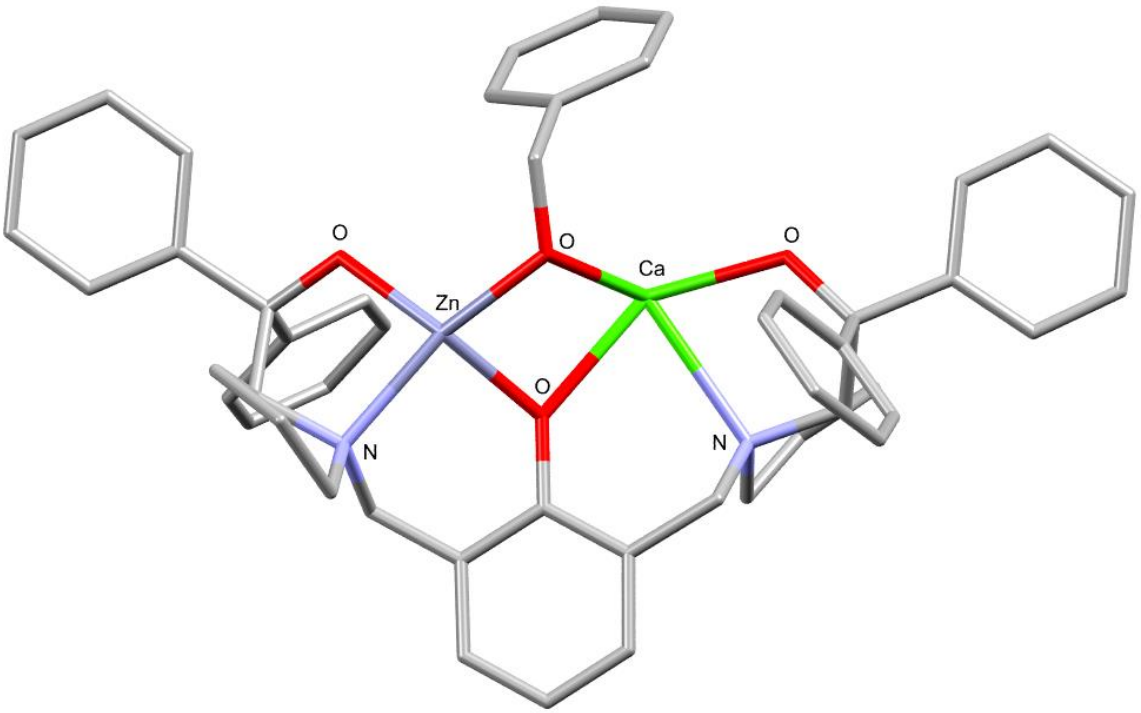

Figure S75. Molecular structure of complex **9'**, computed at the rωB97XD/6-311++g(d,p)/6-31g(d)/cpcm=tetrahydrofuran/298K level of theory.

The coordination of THF and HMDSH molecules to **9'** was also investigated. In agreement with results in Table S13, a bridging benzoxide between the zinc and calcium atoms was also favoured in the presence of THF and HMDSH and only those structures are detailed in Table S14.

Table S14. Free enthalpies computed for complex **9'** in the presence of THF and HMDSH at the rωB97XD/6-311++g(d,p)/6-31g(d)/cpcm=tetrahydrofuran/298K level of theory.

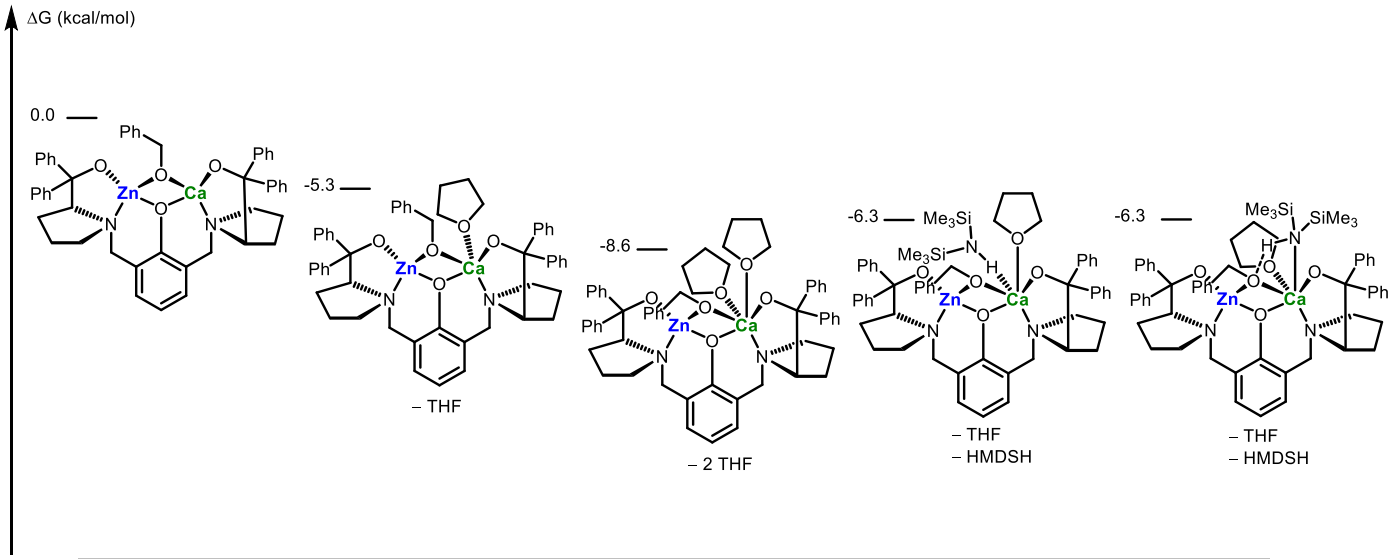

Structure	G (Hartree)	ΔG (kcal mol^{-1})
THF	–232.315175	
HMDSH	–873.63778	
[LCaZn(OBn)]' (bridging)	–4762.370302	+0.0 (reference)
[LZn(OBn)Ca(THF)]' – THF	–4762.378819	–5.3
[LZn(OBn)Ca(THF)$_2$]' – 2 THF	–4762.383962	–8.6
[LZn(OBn)Ca(THF)(HMDSH)]' – THF – HMDSH	–4762.380351	–6.3
[LZn(OBn)Ca(HMDSH)(THF)]' – THF – HMDSH	–4762.380375	–6.3

According to the calculations detailed in Table S14, a bridging benzoxide between the zinc and calcium atoms in **9'** is favoured, as well as the coordination of one or two molecules of THF and one molecule of HMDSH. Conversely, the coordination of two molecules of HMDSH to **9'** was not found to be possible, with systematic decoordination of the second equivalent of HMDSH occurring.

Coordination of LA to 8' and the first nucleophilic attack

The coordination of one molecule of L-LA or D-LA to **8'** was investigated. The transition state of the nucleophilic attack on the LA carbonyl group by the M-OBn group of **8'** was also studied, modelling the first step of the ROP mechanism. In agreement with results in Table S11, a bridging benzoxide between the zinc and magnesium atoms was also favoured in the presence of LA and only those structures are detailed in Table S15. The calculated molecular structures of **[LZn(OBn)Mg(L-LA)]'** and **[LZn(OBn)Mg(D-LA)]'** are displayed in Figures S76-79, respectively.

Table S15. Free enthalpies computed for the coordination of LA to complex **8'** at the rωB97XD/6-311++g(d,p)/6-31g(d)/cpcm=tetrahydrofuran/298K level of theory.

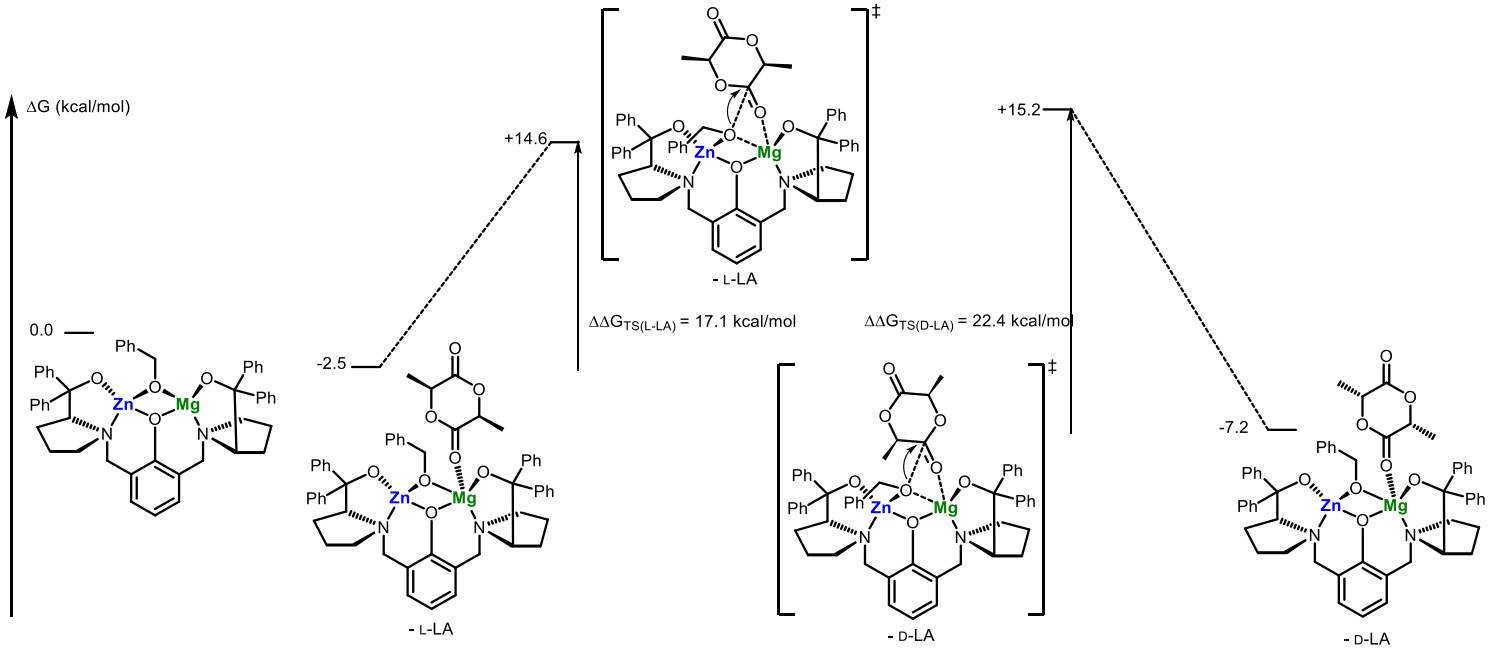

Structure	G (Hartree)	ΔG (kcal mol^{-1})
L-LA	–534.197243	
D-LA	–534.19722	
[LMgZn(OBn)]' (bridging)	–4284.826986	+0.0 (reference)
[LZn(OBn)Mg(L-LA)]' – L-LA	–4284.830968	–2.5
[LZn(OBn)Mg(D-LA)]' – D-LA	–4284.838477	–7.2
TS **[LZn(OBn)Mg(L-LA)]'** – L-LA	–4284.803653	+14.6
TS **[LZn(OBn)Mg(D-LA)]'** – D-LA	–4284.802824	+15.2

According to the calculations detailed in Table S15, the transition state of the nucleophilic attack on the carbonyl group of the coordinated LA molecule by the M-OBn group of **8'** is lower for L-LA than D-LA.

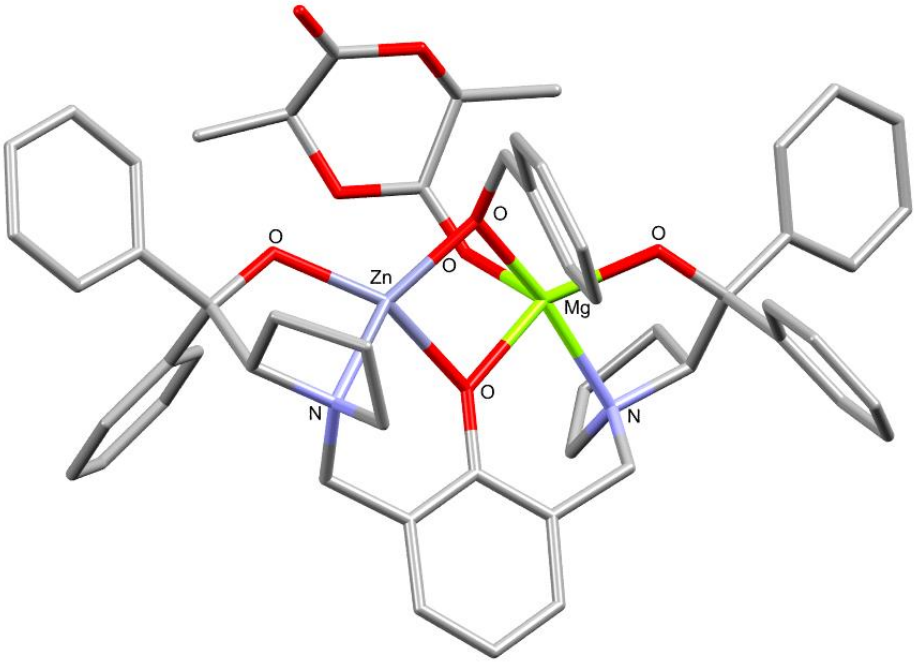

Figure S76. Molecular structure of **[LZn(OBn)Mg(L-LA)]'**, computed at the rωB97XD/6-311++g(d,p)/6-31g(d)/cpcm=tetrahydrofuran/298K level of theory, from the front perspective.

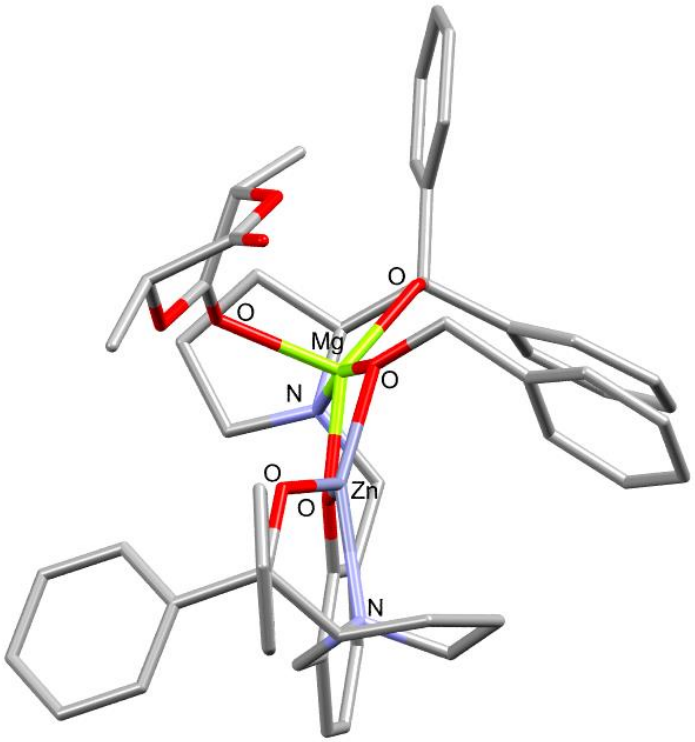

Figure S77. Molecular structure of **[LZn(OBn)Mg(L-LA)]'**, computed at the rωB97XD/6-311++g(d,p)/6-31g(d)/cpcm=tetrahydrofuran/298K level of theory, from the side-on perspective.

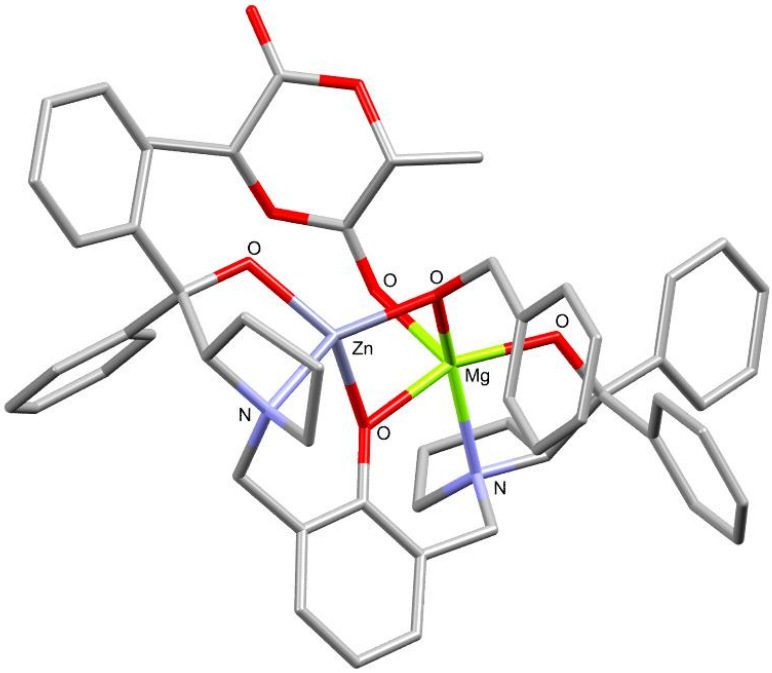

Figure S78. Molecular structure of **[LZn(OBn)Mg(D-LA)]'**, computed at the rωB97XD/6-311++g(d,p)/6-31g(d)/cpcm=tetrahydrofuran/298K level of theory, from the front perspective.

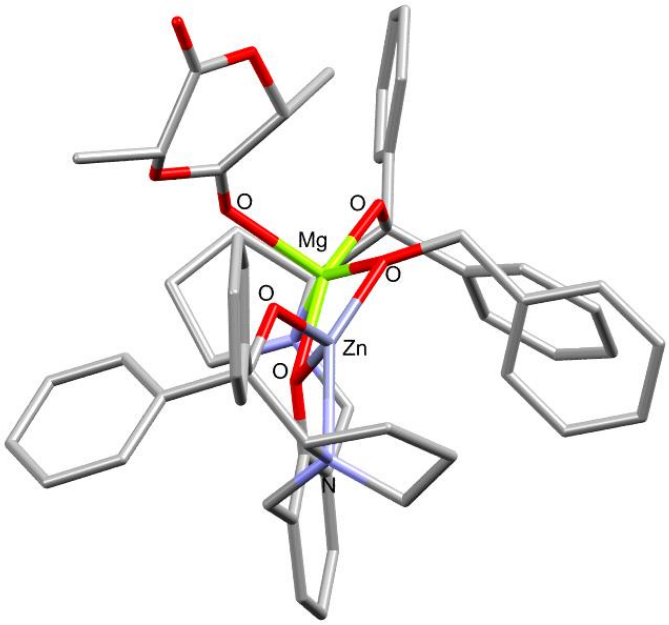

Figure S79. Molecular structure of **[LZn(OBn)Mg(D-LA)]'**, computed at the rωB97XD/6-311++g(d,p)/6-31g(d)/cpcm=tetrahydrofuran/298K level of theory, from the side-on perspective.

The coordination of THF and HMDSH molecules to **[LZn(OBn)Mg(L-LA)]'** and **[LZn(OBn)Mg(D-LA)]'** was also investigated (Table S16). Only structures susceptible to allow for the nucleophilic attack of the LA carbonyl group by the M-OBn moiety were considered.

Table S16. Free enthalpies computed for the coordination of THF and HMDSH to **[LZn(OBn)Mg(L-LA)]'** and **[LZn(OBn)Mg(D-LA)]'** at the rωB97XD/6-311++g(d,p)/6-31g(d)/cpcm=tetrahydrofuran/298K level of theory.

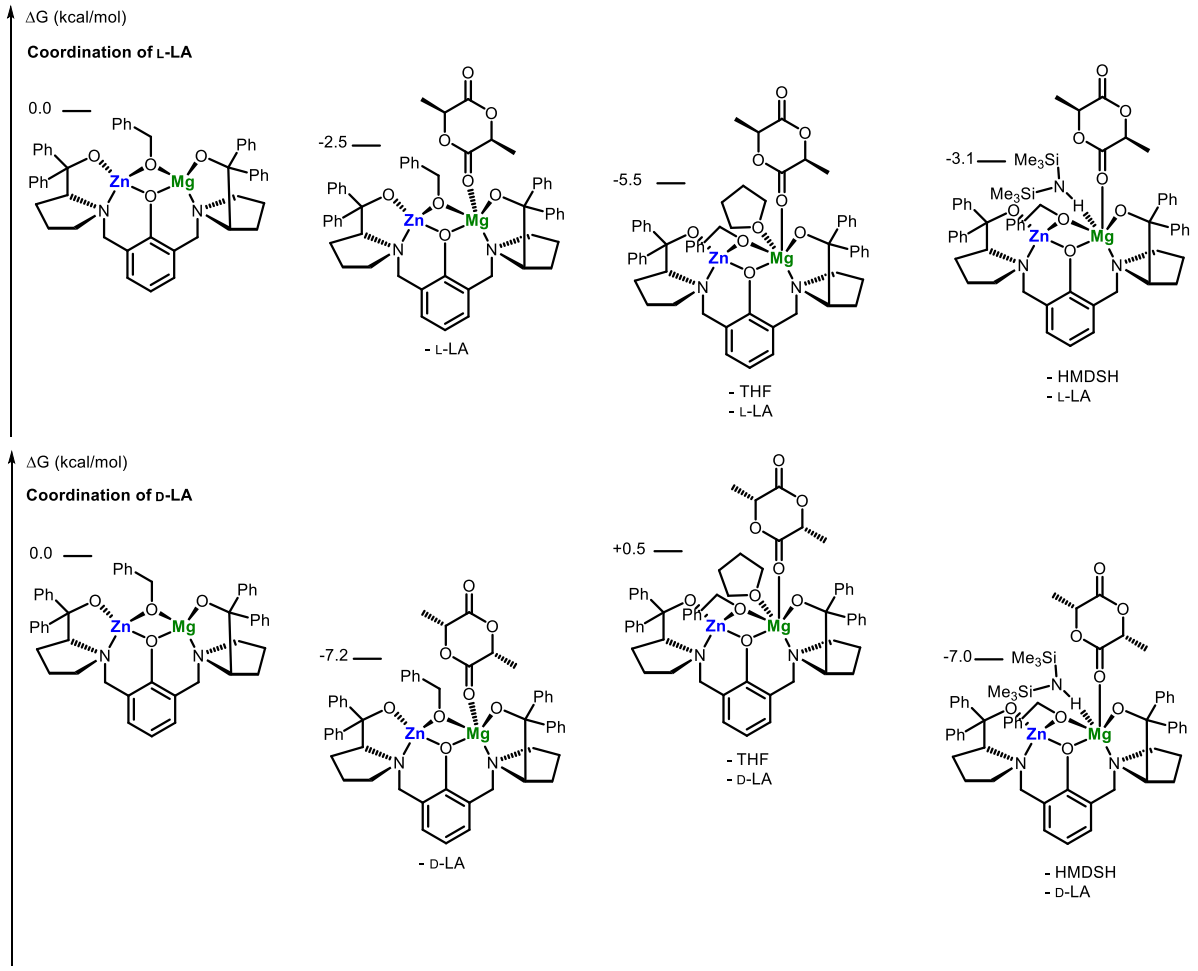

Structure	G (Hartree)	ΔG (kcal mol^{-1})
THF	–232.315175	
HMDSH	–873.63778	
L-LA	–534.197243	
D-LA	–534.19722	
[LMgZn(OBn)]' (bridging)	–4284.826986	+0.0 (reference)
[LZn(OBn)Mg(L-LA)]' – L-LA	–4284.830968	–2.5
[LZn(OBn)Mg(L-LA)(THF)]' – THF – L-LA	–4284.835704	–5.5
[LZn(OBn)Mg(L-LA)(HMDSH)]' – HMDSH – L-LA	–4284.831925	–3.1
[LZn(OBn)Mg(D-LA)]' – D-LA	–4284.838477	–7.2
[LZn(OBn)Mg(D-LA)(THF)]' – THF – D-LA	–4284.826253	+0.5
[LZn(OBn)Mg(D-LA)(HMDSH)]' – HMDSH – D-LA	–4284.838093	–7.0

According to the calculations detailed in Table S16, coordination of one THF molecule to the magnesium centre of **8'** is most favoured in the presence of L-LA, with coordination of one molecule of HMDSH more favoured than no Lewis donor coordination at all. Conversely, in the presence of D-LA, the most stable molecular structure involves no Lewis donors, albeit coordination of one molecule of HMDSH is also favourable.

Coordination of LA to 9' and the first nucleophilic attack

The coordination of one molecule of L-LA or D-LA to **9'** was investigated. The transition state of the nucleophilic attack on the LA carbonyl group by the M-OBn group of **9'** was also studied, modelling the first step of the ROP mechanism. In agreement with results in Table S13, a bridging benzoxide between the zinc and calcium atoms was also favoured in the presence of LA and only those structures are detailed in Table S17. The calculated molecular structures of **[LZn(OBn)Ca(L-LA)]'** and **[LZn(OBn)Ca(D-LA)]'** are displayed in Figures 6 and S80-81.

Table S17. Free enthalpies computed for the coordination of LA to complex **9'** at the rωB97XD/6-311++g(d,p)/6-31g(d)/cpcm=tetrahydrofuran/298K level of theory.

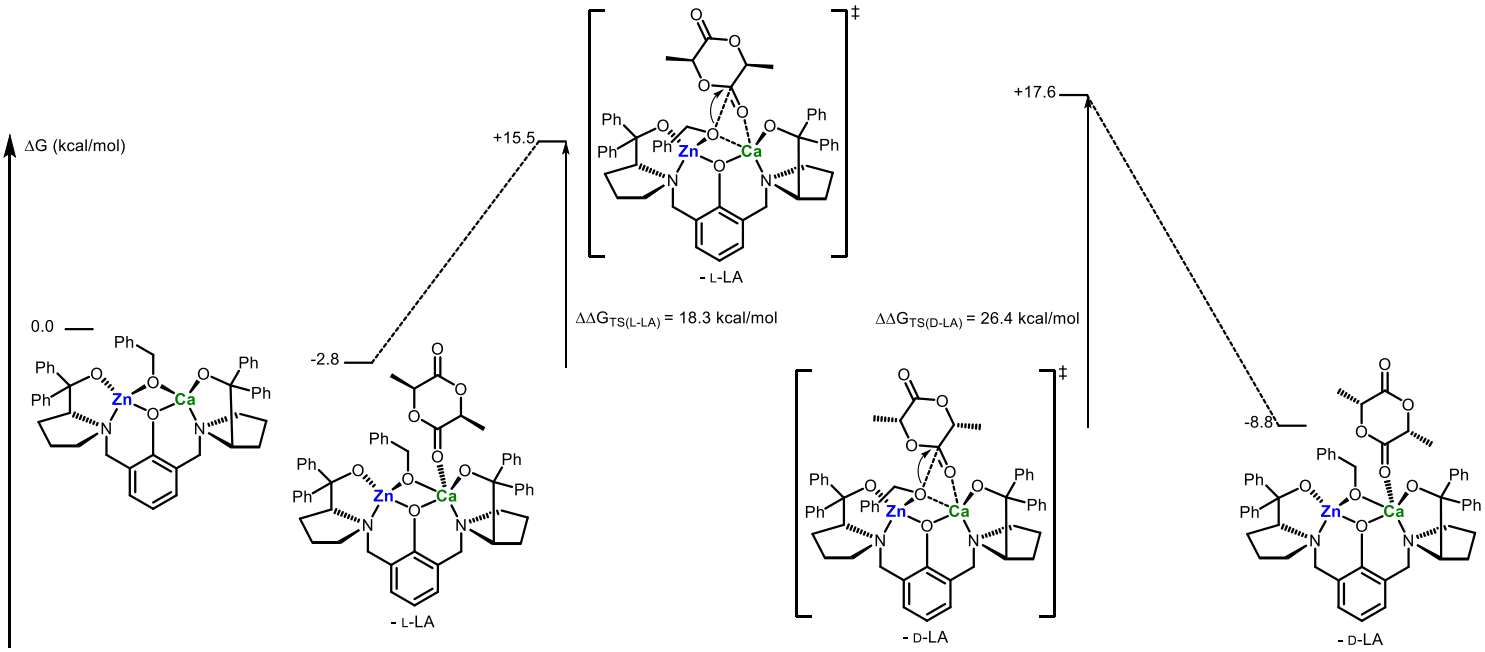

Structure	G (Hartree)	ΔG (kcal mol^{-1})
L-LA	–534.197243	
D-LA	–534.19722	
[LCaZn(OBn)]' (bridging)	– 4762.370302	+0.0 (reference)
[LZn(OBn)Ca(L-LA)]' – L-LA	–4762.374778	–2.8
[LZn(OBn)Ca(D-LA)]' – D-LA	–4762.38427	–8.8
TS **[LZn(OBn)Ca(L-LA)]'** – L-LA	–4762.345528	+15.5
TS **[LZn(OBn)Ca(D-LA)]'** – D-LA	– 4762.342281	+17.6

According to the calculations detailed in Table S17, the transition state of the nucleophilic attack on the carbonyl group of the coordinated LA molecule by the M-OBn group of **9'** is lower for L-LA than D-LA.

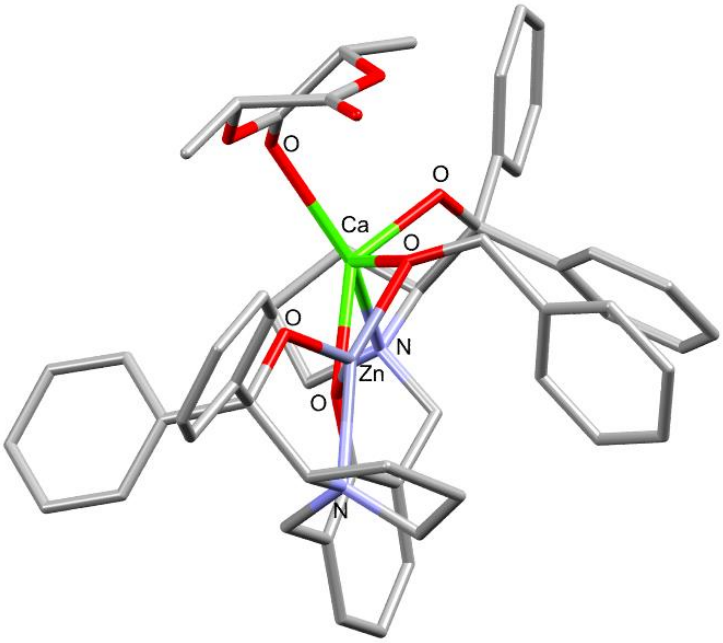

Figure S80. Molecular structure of **[LZn(OBn)Ca(L-LA)]'**, computed at the rωB97XD/6-311++g(d,p)/6-31g(d)/cpcm=tetrahydrofuran/298K level of theory, from the side-on perspective.

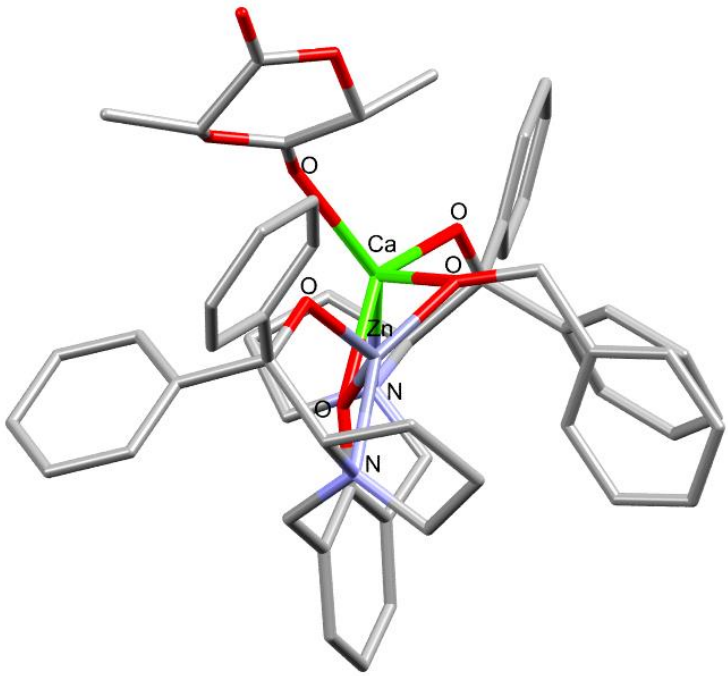

Figure S81. Molecular structure of **[LZn(OBn)Ca(D-LA)]'**, computed at the rωB97XD/6-311++g(d,p)/6-31g(d)/cpcm=tetrahydrofuran/298K level of theory, from the side-on perspective.

The coordination of THF and HMDSH molecules to **[LZn(OBn)Ca(L-LA)]'** and **[LZn(OBn)Ca(D-LA)]'** was also investigated (Table S18). Only structures susceptible to allow for the nucleophilic attack of the LA carbonyl group by the M-OBn moiety were considered.

Table S18. Free enthalpies computed for the coordination of THF and HMDSH to **[LZn(OBn)Ca(L-LA)]'** and **[LZn(OBn)Ca(D-LA)]'** at the rωB97XD/6-311++g(d,p)/6-31g(d)/cpcm=tetrahydrofuran/298K level of theory.

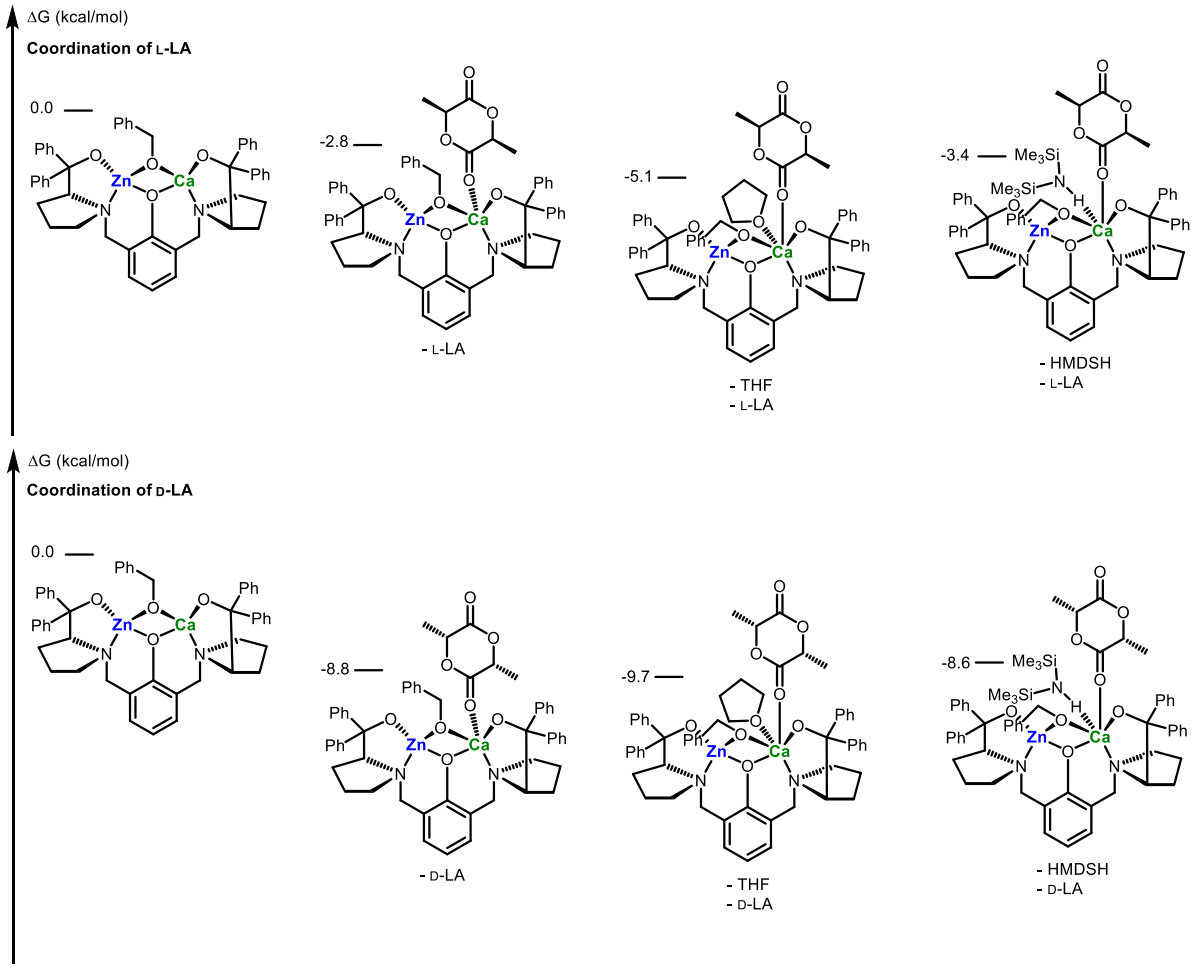

Structure	G (Hartree)	ΔG (kcal mol^{-1})
THF	–232.315175	
HMDSH	–873.63778	
L-LA	–534.197243	
D-LA	–534.19722	
[LCaZn(OBn))]' (bridging)	– 4762.370302	+0.0 (reference)
[LZn(OBn)Ca(L-LA)]' – L-LA	–4762.374778	–2.8
[LZn(OBn)Ca(L-LA)(THF)]' – THF – L-LA	–4762.378472	–5.1
[LZn(OBn)Ca(L-LA)(HMDSH)]' – HMDSH – L-LA	-4762.375746	–3.4
[LZn(OBn)Ca(D-LA)]' – D-LA	–4762.38427	–8.8
[LZn(OBn)Ca(D-LA)(THF)]' – THF – D-LA	–4762.385721	–9.7
[LZn(OBn)Ca(D-LA)(HMDSH)]' – HMDSH – D-LA	–4762.384078	–8.6

According to the calculations detailed in Table S18, coordination of one THF molecule to the calcium centre of **9'** is most favoured in the presence of L-LA, with coordination of one molecule of HMDSH more favoured than no Lewis donor coordination at all. In the presence of D-LA, the most stable molecular structure also involves one molecule of THF, albeit structures involving the coordination of one molecule of HMDSH or no Lewis donor coordination at all are also favourable.

References

1. W. Gruszka, L. C. Walker, M. P. Shaver and J. A. Garden, *Macromolecules*, 2020, **53**, 4294-4302.
2. Gaussian 16, Revision A.03, M. J. Frisch, G. W. Trucks, H. B. Schlegel, G. E. Scuseria, M. A. Robb, J. R. Cheeseman, G. Scalmani, V. Barone, G. A. Petersson, H. Nakatsuji, X. Li, M. Caricato, A. V. Marenich, J. Bloino, B. G. Janesko, R. Gomperts, B. Mennucci, H. P. Hratchian, J. V. Ortiz, A. F. Izmaylov, J. L. Sonnenberg, D. Williams-Young, F. Ding, F. Lipparini, F. Egidi, J. Goings, B. Peng, A. Petrone, T. Henderson, D. Ranasinghe, V. G. Zakrzewski, J. Gao, N. Rega, G. Zheng, W. Liang, M. Hada, M. Ehara, K. Toyota, R. Fukuda, J. Hasegawa, M. Ishida, T. Nakajima, Y. Honda, O. Kitao, H. Nakai, T. Vreven, K. Throssell, J. A. Montgomery, Jr., J. E. Peralta, F. Ogliaro, M. J. Bearpark, J. J. Heyd, E. N. Brothers, K. N. Kudin, V. N. Staroverov, T. A. Keith, R. Kobayashi, J. Normand, K. Raghavachari, A. P. Rendell, J. C. Burant, S. S. Iyengar, J. Tomasi, M. Cossi, J. M. Millam, M. Klene, C. Adamo, R. Cammi, J. W. Ochterski, R. L. Martin, K. Morokuma, O. Farkas, J. B. Foresman, and D. J. Fox, Gaussian, Inc., Wallingford CT, 2016.
3. J. -D. Chai, M. Head-Gordon, *Chem. Phys. Lett.*, 2008, **467**, 176–178.
4. J. -D. Chai, M. Head-Gordon, *Phys. Chem. Chem. Phys.*, 2008, **10**, 6615–6620.
5. G. Scalmani, M. J. Frisch, *J. Chem. Phys.*, 2010, **132**, 114110-114115.
6. D. M. York, M. Karplus, *J. Phys. Chem. A*, 1999, **103**, 11060–11079.
7. W. Gruszka, A. Lykkeberg, G. S. Nichol, M. P. Shaver, A. Buchard, J. A. Garden, *Chem. Sci.*, 2020, **11**, 11785-11790.
8. X. He, B. C. Noll, A. Beatty, R. E. Mulvey, K. W. Henderson, *J. Am. Chem. Soc.*, 2004, **126**, 7444–7445.
9. F. Buch, PhD thesis, Universität Duisburg-Essen, 2008.
10. A. Kowalski, A. Duda, S. Penczek, *Macromolecules,* 1998, **31,** 2114–2122.
11. A. J. Gaston, Z. Greindl, C. A. Morrison, J. A. Garden, *Inorg. Chem.*, 2021, **60**, 2294-2303.